國　立　交　通　大　學
奈 米 科 技 研 究 所

碩 士 論 文

運用溶膠－凝膠法技術製作金屬氧化物奈米結晶粒於快閃記憶體元件之研究

The Study of Flash Memory Devices with Metal Oxide Nanocrystals in Sol-Gel Technique

研 究 生：鄭延宸　　　**Yen-Chen Cheng**

學　　號：9452510

指導教授：柯富祥 博士 **Dr. Fu-Hsiang Ko**

劉增豐 博士 **Dr. Tzeng-Feng Liu**

中華民國九十六年七月

運用溶膠—凝膠法技術製作金屬氧化物奈米結晶粒於快閃記憶體元件之研究

The Study of Flash Memory Devices with Metal Oxide Nanocrystals in Sol-Gel Technique

研 究 生：鄭延宸　　　Student：Yen-Chen Cheng

指導教授：柯富祥　　　Advisor：Fu-Hsiang Ko

劉增豐　　　Tzeng-Feng Liu

國 立 交 通 大 學

奈 米 科 技 研 究 所

碩 士 論 文

A Thesis
Submitted to Institute of Nanotechnology
College of Engineering
National Chiao Tung University
in partial Fulfillment of the Requirements
for the Degree of
Master
in
Nanotechnology
July 2007
Hsinchu, Taiwan, Republic of China

中華民國九十六年七月

運用溶膠－凝膠法技術製作金屬氧化物
奈米結晶粒於快閃記憶體元件之研究

研究生 ： 鄭延宸　　　　　　指導教授 ： 柯富祥 博士

劉增豐 博士

國立交通大學

奈米科技研究所碩士班

摘 要

隨著半導體產業的發展，大眾對於「非揮發性記憶體」的材料與技術也越重視，其中又以具有輕、薄、短、小和可攜帶式的各類電子產品，諸如數位相機、智慧型手機、隨身碟及 PDA 等尤之。

傳統的浮動閘極型結構非揮發性快閃（Flash）記憶體，當記憶體元件的穿隧氧化層膜厚低於 10 奈米時，會使得原先已儲存於複晶矽材料製作成的浮動閘極內電荷，極易藉由在重複多次讀寫週期後造成的氧化層缺陷，形成漏電路徑，導致儲存在浮動閘極內電荷的資料流失。而複晶矽-氧化物-氮化矽-氧化物-單晶矽（SONOS）型結構的快閃記憶體，被提議為解決元件尺寸縮小時，因傳統浮動閘極型結構記憶體所面對的極限問題。在傳統的 SONOS 型結構記憶體元件上，其儲存電荷的捕陷層材料是氮化矽。此種結構中，因為電荷是被儲存在不同捕陷位置的分散區域內，所以相對可提升傳統浮動閘極型結構對於資料保存性的問題；

不過，由於氮化矽材料與二氧化矽之間的導電帶位能差不高，如此會使得記憶體元件的寫入及抹除速度降低。

當利用分離的奈米結晶粒做為電荷儲存之傳導媒介時，此時奈米結晶粒快閃記憶體對於局部性的氧化物缺陷擁有較佳的免疫能力。而它在很多方面也具有益處：如較多的電荷捕陷區域、較大的臨限電壓變化、較長的電荷保存時間，以及良好的耐用特性。因此藉由高介電材料形成奈米結構結晶粒取代快閃記憶體元件電荷捕陷層之研究，目前正被大量探討中。

現今雖然高介電材料的沉積方式繁多，例如:原子層沉積法、物理氣相沉積法(如雙電子槍蒸鍍系統、真空濺鍍系統)、化學氣相沉積法、有機金屬化學氣相沉積法，但是上述幾種沉積法需要的成本皆相當昂貴。在本篇論文中則提出了使用溶膠-凝膠法技術來沉積高介電與金屬氧化物材料，以作為奈米結晶粒快閃記憶體元件電荷捕陷層的製作方法。相較其他方法而言，溶膠-凝膠法的優點在於價格較便宜，又可迅速的配出兩元或三元成份以上組成的奈米結晶粒，對比於一般的高真空沉積環境設備上，更具省時及便利性。

在本研究論文的第二、三章中，我們依序製作出奈米結晶粒快閃記憶體元件以及充分利用了溶膠-凝膠法技術，將二氯化鈷、四氯化鍺、四氯化金、四氧氯化鋰、二氯化鎳、四氯化矽、四氯化鋯等元素做為前驅物，來製備多元化學複合物成份的奈米結晶粒。個別先將前驅氯化物溶入異丙醇及酒精溶劑中，藉由溶膠-凝膠法在穿隧氧化層上沉積金屬氯化物材料，再經過 1050 度、60 秒的快速熱退火與氧化步驟後，形成多種不同種類組成的金屬氧化物薄膜及奈米結晶粒，即是為快閃記憶體元件的電荷捕陷層。在元件電性方面，顯示了使用溶膠-凝膠法沉積出的金屬氧化物電荷捕陷層，確實具有良好的記憶體儲存效應，例如較大的記憶區間、快速的寫入/抹除速度、持久的電荷保存/耐用率、極小的閘/汲極干擾等優點。此外，從論文內的高解析度穿透式電子顯微鏡（HRTEM）儀器圖像中也可看出，元件的電荷捕陷層經過了 1050 度、60 秒的快速熱退火與氧化步驟後，的確已形成了奈米尺度之球狀體或橢圓形狀奈米結晶粒或複合物薄膜。

最後，由此實驗的顯著性奈米結構特徵，使我們相信溶膠–凝膠法技術是一種既低價位、快速又具效率，可應用於製作金屬氧化物薄膜或奈米結晶粒，作為快閃記憶體元件電荷捕陷層的好方法。

The Study of Flash Memory Devices with Metal Oxide Nanocrystals in Sol-Gel Technique

Student: Yen-Chen Cheng Advisor: Dr. Fu-Hsiang Ko

Dr. Tzeng-Feng Liu

Institute of Nanotechnology

National Chiao Tung University

Abstract

As overall semiconductor industry development, the technology of material science is extremely significant on non-volatile memory (NVM) in every field of human's life, especially in lightness, thinness, shortness, and smallness with portable electronic products like digital camera, smart cell phone, flash drive disk, and PDA, etc.

On non-volatile Flash memory of the conventional floating-gate (FG) structure, when the tunnel oxide thickness of a memory device is less than 10 nm, storage charges in the polysilicon floating gate are easy to leak along the path through oxide bulk defects during programming/erasing (P/E) cycles. The polysilicon-oxide-nitride-oxide-silicon (SONOS) Flash memory structure is recommended that we resolve this limitation with a device scaling down. The

charge-trapping layer of a customary SONOS memory device is silicon nitride (Si_3N_4). Because storage charges are trapped in discrete traps diversely, they can enhance charge retention of the FG structure. The traditional SONOS memory device has good data storage; however, the conduction band offset between Si_3N_4 and silicon dioxide (SiO_2) is not large. This result leads to slower P/E speed of the memory device.

By using discrete nanocrystals (NCs) as the charge storage medium, the nanocrystal (NC) Flash memory is more immune to local oxide defects. It is considered to be more beneficial in many aspects: more charge-trapping sites, larger Vth or V_T shift (△Vth or △V_T) memory window, longer retention time, and good endurance cycles. Thus, applying high-k dielectric materials to form nano-composite NCs to substitute for the charge-trapping layer in a Flash memory device has been extensively researched.

Up to now, despite the fact that such numerous high-k dielectric deposition methods have been supplied for atomic layer deposition (ALD), physical vapor deposition (PVD) (e.g., Dual E-Gun Evaporation System, Sputtering System), chemical vapor deposition (CVD), and metal-organic chemical vapor deposition (MOCVD), they are high cost. In this study, we present Sol-Gel technique as a way to deposit high-k dielectrics and metal oxide (M_xO_y) materials for the charge-trapping layer in the NC Flash memory devices. Contrary to high vacuum compatible equipments, many advantages of the Sol-Gel spin coating method are lower costs, more convenient tools, and easier processes to synthesize the combination of binary or ternary M_xO_y NCs in the normal pressure environment.

In the chapter 2 and 3, we gradually fabricated the NC Flash memory devices and made good use of Sol-Gel technique with ($CoCl_2 \cdot 6H_2O$), $GeCl_4$, ($HAuCl_4 \cdot 3H_2O$), $LiClO_4$, ($NiCl_2 \cdot 6H_2O$), $SiCl_4$, and $ZrCl_4$ elements as precursors to deposit the NCs consisting of several chemical compounds. These precursors of distinct metal chloride

(M_xCl_y) powder were mixed and dissolved into isopropanol (IPA) and C_2H_5OH, deposited on the tunnel oxide layer by the Sol-Gel spin coating procedure, and followed with the 1050°C 60 sec. oxide rapid thermal annealing (ORTA) step in the O_2 environment to form various kinds of the M_xO_y thin film or NCs as the charge-trapping layer of the Flash memory devices, respectively. This M_xO_y NC charge-trapping layer extracted from the Sol-Gel spin coating method included in the device exhibited good electrical properties, such as relatively large memory window, high P/E speed, long data retention/endurance time, little gate/drain (G/D) disturbance, and so on. Moreover, the high-resolution transmission microscopy (HRTEM) instrument was conducted to research the physical properties of binary or ternary M_xO_y NCs as well. From the HRTEM images, each trapping layer of the devices truly was shaped into nano-sized round balls or oval-shaped NCs or a composite thin film after the 1050° C 60 sec. oxide rapid thermal annealing (ORTA) step.

In the long run, by reason of prominently nano-structured features in the memory devices for our experiments, we believe Sol-Gel technique is a low-priced, instant, and efficient method to fabricate the M_xO_y thin film or NCs as the charge-trapping layer of Flash memory devices.

致 謝 詞

在這兩年的研究生活中，首先要向我的指導教授柯富祥、劉增豐博士，致上最高的謝意，謝謝老師兩年來的關心、指導與教誨，我的論文才得以順利完成。老師採取了信任學生的態度，讓我自由的發揮創意，並在實驗上適時的提供了非常寶貴的意見，使得我在研究生的學習生涯中，培養出了做事方法和解決問題的能力。這段學業研究期間，在老師的教育及鼓勵下，讓我的人生成長了許多。

此外，須向其昌學長、俊淇學長、佳典學長在實驗過程中的細心指導與電子所紹明學長在元件量測上的熱心幫忙，表達深深的感謝，若無你們從旁的協助與解惑，此研究論文將不盡完備。另外，也要感謝志杰、奕儂、群芳、敬雅同學在課業及生活上的互相幫忙，使我們順利的度過了這兩年。實驗室的中書、宜生學弟及德玲、依蓁、美榕學妹們，當然也不會忘記和你們一起度過的歡樂時光。

最後，要將此篇論文獻給我最摯愛的家人、女友雅雯，感謝你們對我的全力支持與關懷，讓我能夠無後顧之憂，順利的完成研究所學位，若沒有你們的體諒、包容，相信這兩年的生活會是黯淡無光的!在此將這份小小的榮耀和你們共同分享之。

Contents

Abstract (Chinese) i

Abstract (English) ………………………………………………………………......iv

Acknowledges (Chinese) vii

Contents …………………………..……………………………….…………..viii

Table Lists ………………………….…………………………………………....xi

Figure Captions ……………………………………………..…….……………xii

Chapter 1 Introduction ……………………...1

1-1 Overview of Non-volatile Memory (NVM) 1

1-2 Motivation ………………………………………………………………………..11

1-3 Thesis Organization 12

Chapter 2 Electrical and Physical Properties of Metal Oxide Nanocrystal Flash Memory Devices by the Sol-Gel Spin Coating Method with IPA Solvent 14

2-1 Introduction 14

2-2 The Sol-Gel Technique ………...17

2-3 Experiments 20

2-4 Results and Discussion …………………………………………………….30

2-4.1 Electrical Properties …………………………………………………..30

2-4.1.1 Id-Vg Transfer Curves 30

2-4.1.2 Programming/Erasing Speed 33

2-4.1.3 Retention Time 37

2-4.1.4 Endurance Cycles 39

2-4.1.5 Gate/Drain Disturbance 41

2-4.2 Physical Properties 46

2-5 Summary 48

Chapter 3 Electrical and Physical Properties of Metal Oxide Nanocrystal Flash Memory Devices by the Sol-Gel Spin Coating Method with C_2H_5OH Solvent 50

3-1 Introduction 50

3-2 Experiments 51

3-3 Results and Discussion 55

3-3.1 Electrical Characteristics 55

3-3.1.1 Id-Vg Transfer Curves 55

3-3.1.2 Programming/Erasing Speed 58

3-3.1.3 Retention Time 61

3-3.1.4 Endurance Cycles 63

3-3.1.5 Gate/Drain Disturbance 65

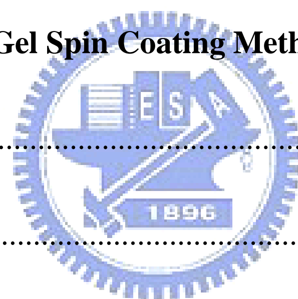

3-3.2 Physical Properties 69

3-4 Summary 72

Chapter 4 Conclusions and Recommendations for Future Research 74

4-1 Conclusions 74

4-2 Recommendations for Future Research 75

References 76

Table Lists

Chapter 1

Tab. 1-1 The next generation trend on NVM technology for the ITRS update list 9

Figure Captions

Chapter 1

Fig. 1-1 The increased demand for portable electronic devices to memory technology 1

Fig. 1-2 The semiconductor memory tree 2

Fig. 1-3 The floating-gate (FG) structure with polysilicon used as the floating gate for data storage 3

Fig. 1-4 The current vs. voltage characterization of a FG memory device under the programmed and erased states for the △ Vth or △ V_T and memory window 4

Fig. 1-5 The structure of well-known commercial ETOX Flash memory cell for floating gate 5

Fig. 1-6 The energy-band diagrams of ETOX Flash memory showing electron and hole injection states with "written" by CHEI and "erased" by BTBHHI or FN tunneling mechanism 5

Fig. 1-7 The conventional SONOS memory structure, silicon nitride (Si_3N_4) as the charge-trapping layer 7

Fig. 1-8 The energy-band diagram of nitride-based SONOS memory 8

Fig. 1-9 The band diagram comparison of SONOS memory of Si_3N_4 and HfO_2 materials when programming (solid line as Si_3N_4, dash line as HfO_2) 8

Fig. 1-10 The nanocrystal (NC) charge storage distribution structure for the Flash memory cell 10

Chapter 2

Fig. 2-1 The band diagram of ZrO_2 dielectric SONOS-type memory 15

Fig. 2-2 The band diagram of nitride-based SONOS memory 15

Fig. 2-3 The energy-band diagram comparison of SONOS memory of Si_3N_4 and HfO_2 materials when programming (solid line as Si_3N_4, dash line as HfO_2) 16

Fig. 2-4 The diagram of the spin coating method with controllable spin motor 18

Fig. 2-5 Three main product applications of the Sol-Gel method (dash line as the step-by-step coating procedures of our experiments) 19

Fig. 2-6 The flow chart of IPA Sol-Gel derived Flash memory devices 21

Fig. 2-7 The process flow of proposed IPA Sol-Gel derived NC Flash memory cells 30

Fig. 2-8 The Id-Vg transfer curves of (CoLi)Si_xO_y-M_xO_y NC devices 32

Fig. 2-9 The Id-Vg transfer curves of (CoLi)Ge_xO_y-M_xO_y NC devices 32

Fig. 2-10 The Id-Vg transfer curves of (CoLiZr)Si_xO_y-M_xO_y NC devices 33

Fig. 2-11 The programming speed of (CoLi)Si_xO_y-M_xO_y NC devices 34

Fig. 2-12 The programming speed of (CoLi)Ge_xO_y-M_xO_y NC devices 35

Fig. 2-13 The programming speed of (CoLiZr)Si_xO_y-M_xO_y NC devices 35

Fig. 2-14 The erasing speed of (CoLi)Si_xO_y-M_xO_y NC devices 36

Fig. 2-15 The erasing speed of (CoLi)Ge_xO_y-M_xO_y NC devices 36

Fig. 2-16 The erasing speed of (CoLiZr)Si_xO_y-M_xO_y NC devices 37

Fig. 2-17 The data retention time of (CoLi)Si_xO_y-M_xO_y NC devices 38

Fig. 2-18 The data retention time of (CoLi)Ge_xO_y-M_xO_y NC devices ……………...38

Fig. 2-19 The data retention time of (CoLiZr)Si_xO_y-M_xO_y NC devices 39

Fig. 2-20 The data endurance of (CoLi)Si_xO_y-M_xO_y NC devices 40

Fig. 2-21 The data endurance of (CoLi)Ge_xO_y-M_xO_y NC devices 40

ES 1896

Fig. 2-22 The data endurance of (CoLiZr)Si_xO_y-M_xO_y NC devices 41

Fig. 2-23 The G/D Disturbance schematic structure of Flash memory cells 42

Fig. 2-24 The gate disturbance of (CoLi)Si_xO_y-M_xO_y NC devices 42

Fig. 2-25 The gate disturbance of (CoLi)Ge_xO_y-M_xO_y NC devices 43

Fig. 2-26 The gate disturbance of (CoLiZr)Si_xO_y-M_xO_y NC devices 43

Fig. 2-27 The drain disturbance of (CoLi)Si_xO_y-M_xO_y NC devices 44

Fig. 2-28 The drain disturbance of (CoLi)Ge_xO_y-M_xO_y NC devices 45

Fig. 2-29 The drain disturbance of (CoLiZr)Si_xO_y-M_xO_y NC devices 45

Fig. 2-30 The HRTEM image of the (CoLi)Si_xO_y-composite thin film on SiO_2 after the 1050° C 60 sec. ORTA step 46

Fig. 2-31 The HRTEM image of the (CoLi)Ge_xO_y-composite thin film on SiO_2 after the 1050° C 60 sec. ORTA step 47

Fig. 2-32 The HRTEM image of (CoLiZr)Si_xO_y-composite NCs on SiO_2 after the 1050° C 60 sec. ORTA step 48

Chapter 3

Fig. 3-1 The energy-band diagram of ZrO_2 dielectric SONOS-type memory 51

Fig. 3-2 The flow chart of C_2H_5OH Sol-Gel derived Flash memory devices 53

Fig. 3-3 The semiconductor process flow of C_2H_5OH Sol-Gel derived NC Flash memory cells 54

Fig. 3-4 The presented C_2H_5OH Sol-Gel derived NC Flash memory cross section ..55

Fig. 3-5 The Id-Vg transfer curves of $AuGe_xO_y$-M_xO_y NC devices 56

Fig. 3-6 The Id-Vg transfer curves of (CoZr)Ge_xO_y-M_xO_y NC devices 57

Fig. 3-7 The Id-Vg transfer curves of (NiZr)$Si_xGe_zO_y$-M_xO_y NC devices 57

Fig. 3-8 The programming speed of $AuGe_xO_y$-M_xO_y NC devices 58

Fig. 3-9 The programming speed of (CoZr)Ge_xO_y-M_xO_y NC devices 59

Fig. 3-10 The programming speed of (NiZr)$Si_xGe_zO_y$-M_xO_y NC devices 59

Fig. 3-11 The erasing speed of $AuGe_xO_y$-M_xO_y NC devices 60

Fig. 3-12 The erasing speed of (CoZr)Ge_xO_y-M_xO_y NC devices 60

Fig. 3-13 The erasing speed of (NiZr)$Si_xGe_zO_y$-M_xO_y NC devices 61

Fig. 3-14 The data retention time of $AuGe_xO_y$-M_xO_y NC devices 62

Fig. 3-15 The data retention time of (CoZr)Ge_xO_y-M_xO_y NC devices 62

Fig. 3-16 The data retention time of (NiZr)$Si_xGe_zO_y$-M_xO_y NC devices 63

Fig. 3-17 The data endurance of $AuGe_xO_y$-M_xO_y NC devices 64

Fig. 3-18 The data endurance of (CoZr)Ge_xO_y-M_xO_y NC devices 64

Fig. 3-19 The data endurance of (NiZr)$Si_xGe_zO_y$-M_xO_y NC devices 65

Fig. 3-20 The gate disturbance of $AuGe_xO_y$-M_xO_y NC devices 66

Fig. 3-21 The gate disturbance of (CoZr)Ge_xO_y-M_xO_y NC devices 66

Fig. 3-22 The gate disturbance of (NiZr)$Si_xGe_zO_y$-M_xO_y NC devices 67

Fig. 3-23 The drain disturbance of $AuGe_xO_y$-M_xO_y NC devices 68

Fig. 3-24 The drain disturbance of (CoZr)Ge_xO_y-M_xO_y NC devices 68

Fig. 3-25 The drain disturbance of (NiZr)$Si_xGe_zO_y$-M_xO_y NC devices 69

Fig. 3-26 The HRTEM image of $AuGe_xO_y$-composite NCs on SiO_2 after the 1050° C 60 sec. ORTA step 70

Fig. 3-27 The HRTEM image of (CoZr)Ge_xO_y-composite NCs on SiO_2 after the 1050° C 60 sec. ORTA step 71

Fig. 3-28 The HRTEM image of (NiZr)$Si_xGe_zO_y$-composite NCs on SiO_2 after the 1050° C 60 sec. ORTA step 72

Chapter 1

Introduction

1-1 Overview of Non-volatile Memory (NVM)

Recent years have been increased attention and demand for portable electronic devices like digital camera, smart cell phone, flash drive disk, and personal digital assistant (PDA) in every field of human's life being given to memory technology as demonstrated in Fig. 1-1. The Semiconductor memory based on the complementary metal-oxide-semiconductor (CMOS) technology has been split into two main categories by whether storage charges in the polysilicon floating gate can be influenced with the power supply or not as illustrated in Fig. 1-2. One is volatile memory, and the other is non-volatile memory (NVM).

Fig. 1-1 The increased demand for portable electronic devices to memory technology

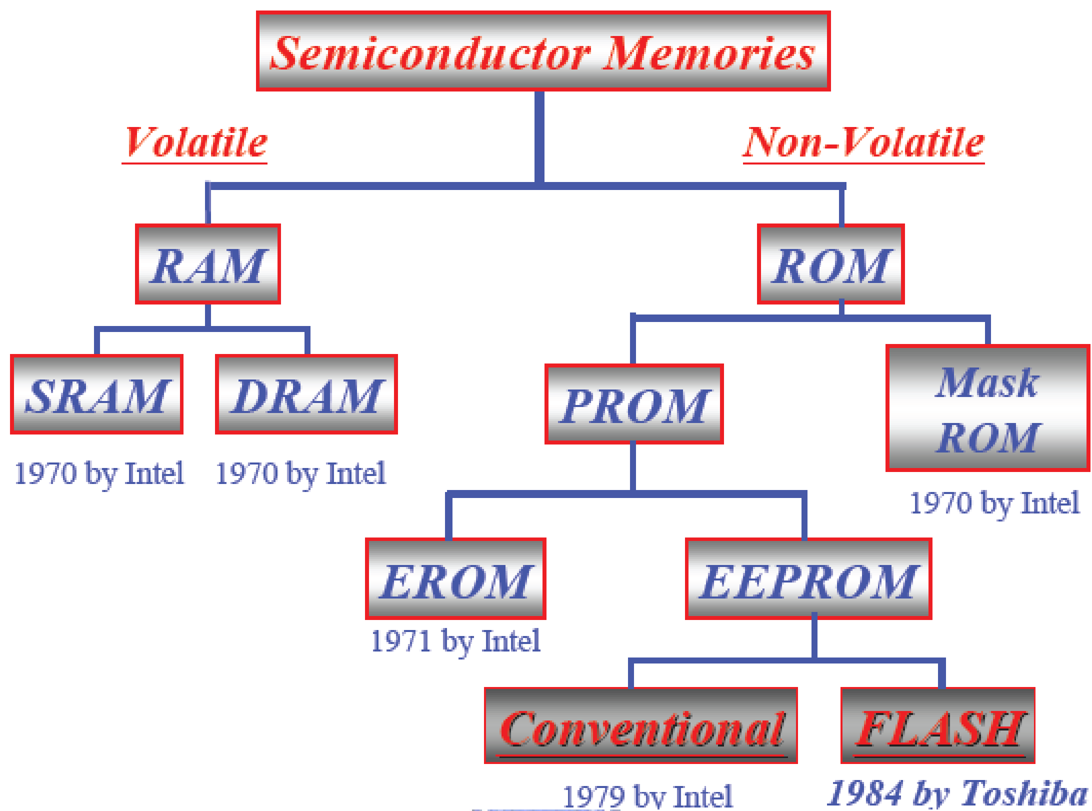

Fig. 1-2 The semiconductor memory tree

Volatile memory such as static random access memory (SRAM) and dynamic random access memory (DRAM) will lose storage charges when the power supply is off; on the other hand, non-volatile memory (NVM), such as electrically programmable read-only memory (EPROM), electrically erasable programmable read-only memory (EEPROM), and Flash memory will keep storage charges even though the power supply is off.

NVM devices have been extensively utilized in integrated circuits (IC) like electrically alterable read-only memory (EAROM), erasable programmable read-only memory (EPROM), electrically erasable programmable read-only memory (EEPROM), and non-volatile random access memory (NVRAM). Flash memory devices exhibit better characteristics on high programming/erasing (P/E) speed, small chip cell area, and low price. Up to now, the most far-flung cross-bar NVM array is

Flash memory. It has the byte-selectable and programmable operation joint with erasable sector size at the same time. The technology of material science nowadays is extremely significant on NVM applications especially in lightness, thinness, shortness, and smallness with portable commercial products.

In 1967, *D. Kahng* and *S. M. Sze* invented the first floating-gate non-volatile memory (FGNVM) at Bell Labs. As indicated in Fig. 1-3, the conventional floating-gate (FG) memory used polysilicon as a charge-trapping layer surrounded by the silicon dioxide (SiO_2) dielectric layer [1]. Fig. 1-4 displays the typical drain current (Id) versus gate voltage (Vg) characterization of a programmed and erased FG memory device for the threshold voltage Vth or V_T shift (△Vth or △V_T) and memory window. The "0" or "1" memory state of FGNVM can be determined by sensing current value in a CMOS device when the control gate, drain, and source electrodes are biased within the memory operation range.

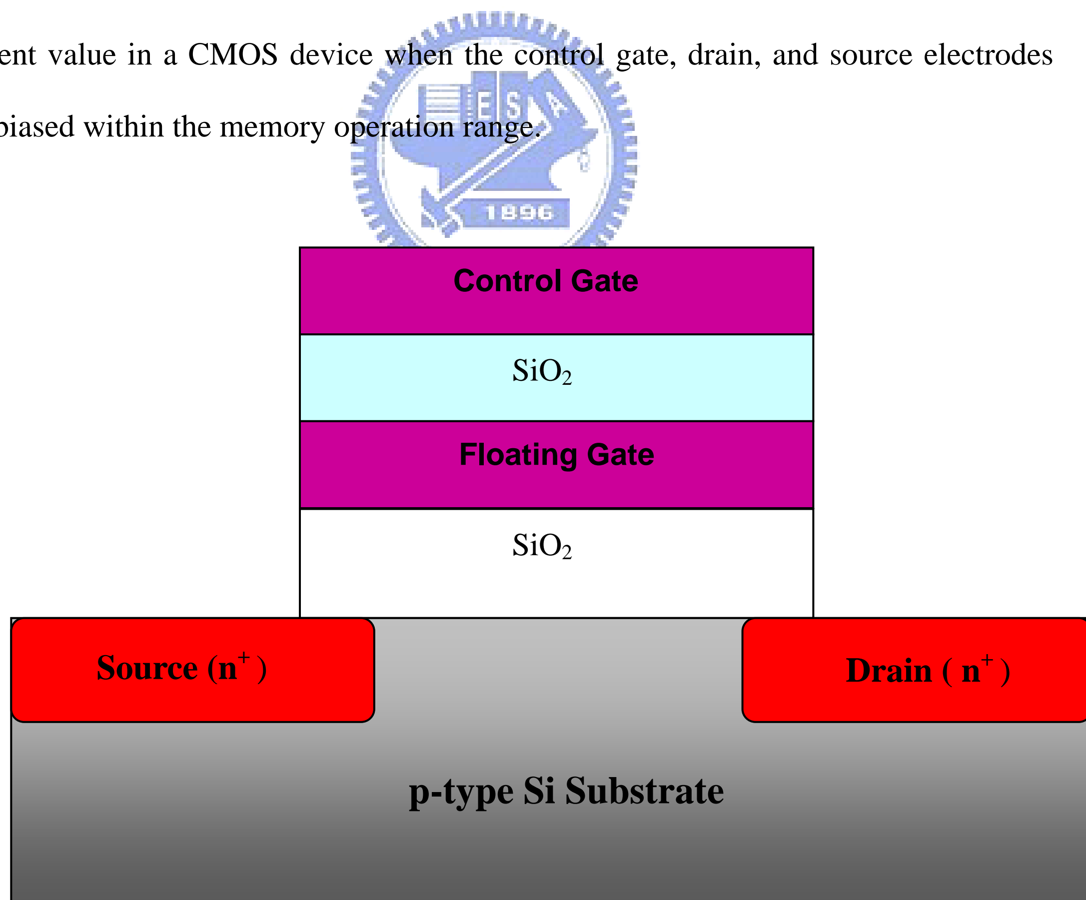

Fig. 1-3 The floating-gate (FG) structure with polysilicon used as the floating gate for data storage

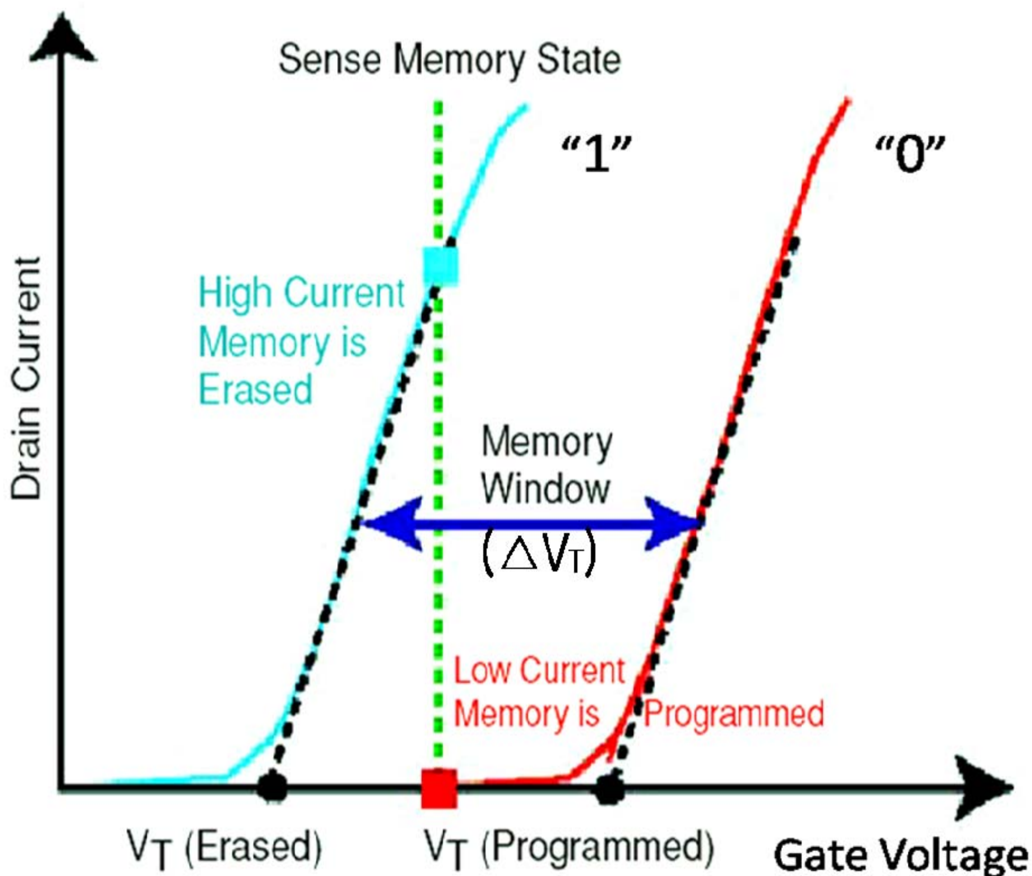

Fig. 1-4 The current vs. voltage characterization of a FG memory device under the programmed and erased states for the △Vth or △V_T and memory window

The well-known commercial Flash memory is Intel EPROM Tunnel Oxide (ETOX) memory structure as presented in Fig. 1-5 [2]. As given in Fig. 1-6, the ETOX is "written" by channel hot electron injection (CHEI) and "erased" by band to band hot hole injection (BTBHHI) or Fowler-Nordheim (FN) tunneling mechanism, respectively [3]. As mentioned above, the operation principles for the Flash memory devices of our experiments are "programmed" by CHEI and "erased" by BTBHHI. The memory storage charges in the floating gate change the threshold voltage (Vth or V_T) of FG transistors by the △Vth or △V_T named memory window between a programmed state and an erased or initial state (Fig. 1-4).

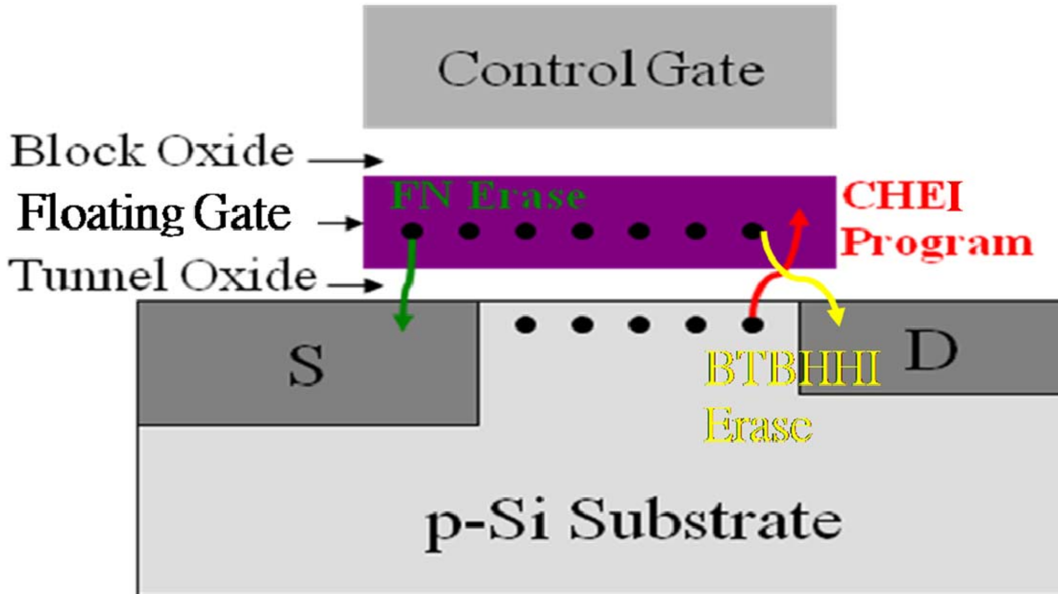

Fig. 1-5 The structure of well-known commercial ETOX Flash memory cell for floating gate

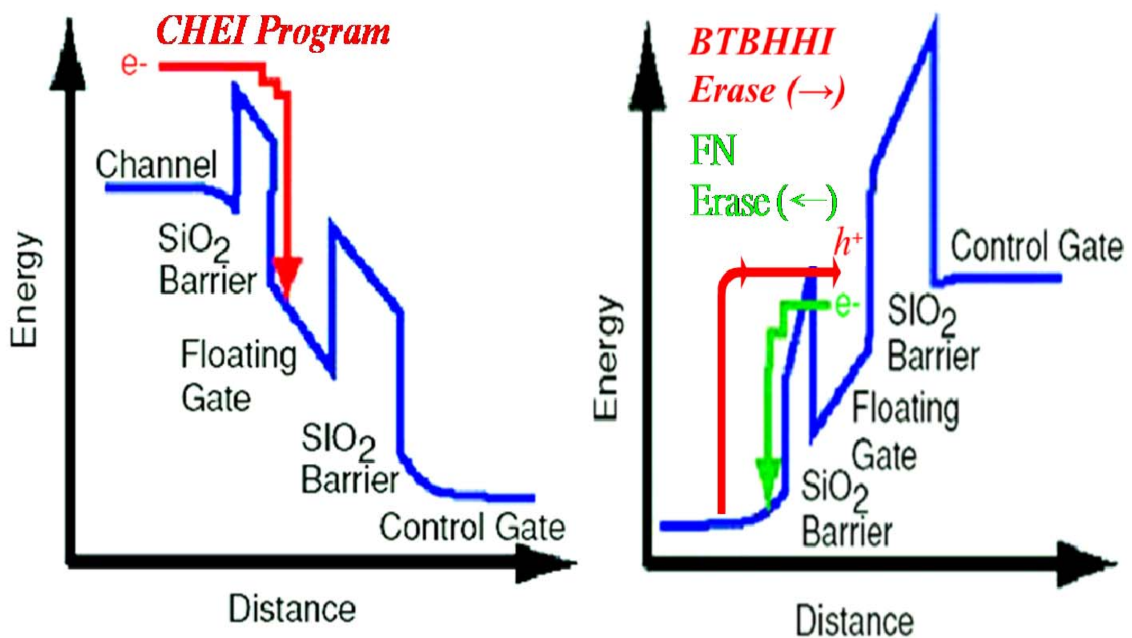

Fig. 1-6 The energy-band diagrams of ETOX Flash memory showing electron and hole injection states with “written” by CHEI and “erased” by BTBHHI or FN tunneling mechanism

The invention of Flash memory is the most revolutionary of all NVSM inventions. Many advantages of Flash memory are what they can be electrically programmed more than 10^6 times, and fabricated with smaller transistor chip cell size [4]-[5]. The Flash memory cell is utilized in FG structure as described in Fig. 1-5.

The FG structure can improve charge density, P/E operation and device reliability for Flash memory applications; however, it has several disadvantages. First, not only does it need a thick tunnel oxide layer about 10-15 nm to keep long retention and endurance time, but it causes higher power consumption, slower P/E speed, and poor scalability. Next, since the polysilicon floating gate is conductivity and hence storage charges in it to leak easily along the path through oxide bulk defects during P/E cycles [6].

With the non-volatile semiconductor memory (NVSM) technology scaling down to nano-structured features, the oxide quality of an ultra-thin isolated film needs to be enhanced. For this scaling limitation of the FGNVM structure, the polysilicon-oxide-nitride-oxide-silicon (SONOS) Flash memory structure is recommended that we resolve this issue with a device scaling down. SONOS memory has longer data retention because of its storage charges trapped in discrete traps diversely than FGNVM when a FG bitcell's tunnel oxide thickness is less than 10 nm. Thus, a single oxide defect in the tunnel oxide layer will not affect the discharge of the memory chip cell [6].

Fig. 1-7 depicts the conventional SONOS memory structure. The charge-trapping layer of a customary SONOS memory device is silicon nitride (Si_3N_4), and energy-band diagram is shown in Fig. 1-8. The conduction band offset between silicon substrate and Si_3N_4 is 2.05 eV. When a positive voltage is supplied to the control gate, the energy band will bend down as revealed in Fig. 1-9. The conduction band electrons trapped in the charge-trapping layer in p-type silicon substrate are

partially a result of penetrating through the tunnel oxide and Si_3N_4 layer. As electrons early trapped in Si_3N_4, parts of the Si_3N_4 material must be tunneled; for this reason, the SONOS memory P/E speed has been declined. In addition to all of the above, the conduction band offset between Si_3N_4 and SiO_2 is not large, and trapped electrons may also penetrate back. In the next generation NVM technology, the SONOS Flash memory has attracted a lot of attention for applications with portable electronic products [7].

According to the International Technology Roadmap for Semiconductors (ITRS) roadmap as listed in Tab. 1-1, high-k dielectric materials would be capable of maintaining a parallel potential difference between the FG structure and the device itself for a larger thickness in comparison with SiO_2 [8]. The problems of charge leakage and scale limit in the charge-trapping layer would be resolved. Today, high dielectric constant materials may be the good substitutes for nitride-based ones as the charge-trapping layer on SONOS memory.

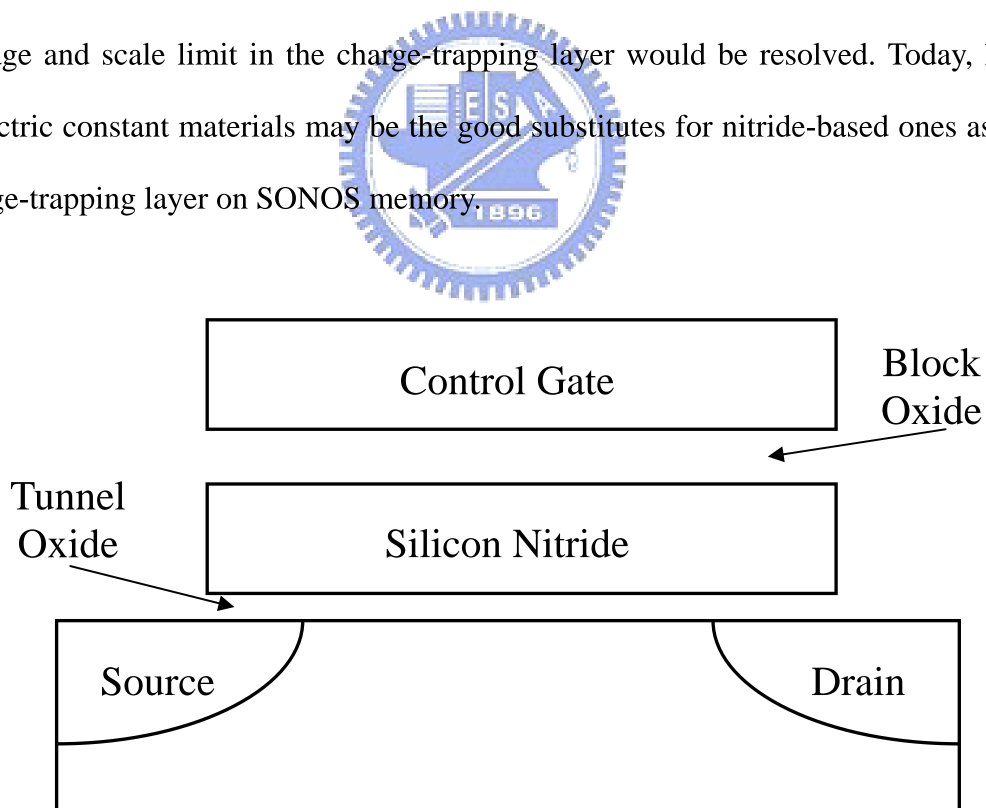

Fig. 1-7 The conventional SONOS memory structure, silicon nitride (Si_3N_4) as the charge-trapping layer

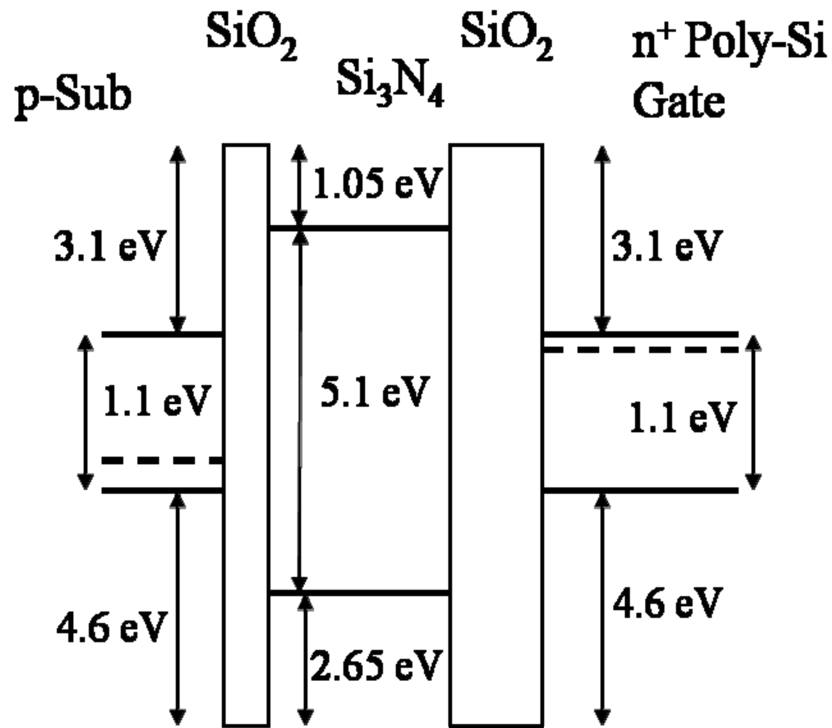

Fig. 1-8 The energy-band diagram of nitride-based SONOS memory

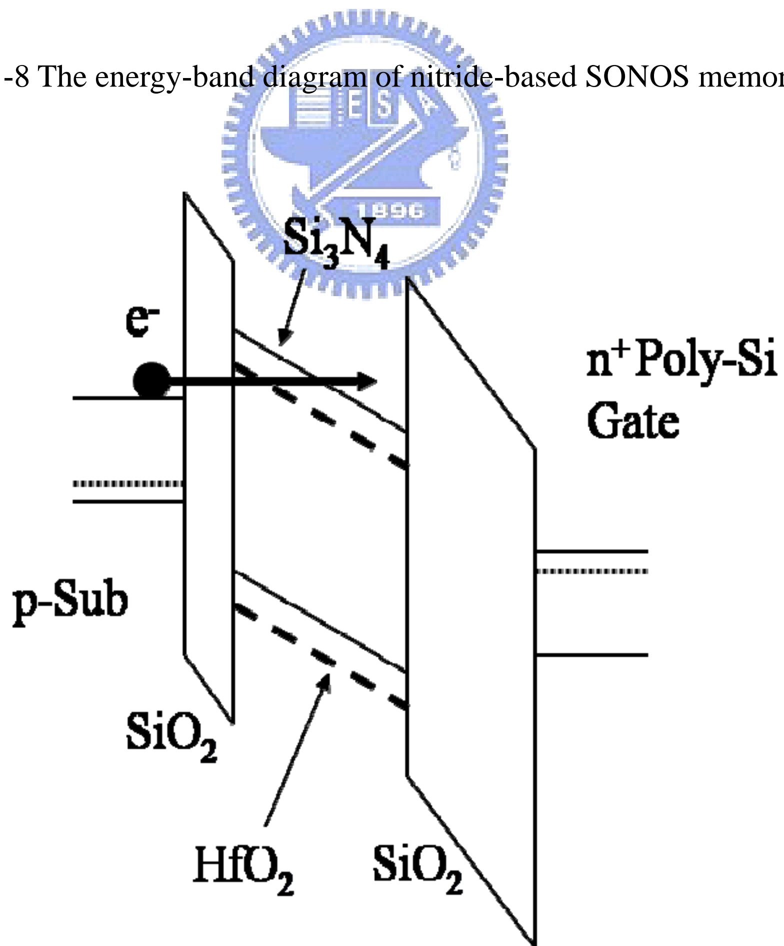

Fig. 1-9 The band diagram comparison of SONOS memory of Si_3N_4 and HfO_2 materials when programming (solid line as Si_3N_4, dash line as HfO_2)

Tab. 1-1 The next generation trend on NVM technology for the ITRS update list

The ITRS - red lights ahead for memory!

International Technology Roadmap for Semiconductors 2000 Update

Year	2002	2003	2004	2005	2008	2011	2014
Half-pitch (nm)	130	120	110/90	100	70/60	50/40	35/30
Min Vdd (V)	1.2	1.2	0.9	0.9	0.6	0.5	0.3
DRAM cell (um2)	0.1	0.08	0.07	0.044	0.018	0.008	0.003
DRAM ret. (msec)	250	250	250	500	500	500	500
NVM ret. (yrs)	10	10	10	10	10	10	0.1
Endur. (cycles)	100k	100k	100k	100k	100k	1M	1M
Cost/bit (uc)	17	11	8	5.3	1.9	0.6	0.2

We know how to do this

We pretty-much know how to do this

We really don't know how to do this

Besides, applying high-k dielectrics for the trapping layer has many advantages. The following are examples of high P/E speed, low power dissipation, simple process execution, and great potential development for scalability under the 65 nm node technology. In accordance with the ITRS roadmap, high dielectric constant materials should be advised to take the place of Si_3N_4 of SONOS memory. High-k dielectric materials are expected to have better charge-trapping characteristics than the traditional Si_3N_4 film in performing long charge retention by the defect trap density and deep level states [9]-[11].

By using discrete nanocrystals (NCs) as the charge storage medium, the nanocrystal (NC) Flash memory is more immune to local oxide defects. It is considered to be more beneficial in many aspects: more charge-trapping sites, larger $\triangle$Vth or $\triangle V_T$ window, longer retention time, and better endurance cycles. Unlike the volume-distributed charge trap, NCs could be uniformly deposited as

two-dimensional (2D) distribution on the thin tunnel oxide layer. As demonstrated in Fig. 1-10, NCs could keep the charge locally because of the well isolation of NCs apart from each other and mainly materialization of good conductive paths between the close nodes. Generally, the NCs are separately nano-scaled agglomerations of a variety of metal oxide (M_xO_y) atoms with sizes of 5 to 10 nm in diameter.

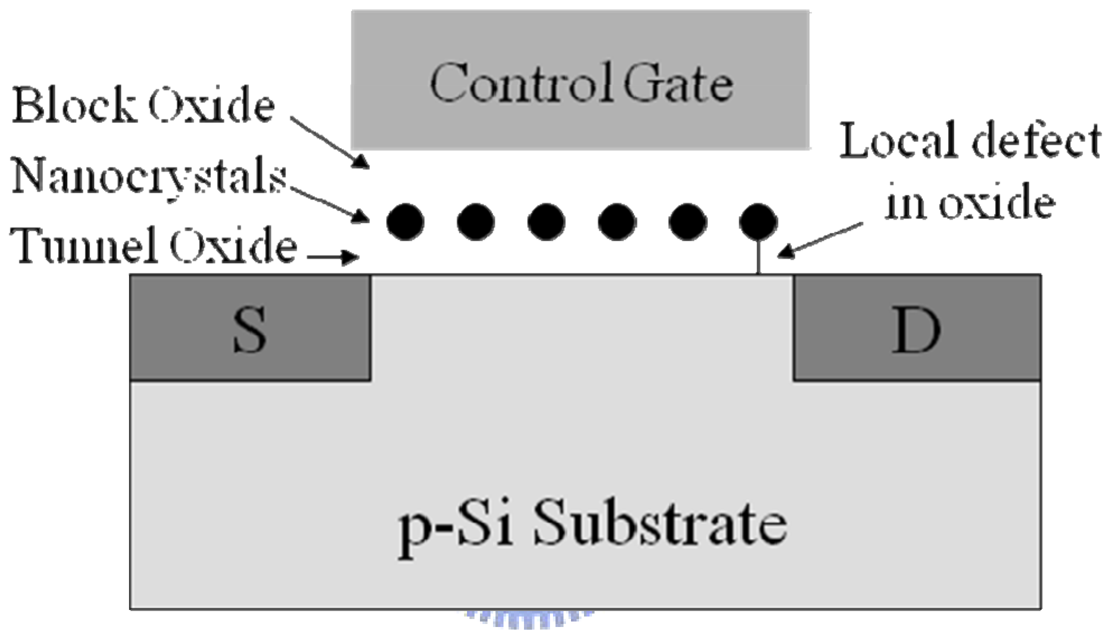

Schematic Diagram of Nano-Crystal memory

Fig. 1-10 The nanocrystal (NC) charge storage distribution structure for the Flash memory cell

The advantages of high-k dielectrics are more trapping centers than Si_3N_4 material and smaller barrier height between silicon substrate and the high-k charge-trapping layer. More trapping centers could have larger △Vth or $\triangle V_T$ window. Smaller barrier height can provide faster speed than it of Si_3N_4 under the same stress condition. For high-k dielectric materials, when programming, the trapped electrons will tunnel shorter distance in the high-k dielectric than in Si_3N_4 (Fig. 1-9).

This result leads to higher P/E speed. Thence, utilizing high-k materials as the charge-trapping layer has great benefits on SONOS Flash memory. The electron trap level of ZrO_2 with 1.0 eV or HfO_2 with 1.5 eV is deeper than Si_3N_4 with 0.8 eV [12]-[13]. It is satisfying to choose high-k materials with small barrier height on silicon substrate for achieving high P/E speed, long data retention/endurance, and little noise disturbance due to deep trapping level. Contrary to the nitride-based SONOS memory, high-k materials have large dielectric constant, high trapping density, wide bandgap, and adequate solutions to Flash memory [14]-[16].

1-2 Motivation

In this thesis, we have designed the greatly characteristic NVSM with a M_xO_y NC charge-trapping layer [17]. This NC charge-trapping layer has taken place of the Si_3N_4 layer in SONOS memory. Prominently features of a lot of M_xO_y NC materials in the Flash memory devices were also presented for low stress operation. This NC Flash memory structure had good characteristics in terms of so large memory window, high P/E speed, long retention time, good data endurance, little gate/drain (G/D) disturbance, and so forth.

The high-k dielectric materials like HfO_2 and ZrO_2 are used to deposit the charge-trapping layer. These materials provide several deep trapping sites. As a result, they can improve charge retention of the FGNVM structure. The charge-trapping efficiency can be enhanced, and relative memory window can be enlarged. With numerous applications of high-k materials, we made good use of various M_xO_y NC approaches as a charge-trapping layer formation for the NC Flash memory devices having lower power consumption, larger memory status, longer data storage time, and less G/D disturbance.

1-3 Thesis Organization

The thesis includes four chapters. In this thesis, we study the NC Flash memory performance with synthesizing high dielectric constant materials and M_xO_y mixtures as a charge-trapping layer deposited by the Sol-Gel spin coating method.

In the chapter 1, we introduced the overview of NVM and Flash memory. Furthermore, we pointed out that charge-trapping materials greatly influenced how the memory trapping functions operate on Flash memory versus SONOS structure.

In the chapter 2, the NC Flash memory process and Sol-Gel technique with five chemical metal chloride (M_xCl_y) precursors were mentioned. We also fabricated the NC Flash memory devices in this section. These experimental memory devices contained the thin film of M_xO_y mixtures or NCs as the charge-trapping layer by the Sol-Gel spin coating procedure from isopropanol (IPA) solvent. The electrical properties such as Id-Vg transfer curves, P/E speed, G/D disturbance, and data storage retention/endurance were measured to obtain the device performance; moreover, the high-resolution transmission microscopy (HRTEM) instrument was conducted to research the physical properties of binary or ternary M_xO_y NCs as well. From the HRTEM images, each trapping layer of the devices truly was shaped into nano-sized round balls or oval-shaped NCs or a composite thin film after the 1050° C 60 sec. oxide rapid thermal annealing (ORTA) step in the O_2 environment.

In the chapter 3, we utilized the Sol-Gel spin coating method with six chemical M_xCl_y precursors to deposit the NCs consisting of several chemical compounds from ethanol (C_2H_5OH) solvent for the NC Flash memory devices, and the HRTEM instrument was set up to research the prominently nano-structured features. In addition to the physical analysis of the M_xO_y thin film and NCs, the NC Flash memory electrical properties were also measured.

At the end of this thesis, the conclusions and recommendations for future research were given in the chapter 4.

Chapter 2
Electrical and Physical Properties of Metal Oxide Nanocrystal Flash Memory Devices by the Sol-Gel Spin Coating Method with IPA Solvent

2-1 Introduction

The conventional SONOS flash memory utilizes Si_3N_4 as a charge storage layer. The Si_3N_4 dielectric constant is 7.5 eV and 2.05 eV barrier height (BH) versus silicon. The electron trap level of Si_3N_4 is 0.8 eV below the nitride conduction band [1]-[2]. The SONOS memory has better charge retention storage than FG memory because of its discrete trap centers diversely with the tunnel oxide thickness less than 10 nm, but one issue of some challenging tasks for SONOS structure is programming speed. The band diagram of ZrO_2 dielectric SONOS-type memory is illustrated in Fig 2-1.

Fig 2-2 indicates the conduction band offset with 1.05eV between SiN and SiO_2. The comparison of Si_3N_4 and HfO_2 high-k material is also displayed in Fig. 2-3. When a positive voltage is applied, silicon substrate electrons need to tunnel a long path of Si_3N_4 to be trapped in the charge-trapping layer for small conduction band offset [3]. Another issue of Si_3N_4 is 1.05 eV conduction band offset between nitride and tunnel oxide. Data retention loss is due to the trapped electron or hole charges easily thermally de-trapped from this shallow well. With the reasons of small BH to silicon and large conduction band offset to SiO_2, high-k materials such as ZrO_2 and HfO_2 are required to perform high P/E speed, long retention/endurance storage, and little G/D disturbance characteristics for the Flash memory charge-trapping storage layer.

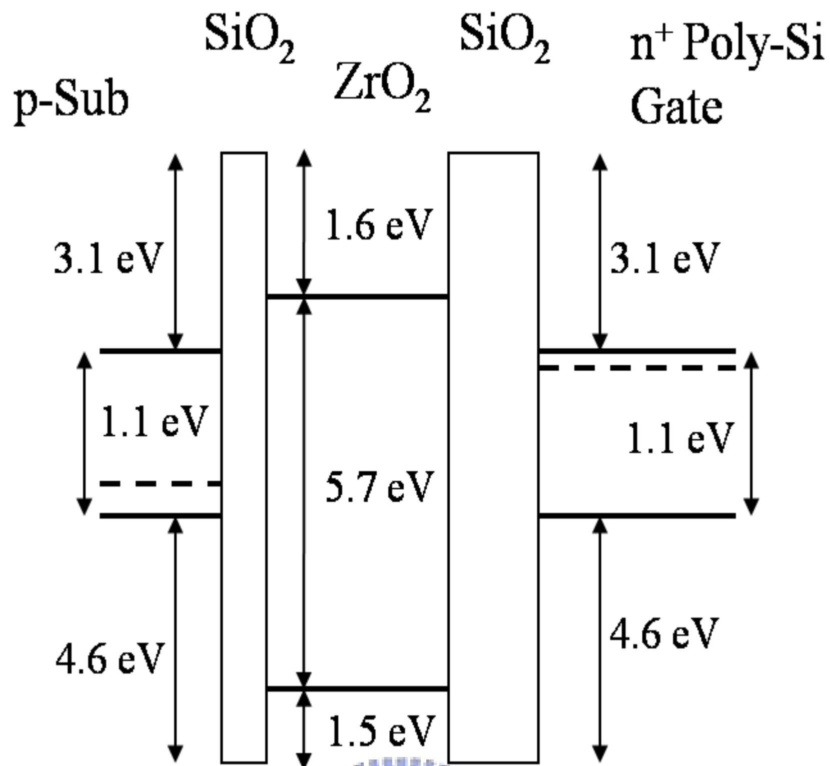

Fig. 2-1 The band diagram of ZrO_2 dielectric SONOS-type memory

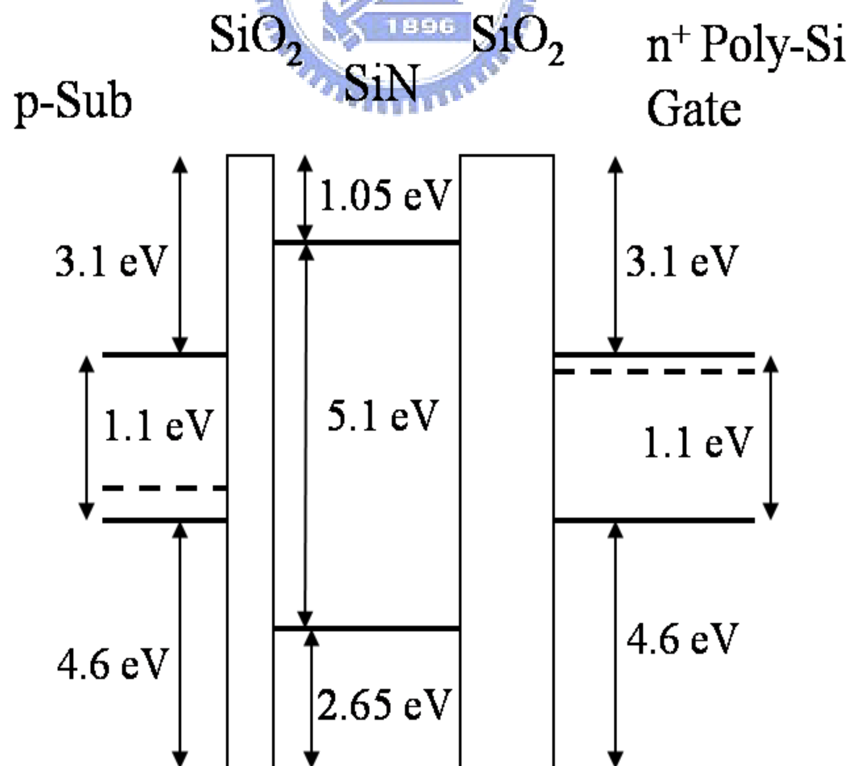

Fig. 2-2 The band diagram of nitride-based SONOS memory

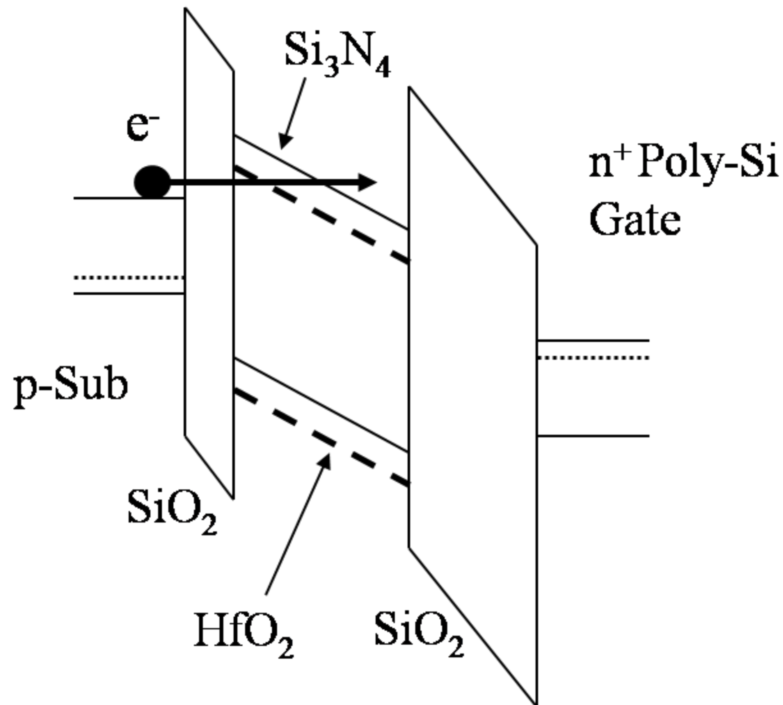

Fig. 2-3 The energy-band diagram comparison of SONOS memory of Si_3N_4 and HfO_2 materials when programming (solid line as Si_3N_4, dash line as HfO_2)

Nowadays the NC Flash memory can tightly keep the trapped electrons or holes to avoid the loss and degradation of charges for data retention time. Contrary to SONOS memory, NC Flash memory is considered to be more advantageous in lots of aspects: low power dissipation, high P/E speed, little disturbance, and so on. The high-k materials have smaller BH to silicon substrate and larger conduction band offset to tunnel oxide than nitride-based ones, so they are adequate to form the thin film of M_xO_y mixtures or NCs for the NC Flash memory trapping layer application [4]-[5].

In this chapter, we presented Sol-Gel technique as a way to deposit high-k dielectrics and M_xO_y materials for the charge-trapping layer in the NC Flash memory devices. We gradually fabricated the NC Flash memory devices and made good use of Sol-Gel technique with five metal chlorides as precursors to deposit the NCs consisting of several chemical compounds. These precursors of distinct M_xCl_y powder were mixed and dissolved into IPA, deposited on the tunnel oxide layer by the Sol-Gel spin

coating procedure, and then with the 1050° C 60 sec. ORTA step to form various kinds of the M_xO_y thin film or NCs as the charge-trapping layer of Flash memory devices, respectively.

Contrary to high vacuum compatible equipments, many advantages of the Sol-Gel spin coating method are cheaper, more convenient, and easier to synthesize the combination of binary or ternary M_xO_y NCs in the normal pressure environment. We analyzed the electrical properties in Id-Vg transfer curves, P/E speed, data retention/endurance, and G/D disturbance; moreover, the physical properties of Sol-Gel derived M_xO_y NCs for discretely charge-trapping centers of the NC Flash memory devices were measured in the HRTEM instrument as well [6]-[7].

2-2 The Sol-Gel Technique

The Sol is a colloidal suspension of solid particles with sizes of 100 nm to 1 μm in diameter in a liquid phase, in which the dispersed particles are small enough to remain suspended by Brownian motion; the Gel is a solid material network containing a liquid component, both of which are in a highly dispersed state [8]. The Sol-Gel coating procedure usually consists of four steps. Firstly, the desired colloidal particles once dispersed in a liquid to form the Sol. Secondly, the deposition of Sol solution makes the coating on the silicon substrate by spraying, dipping or spinning. Thirdly, the particles in Sol are polymerized through the removal of the stabilizing components and make the Gel in a state of a continuous network. Ultimately, the eventual heat treatments pyrolyze the remaining organic or inorganic components molded into the amorphous, polycrystalline, or crystalline material coating [9]-[11].

The spin coating method given in Fig. 2-4 has been applied to the fabrication of the inorganic and organic hybrid materials for specific applications. Liquid state

process enables the molecular scale mixing of precursors, leading to homogeneous, multi-component materials. The most interesting feature of Sol-Gel procedure is capability to synthesize a new type of materials called inorganic-organic hybrids; organic materials can be doped into the Sol-Gel matrix as well. In these types of materials, polymeric or monomeric molecules exist as a separate functional phase or molecule in an inorganic or inorganic-organic hybrid matrix. Furthermore, M_xO_y materials with various phases can also be derived from the Sol-Gel coating method in general applicability to much specific utilization [12]-[14].

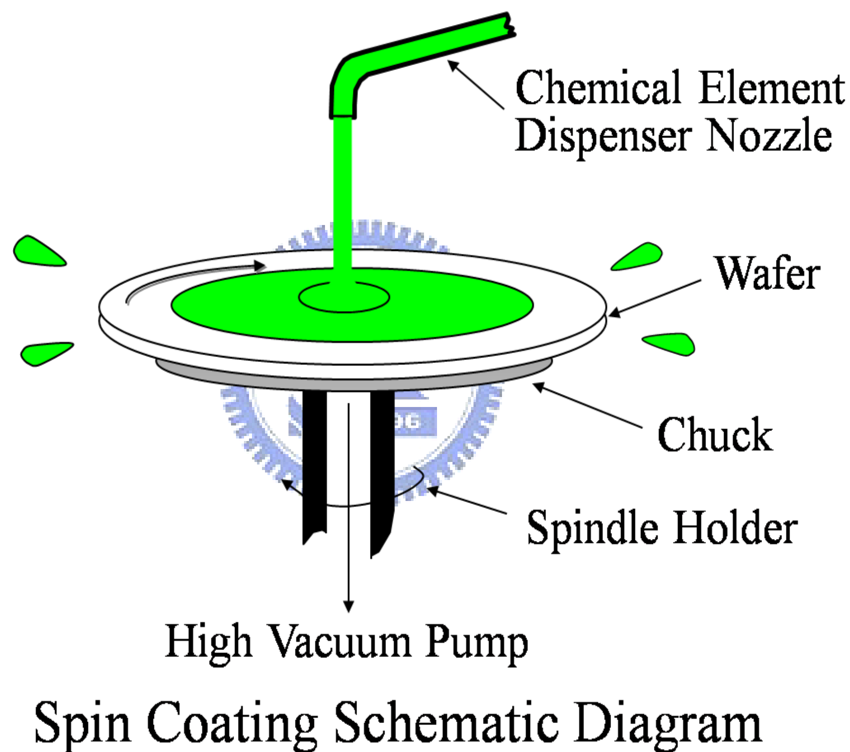

Fig. 2-4 The diagram of the spin coating method with controllable spin motor

The Sol-Gel spin coating advantages are as follows: producing thin bond-coating to make excellent adhesion between the metallic substrate and the top coating, thick coating to obtain corrosion protection performance, easily shaping materials into complex geometries in the Gel state, high purity products, and the highly controllable composition; in addition, Sol-Gel technique has low working temperature with much

wider range from 200° C to 600° C and provides efficiently high quality coatings. If the metal precursor is tethered to the Gel network during Sol-Gel procedure, it allows the non-agglomerated M_xO_y or metal nanoparticles (NPs) preparation for specifically narrow particle size distributions and adjustable metal loading [15].

Fig. 2-5 describes the Sol-Gel method and its relative product applications. These Sol-Gel ceramic fibers are commonly used as optical fiber cores. The majority of fiber cores are easily coated with a Sol-Gel thin film in which there are dopants. For the thin film area of Sol-Gel technique, dense films are produced by coating a substrate material with the Sol and letting it Gel. This result leads to the densely thin-film thickness on the silicon substrate having a lot of uses like catalysts, chemical sensor, electro-optical coupling transmitters, and nano-electronic devices in the material science and engineering field [16].

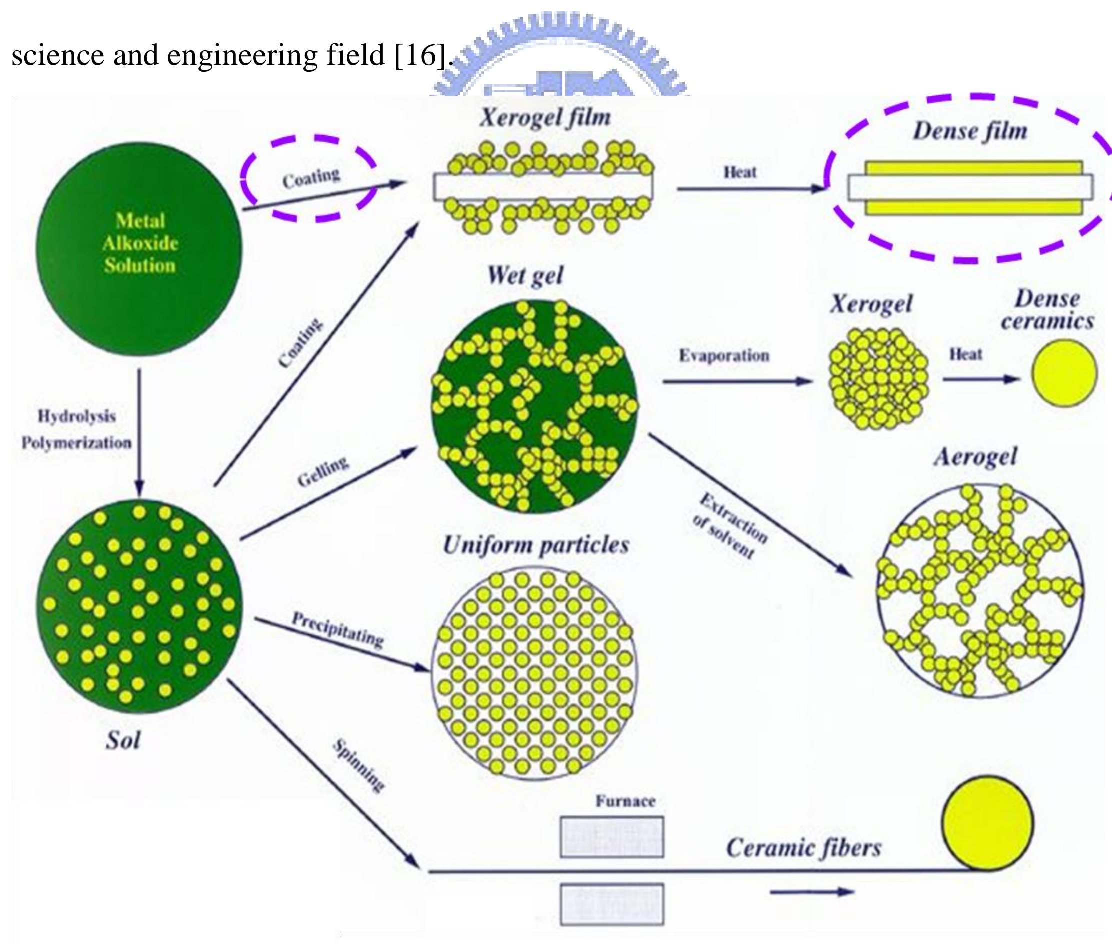

Fig. 2-5 Three main product applications of the Sol-Gel method (dash line as the step-by-step coating procedures of our experiments)

2-3 Experiments

First, ($CoCl_2 \cdot 6H_2O$), $GeCl_4$, $LiClO_4$, $SiCl_4$, and $ZrCl_4$ metal chlorides were used as chemical precursors for the synthesis of M_xO_y NC materials. A mother Sol solution was mixed and dissolved into IPA with vigorous stirring for about 1 hour. Next, the Sol solution was obtained by entirely hydrolyzing metal chlorides with the stoichiometric amount of water in IPA to yield a 1:1000 molar ratio mixture of metal (M_x) : IPA.

The NC Flash memory fabrication of the Sol-Gel spin coating was begun with LOCOS (Local Oxidation of Silicon) isolation process on p-type (100) 150-mm silicon substrate wafers. Then, a 10 nm dry oxide thin film for tunnel oxide was thermally grown at 900° C by vertical furnace oxidation. The chemical solution of a 1:1000 molar ratio mixture of M_x : IPA was deposited on the tunnel oxide layer with the Sol-Gel procedure by spin coater at 3000 rpm for 60 sec. at room temperature (25° C); the as-deposited thin film was followed with the 1050° C 60 sec. ORTA step in the O_2 environment to form various kinds of the M_xO_y thin film or NCs as the charge-trapping layer of the Flash memory devices. The 30-nm-thin block oxide film was coated by the high density plasma enhanced chemical vapor deposition (HDPCVD) process in N_2 densification, and followed with a 200-nm-thick polysilicon gate layer on block oxide.

After polysilicon-gate deposition, the followed steps were polysilicon-gate electrode patterning, source/drain (S/D) extension implanted by the low dose of 2E14 cm^{-2} arsenic (As) at 10 keV ion energy, sidewall spacer formation, gate/source/drain (G/S/D) ion implantation with the high dose of 5E15 cm^{-2} As at 20 keV energy, silicon substrate contact patterning and ion implantation by the high dose of 5E15 cm^{-2} boron fluoride (BF_2) at 40 keV energy, S/D dopant activation at 1050° C, oxide passivation layer deposition by the HDPCVD process, contact hole openings, and metal pads; the rest of the standard MOS manufacturing processes were finished to fabricate the NC

Flash memory devices later.

The flow chart and process flow of the proposed NC Flash memory devices are depicted in Fig. 2-6 and Fig. 2-7.

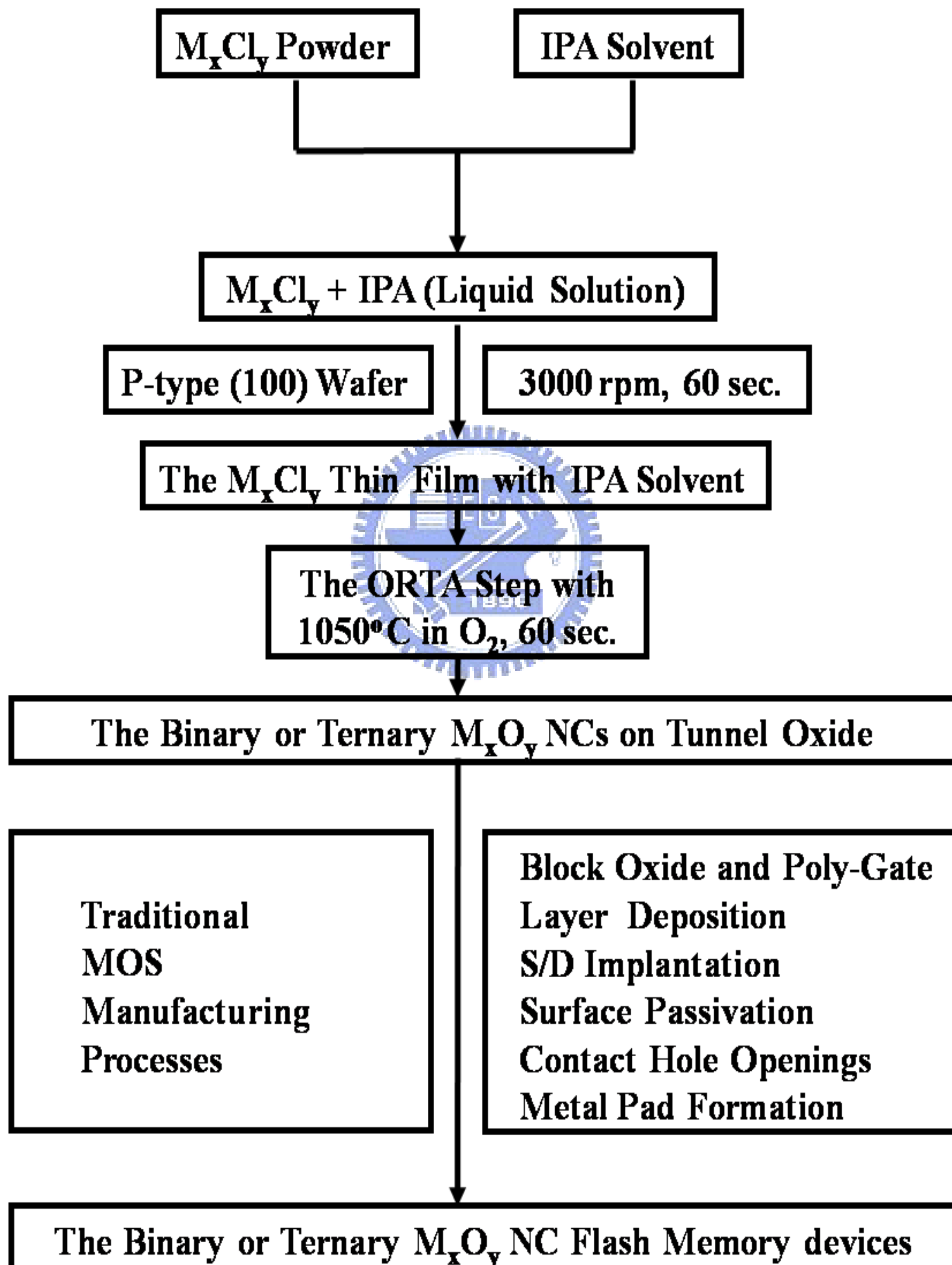

Fig. 2-6 The flow chart of IPA Sol-Gel derived Flash memory devices

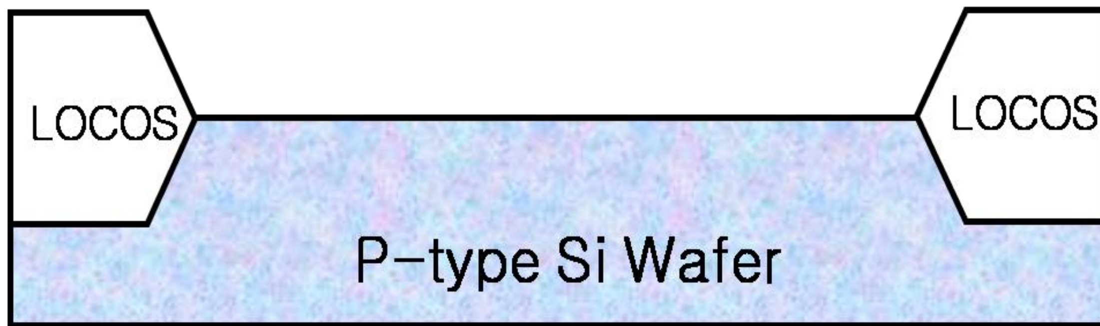

(a) LOCOS isolation process on the p-type (100) 150-mm silicon substrate

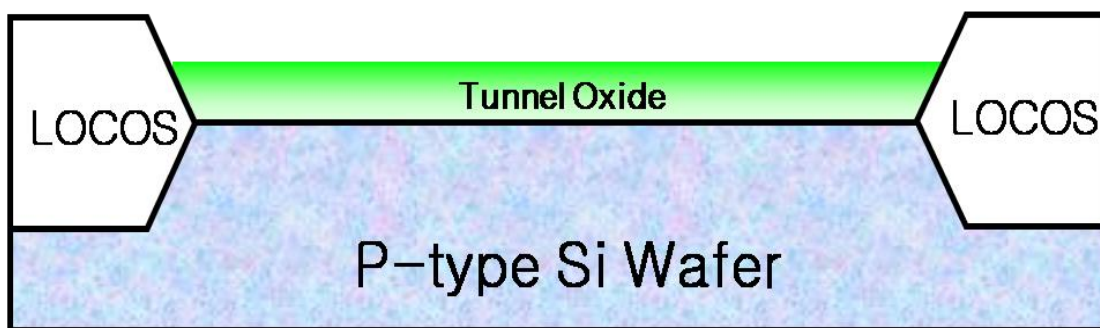

(b) The thin film for tunnel oxide thermally grown at 900° C dry oxidation

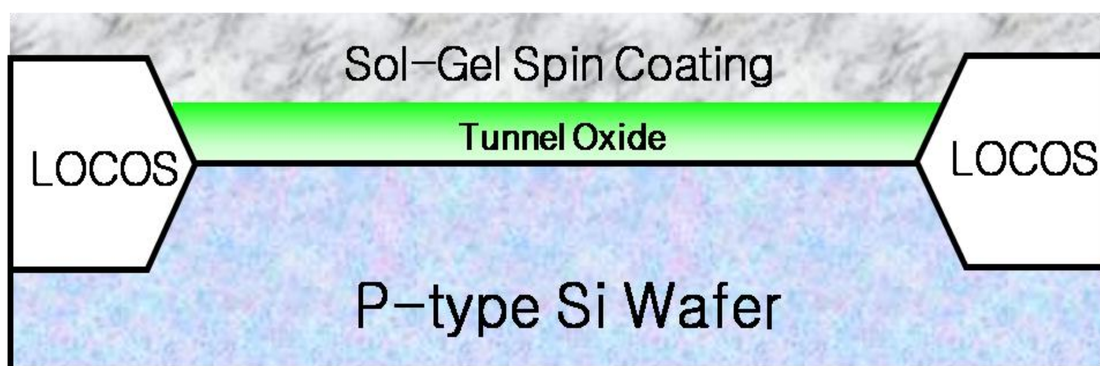

(c) The deposited chemical solution by the Sol-Gel spin coating at 3000 rpm for 60 sec. at room temperature

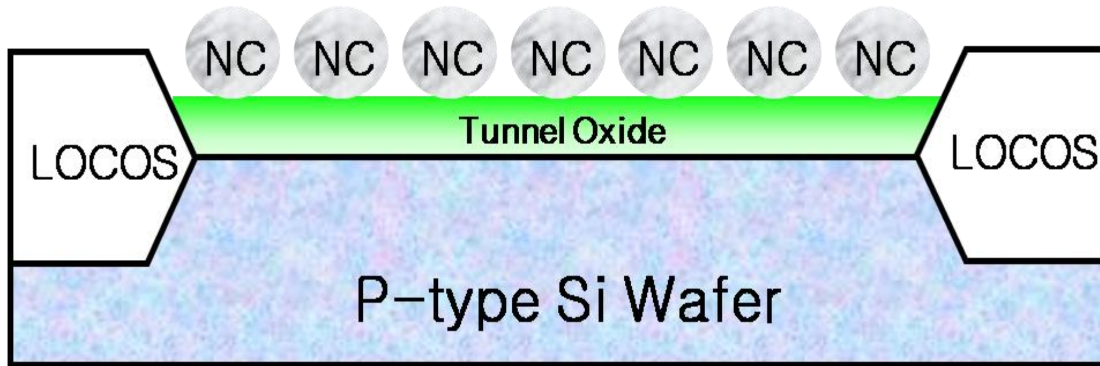

(d) The formation of M_xO_y thin film or NCs with the 1050° C 60 sec. ORTA step

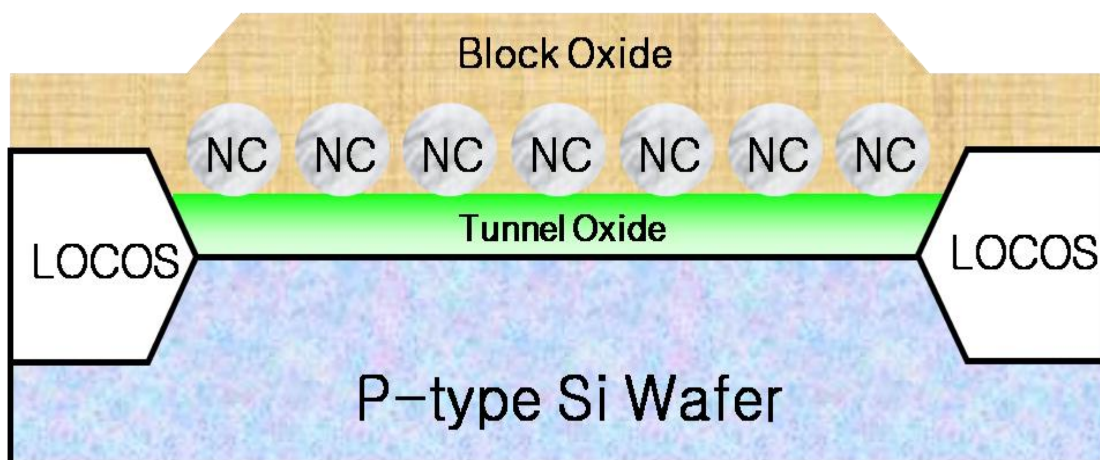

(e) The 30-nm-thin block oxide film coated by the HDPCVD process in N_2 densification

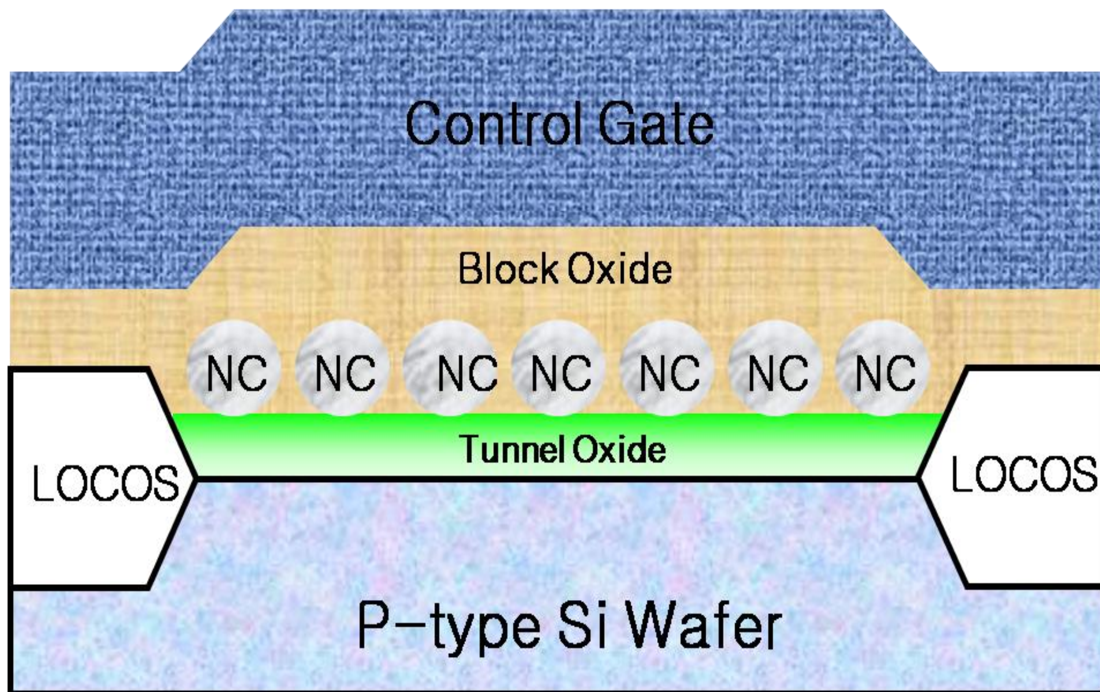

(f) The 200-nm-thick polysilicon control gate layer deposited on the block oxide layer

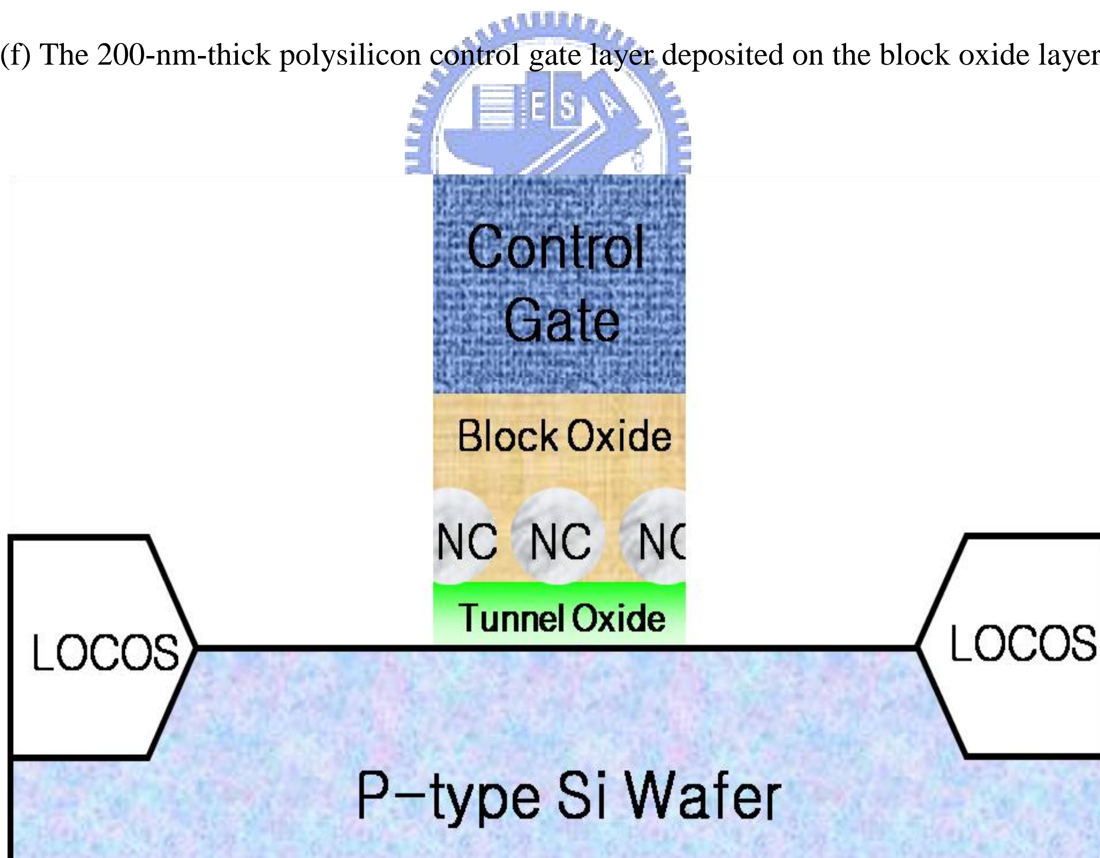

(g) The polysilicon-gate electrode patterning

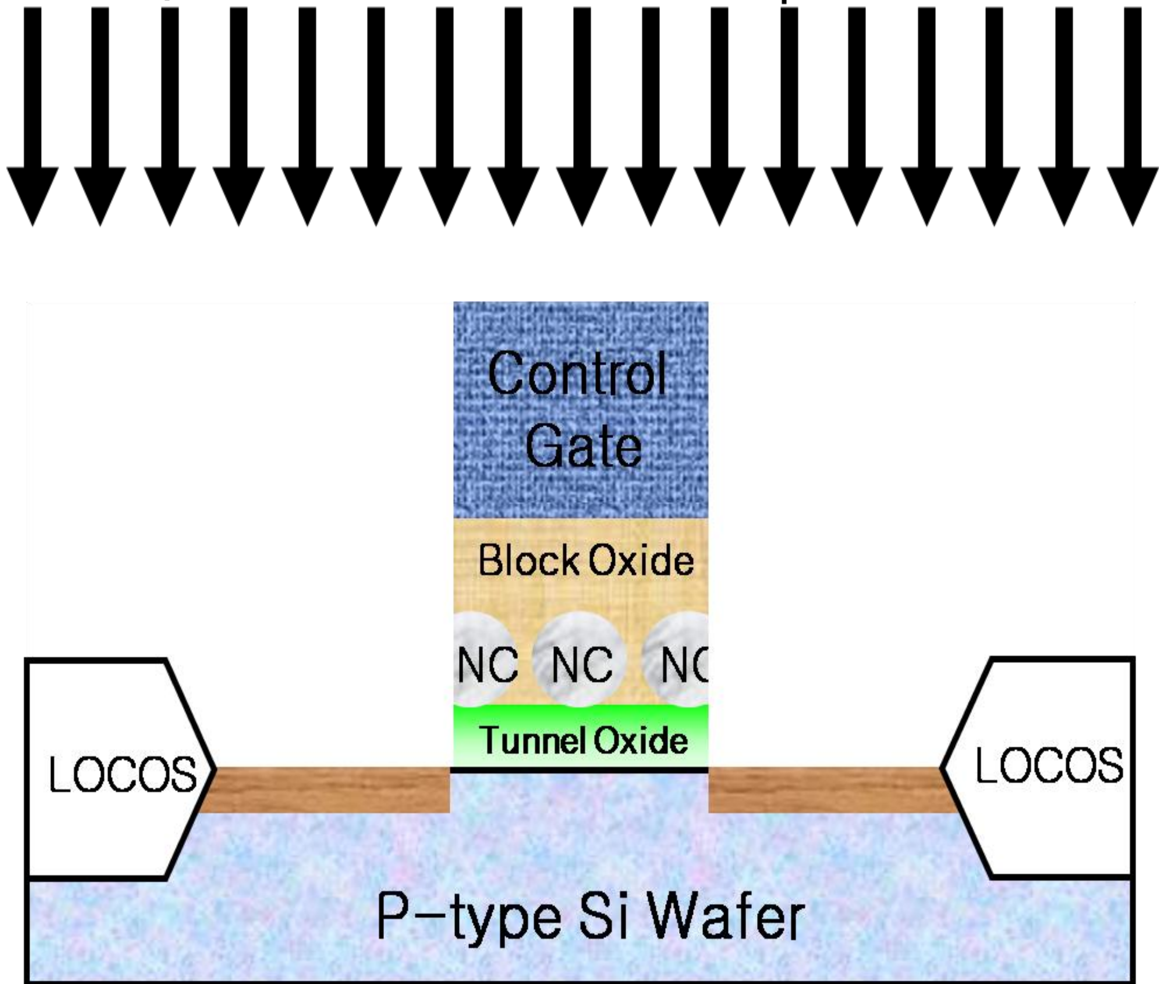

(h) The gate and S/D extension implanted by the low dose of 2E14 cm^{-2} As at 10 keV ion energy

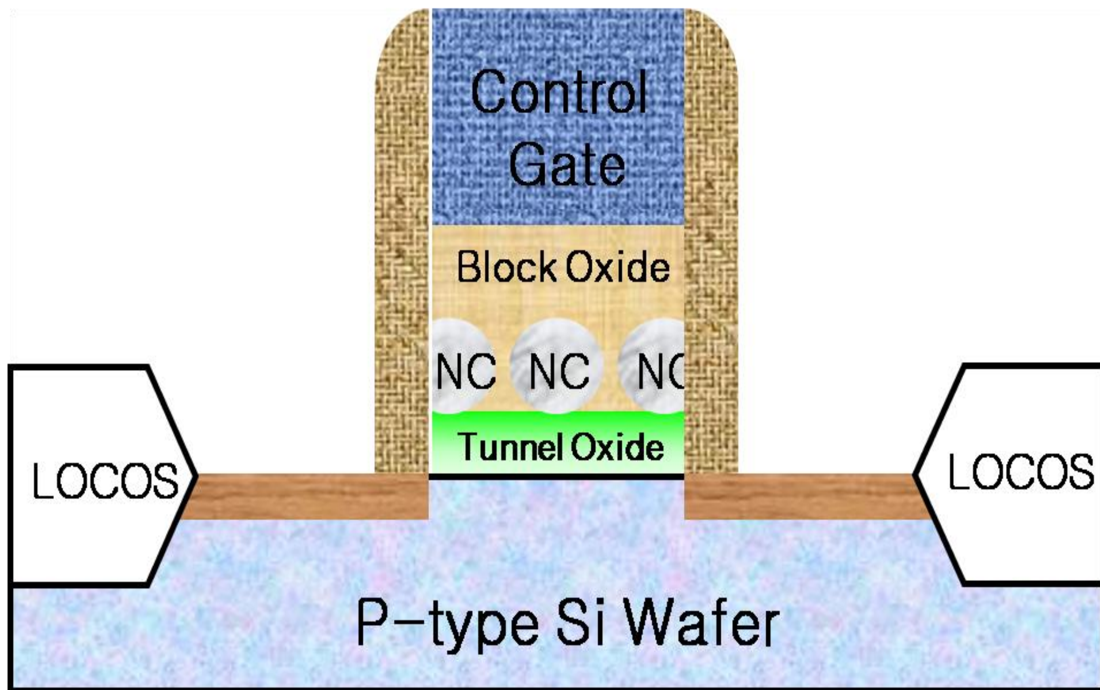

(i) The oxide sidewall spacer formation

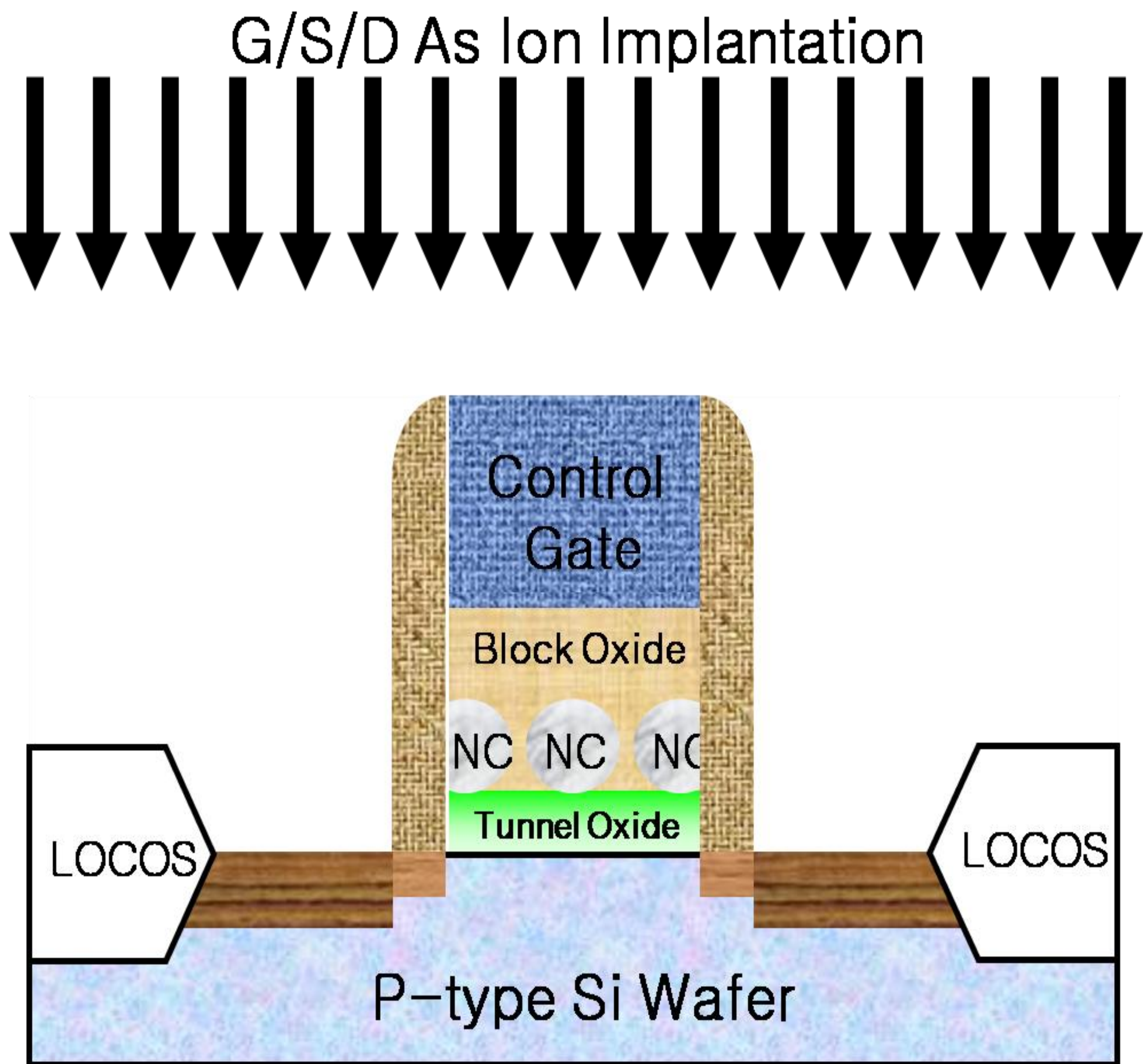

(j) G/S/D ion implantation with the high dose of 5E15 cm^{-2} As at 20 keV energy

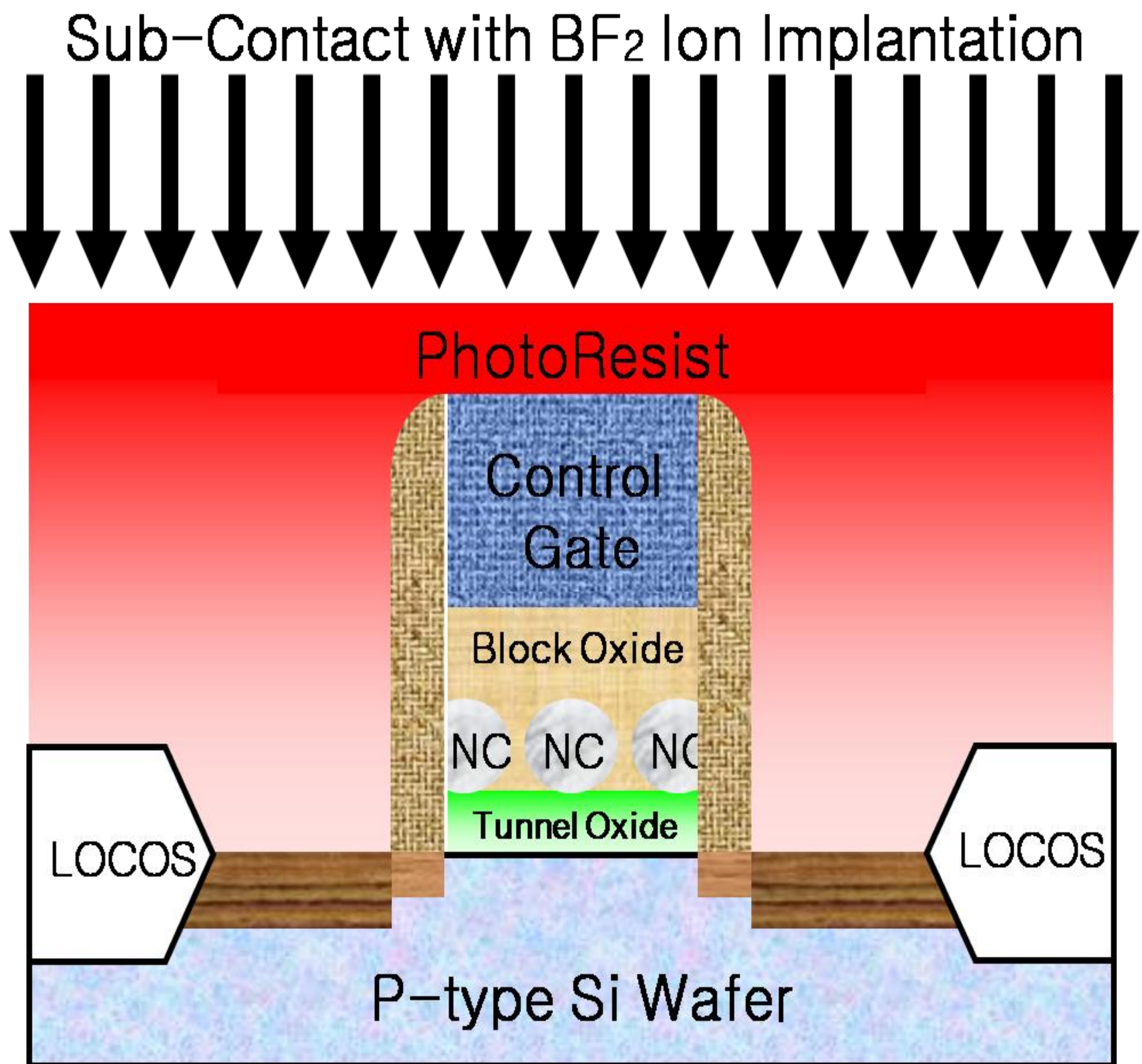

(k) Silicon substrate contact patterning and ion implantation by the high dose BF_2 ions at 40 keV energy

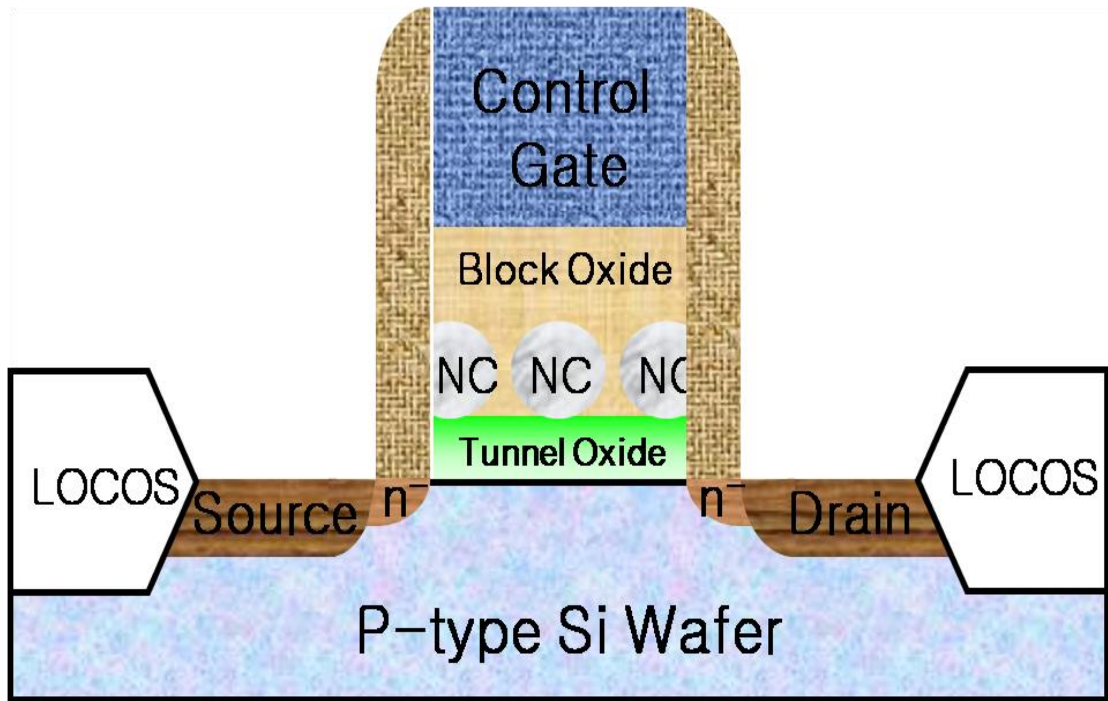

(l) S/D dopant activation at 1050° C

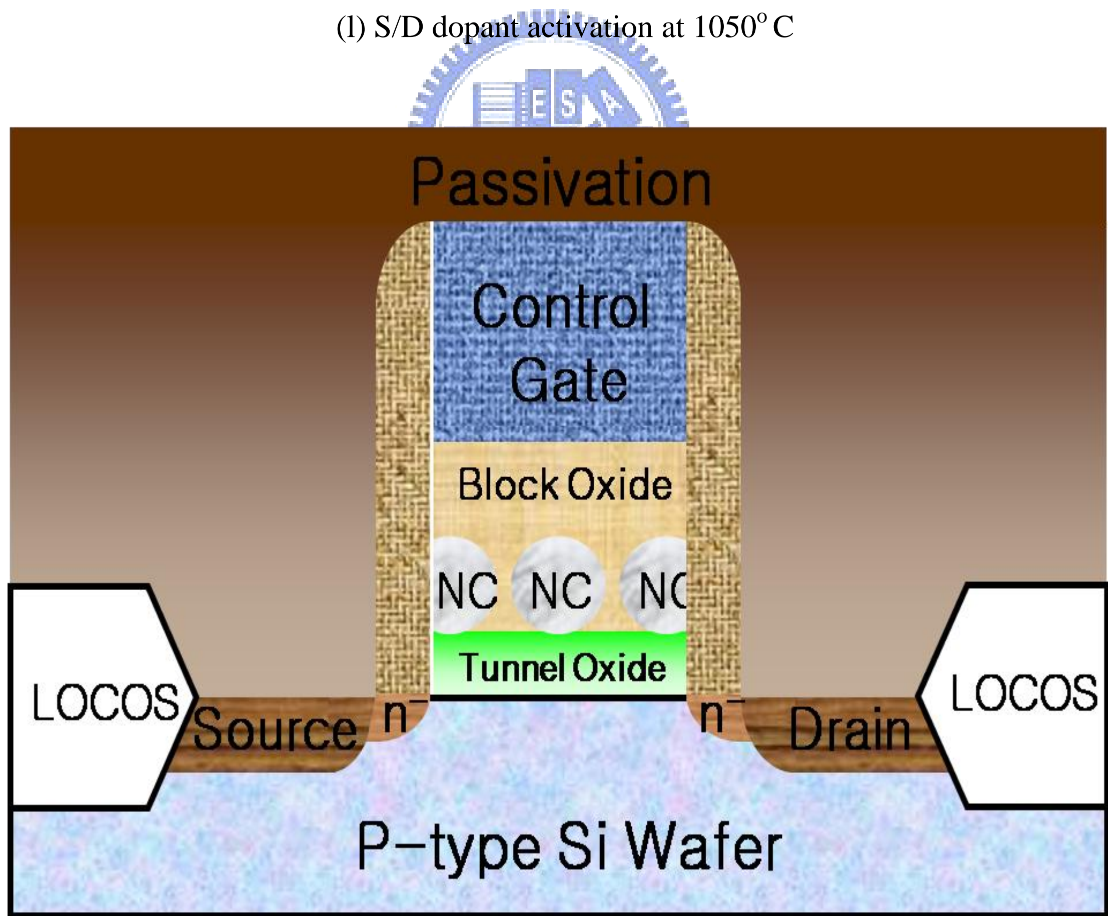

(m) Oxide passivation layer deposition by the HDPCVD process

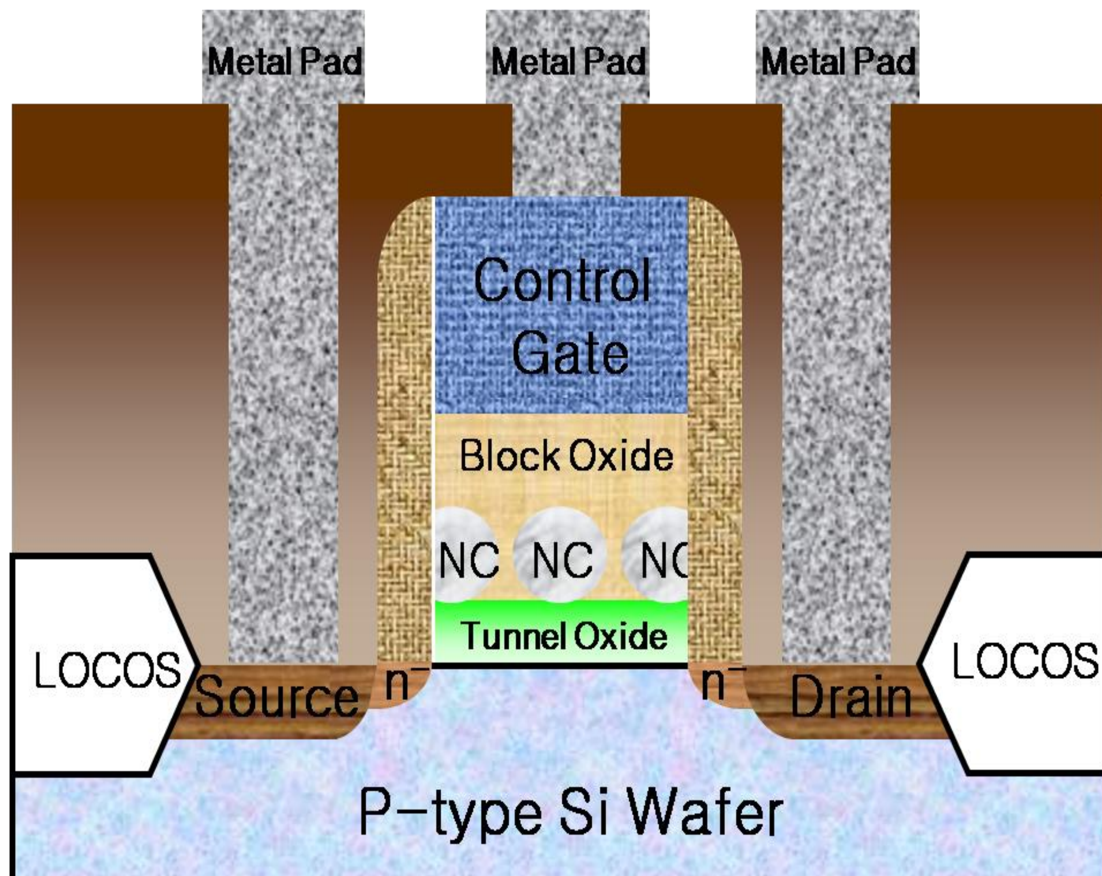

(n) The formation of contact hole openings and metal pads

Fig. 2-7 The process flow of proposed IPA Sol-Gel derived NC Flash memory cells

2-4 Results and Discussion

In this section, the electrical and physical properties of the IPA Sol-Gel derived M_xO_y NC Flash memory devices were discussed.

2-4.1 Electrical Properties

2-4.1.1 Id-Vg Transfer Curves

Fig 2-8, Fig. 2-9, and Fig. 2-10 show the Id-Vg transfer characteristics of $(CoLi)Si_xO_y$, $(CoLi)Ge_xO_y$, and $(CoLiZr)Si_xO_y$ M_xO_y mixtures of the Flash memory

devices under programming and erasing operations, respectively. We utilized CHEI for programming and BTBHHI for erasing mechanism in the NC Flash memory devices [17]-[18]. The programming voltage conditions were as follows: Vg (gate voltage) = 10 V and Vd (drain voltage) = 9 V with 100 msec. stress. The erasing voltage conditions were Vg = -6 V and Vd = 10 V with 10 msec. stress. All the three devices were around 3-4 V memory window.

The results indicated a striking effect of polarization of Vg on relative memory window variation in our devices. Because of the trapped electron charges in the M_xO_y NC charge-trapping layer, the Vth or V_T shifted rightward. When the positive voltage Vg and Vd are supplied, the channel electrons gain energy from them. The negative voltage Vg and positive voltage Vd are applied to generate hot hole charges in the p-type silicon substrate at the same time to balance total trapping charges for erasing; The hot-hole charges in silicon substrate can reach to the M_xO_y NC charge-trapping layer and result in the leftward △Vth or $△V_T$ of following three Id-Vg transfer curves.

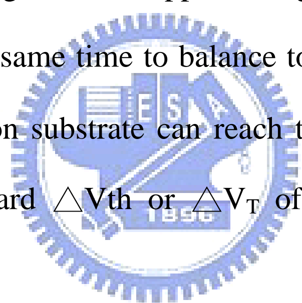

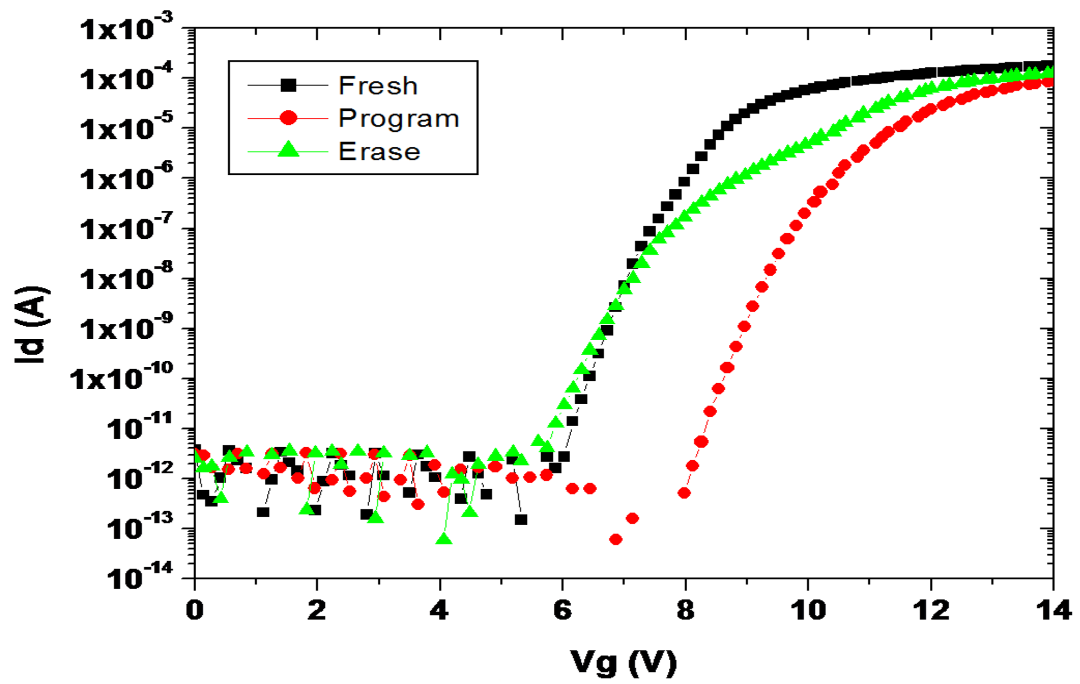

Fig. 2-8 The Id-Vg transfer curves of (CoLi)Si_xO_y-M_xO_y NC devices

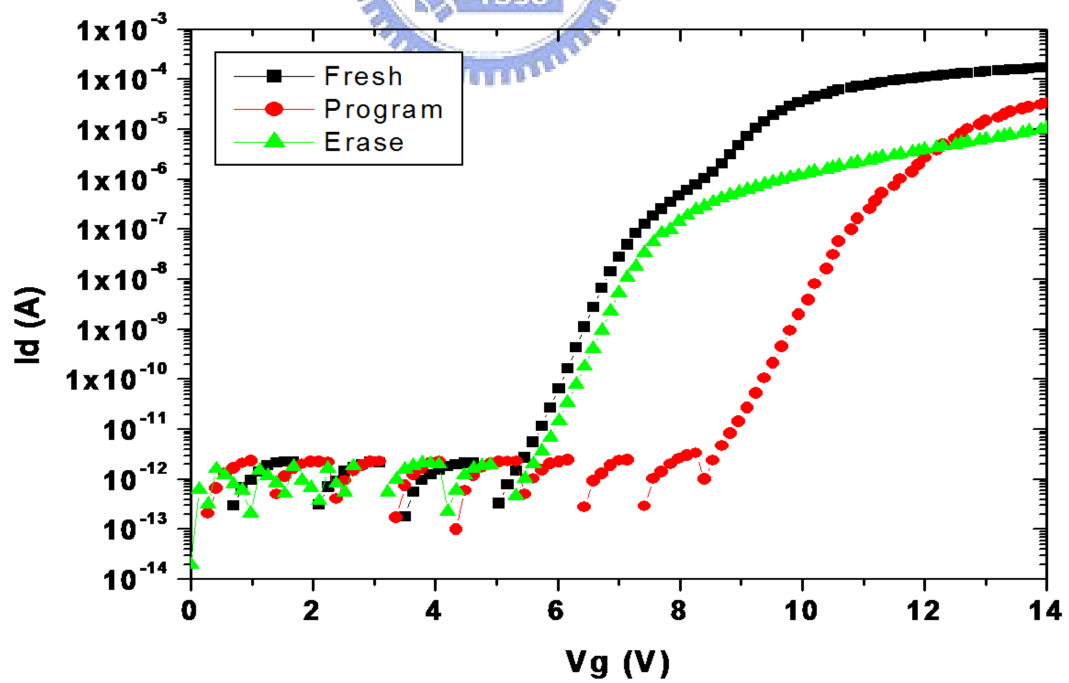

Fig. 2-9 The Id-Vg transfer curves of (CoLi)Ge_xO_y-M_xO_y NC devices

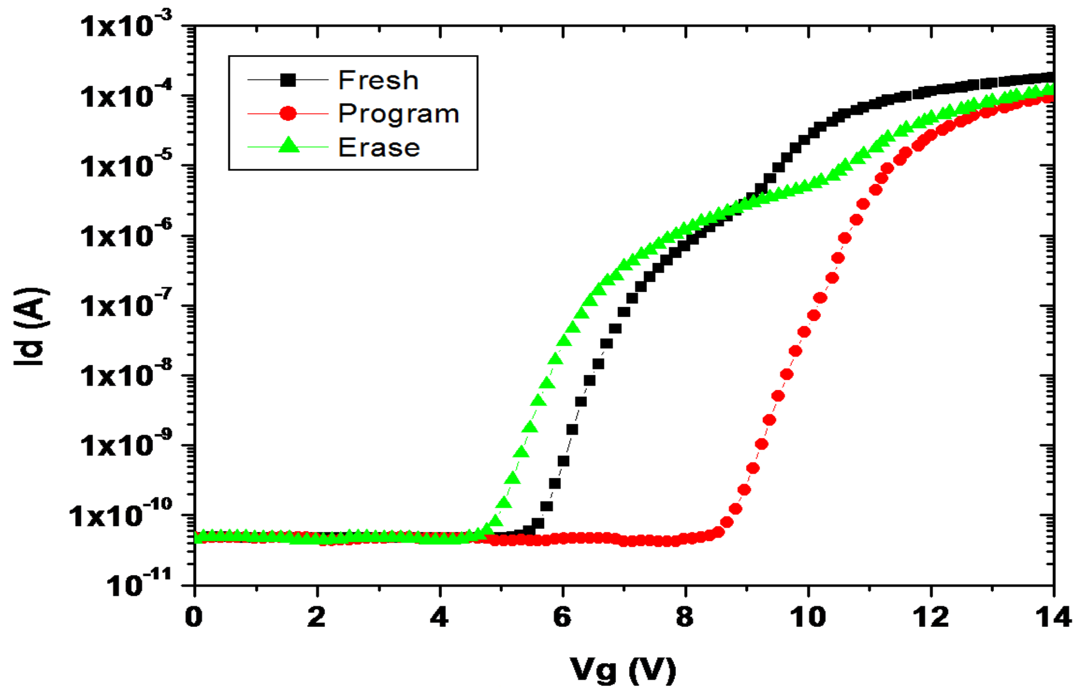

Fig. 2-10 The Id-Vg transfer curves of (CoLiZr)Si_xO_y-M_xO_y NC devices

2-4.1.2 Programming/Erasing Speed

The three memory programming speed curves of (CoLi)Si_xO_y, (CoLi)Ge_xO_y, and (CoLiZr)Si_xO_y M_xO_y mixtures for each device charge-trapping layer are demonstrated in Fig. 2-11, Fig. 2-12, and Fig. 2-13, respectively. They showed different gate and drain voltage stress conditions: Vg = 8 V, 9 V, 10 V, and Vd = 9 V. With the Vg increasing, the △Vth increases and programming speed was also faster.

Fig. 2-14, Fig. 2-15, and Fig. 2-16 illustrate the erasing speed curves of three memory devices for different stress conditions: Vg = -9 V, -10 V, and -6 V with Vd = 9 V and 10 V of (CoLi)Si_xO_y, (CoLi)Ge_xO_y, and (CoLiZr)Si_xO_y M_xO_y mixtures under erasing operation.

As the Vg became more negative, the Vth shifted downward more. The reason why the P/E speed is fast or slow is more channel electrons for programming or more

silicon substrate holes for erasing are induced. These results reveal that channel electrons or hot holes appear to be an important variable in memory speed. Therefore, the increasing or decreasing △Vth as the positive or negative Vg by more and more trapped channel electrons or hot holes in the charge-trapping layer.

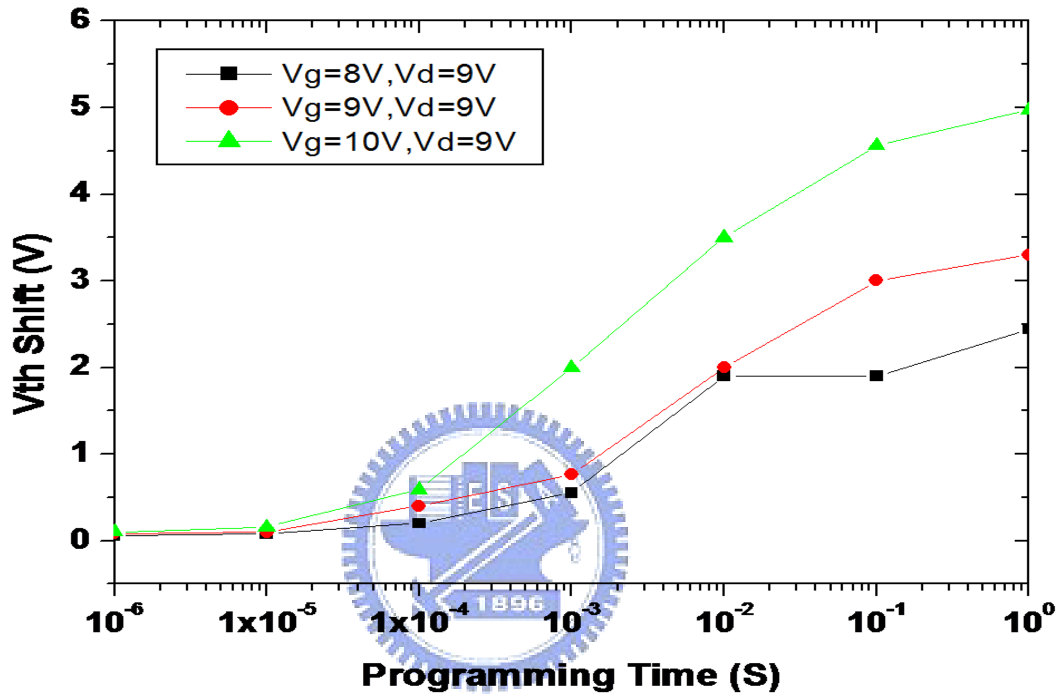

Fig. 2-11 The programming speed of (CoLi)Si_xO_y-M_xO_y NC devices

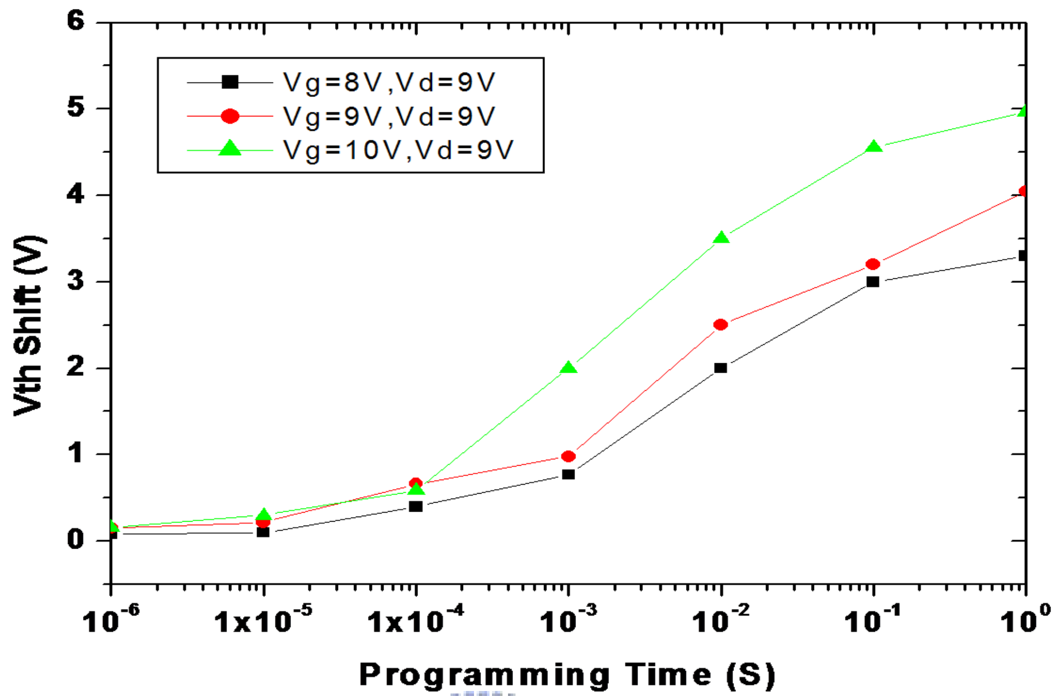

Fig. 2-12 The programming speed of (CoLi)Ge_xO_y-M_xO_y NC devices

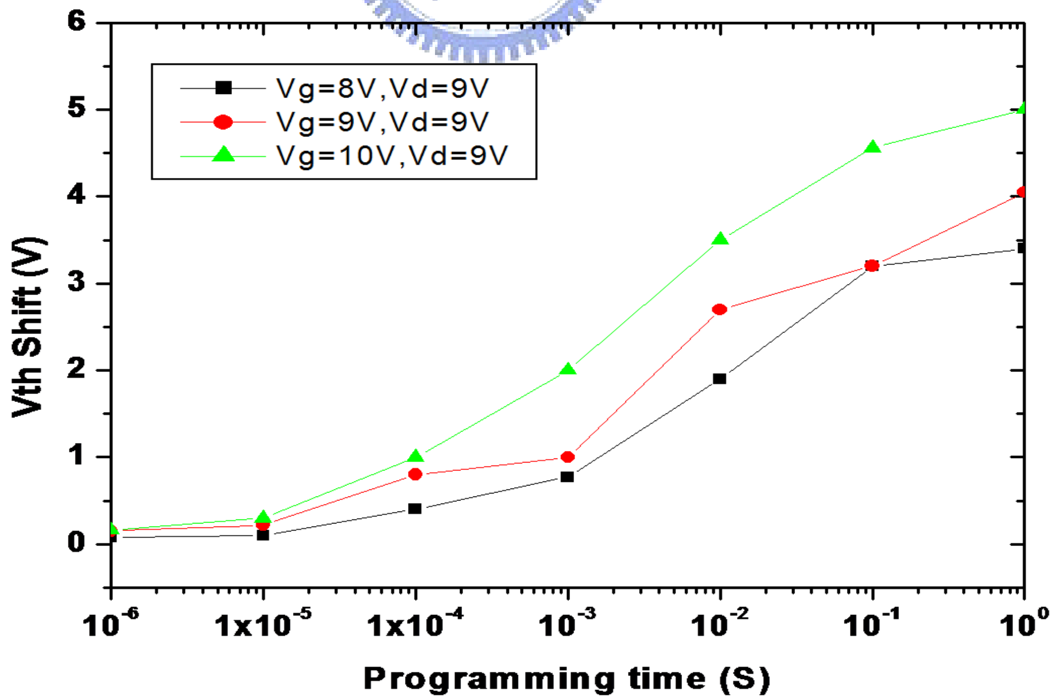

Fig. 2-13 The programming speed of (CoLiZr)Si_xO_y-M_xO_y NC devices

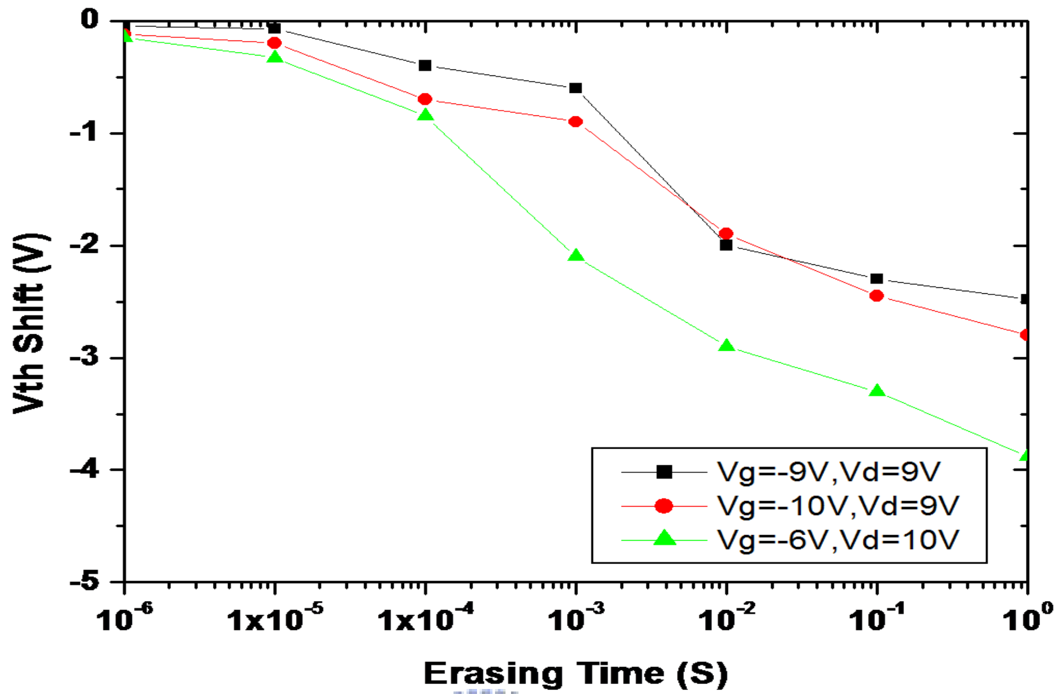

Fig. 2-14 The erasing speed of (CoLi)Si_xO_y-M_xO_y NC devices

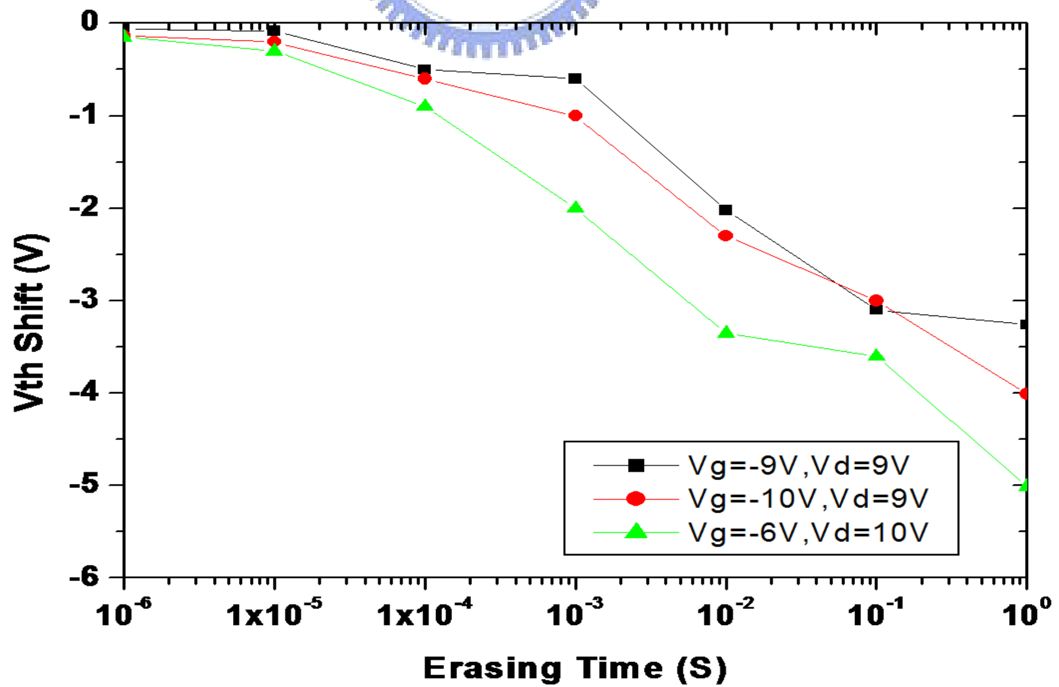

Fig. 2-15 The erasing speed of (CoLi)Ge_xO_y-M_xO_y NC devices

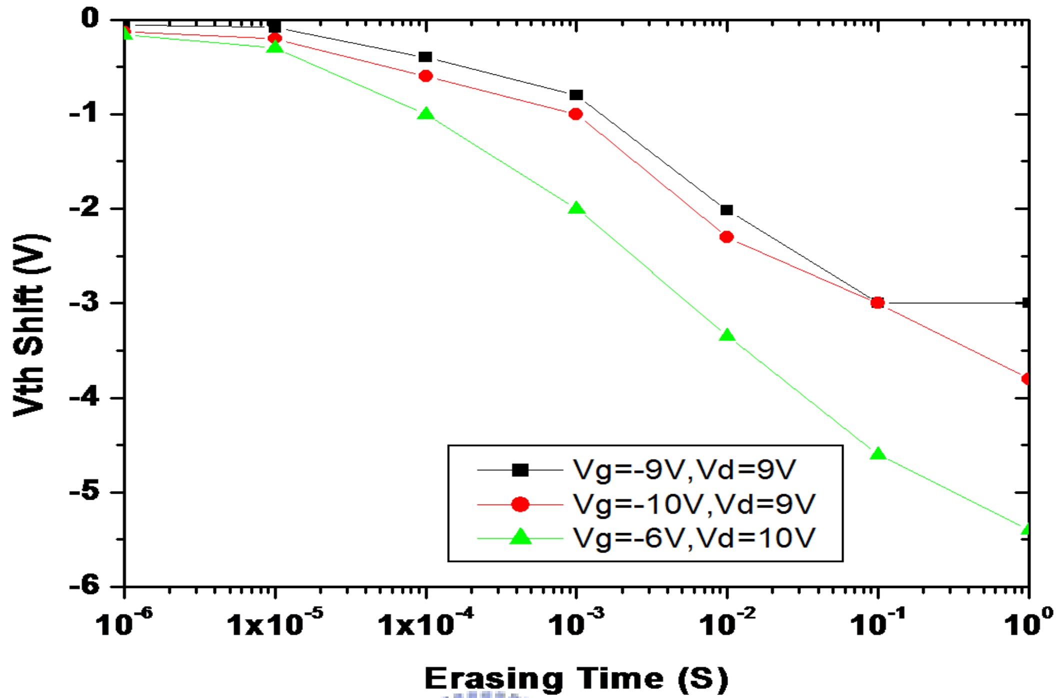

Fig. 2-16 The erasing speed of $(CoLiZr)Si_xO_y$-M_xO_y NC devices

1896

2-4.1.3 Retention Time

As displayed in Fig. 2-17, Fig. 2-18, and Fig. 2-19, the data retention time of M_xO_y NC Flash memory devices was measured at 25° C and 85° C. We normalized the Vth shift scale bar between 0% and 100% versus time from 10^0 to 10^4 sec. The following retention curves presented small charge loss versus time in the devices.

All retention characteristics depicted charge loss below 5% as measure time up to 10^4 sec. at 25° C, and charge loss was less than 12% at 85° C. These charge loss results may be explained by considering the distribution of deep electron traps of the NC charge-trapping layer at 25° C and 85° C as mentioned above.

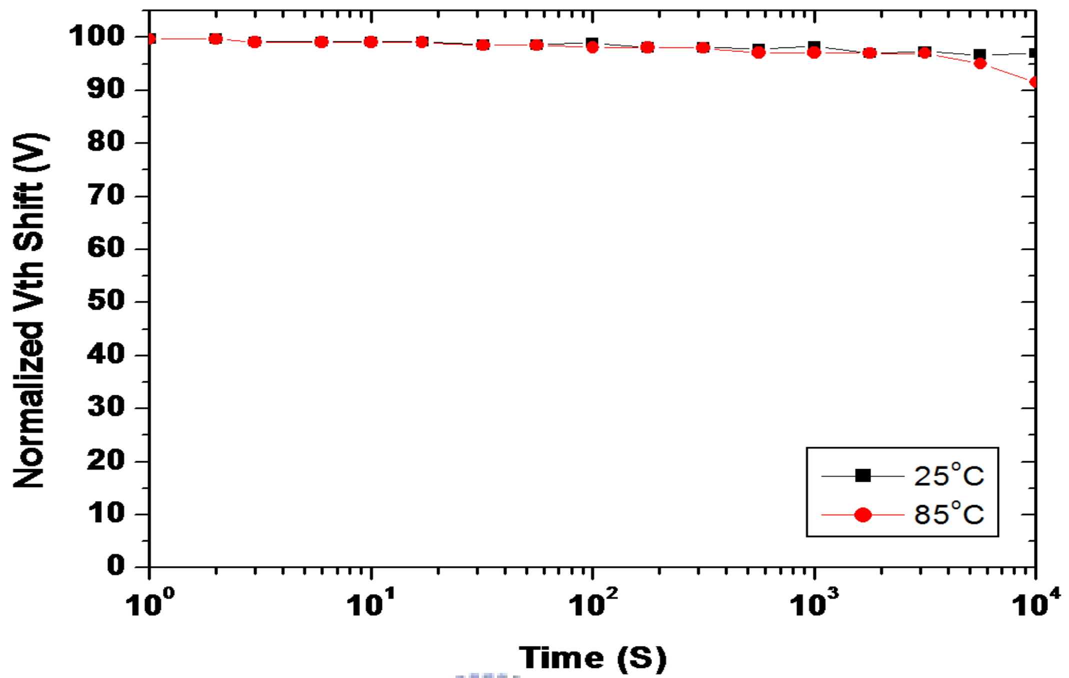

Fig. 2-17 The data retention time of (CoLi)Si_xO_y-M_xO_y NC devices

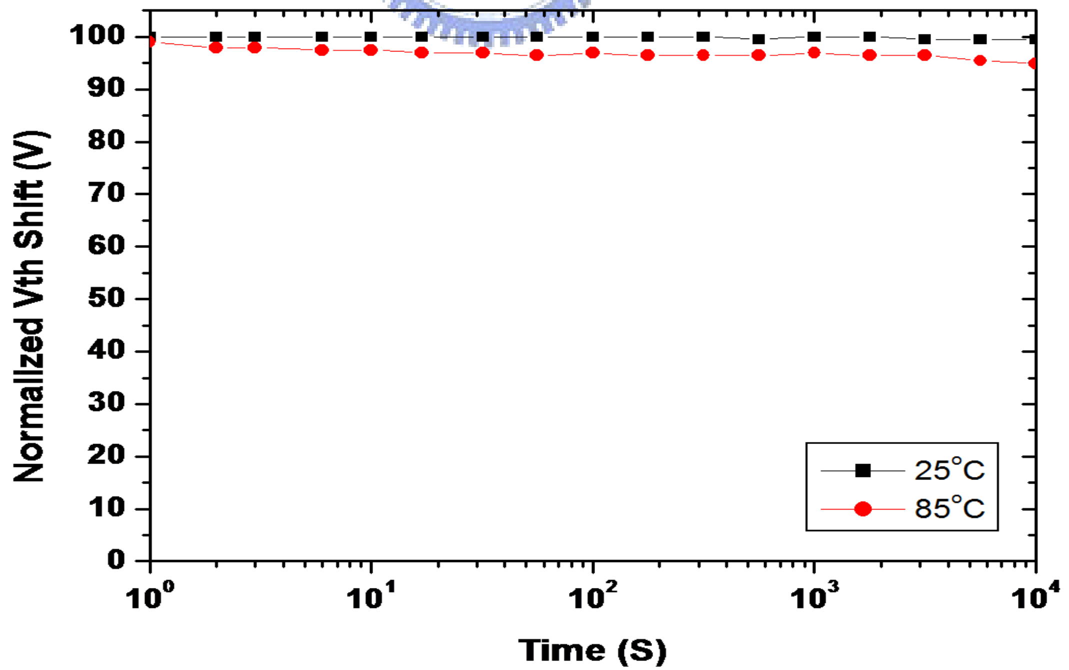

Fig. 2-18 The data retention time of (CoLi)Ge_xO_y-M_xO_y NC devices

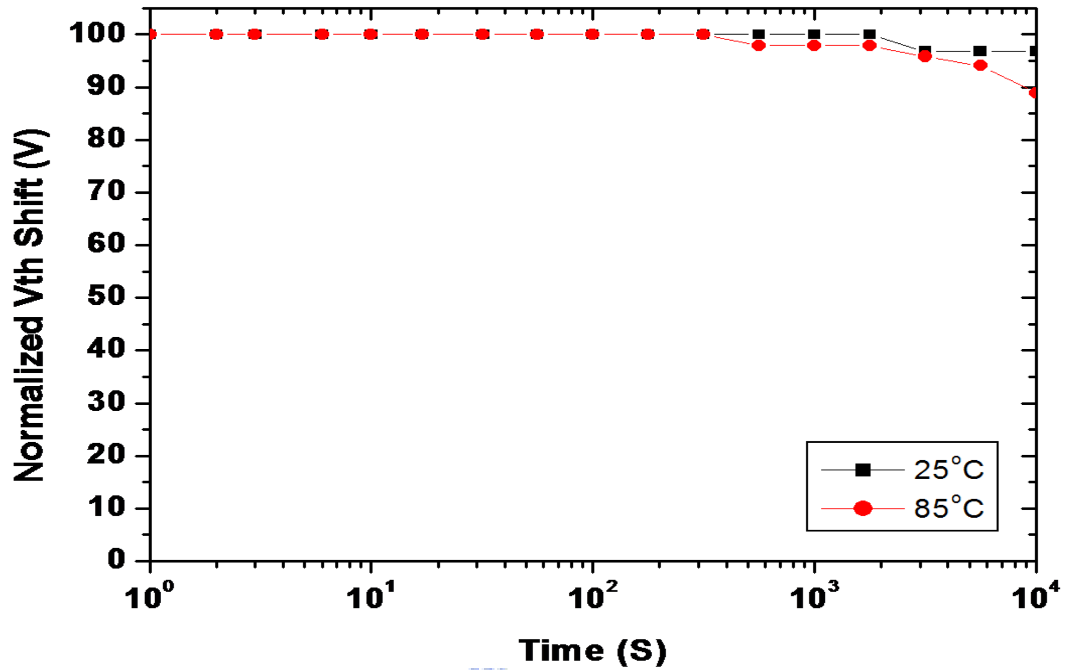

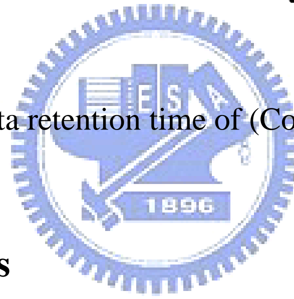

Fig. 2-19 The data retention time of $(CoLiZr)Si_xO_y$-M_xO_y NC devices

2-4.1.4 Endurance Cycles

Fig. 2-20, Fig. 2-21, and Fig. 2-22 give the data endurance curves of the NC Flash memory devices. The measured Vg and Vd conditions for programming and erasing were as follows: Vg = 10 V and Vd = 9 V with 1 msec. and 10 msec. for programming stress, Vg = -10 V and Vd = 9 V with 100 msec. for erasing stress.

Because trapped electrons in deep level traps are erased hard, a small increase of the erasing Vth is observed from the subsequent three Figs.; moreover, only a little window narrowing effect may be found.

After 10^4 P/E cycles, each memory window was fixed to about 2.5 V. These findings led us to believe that the simple Sol-Gel technique should be linked to the novel NC Flash memory fabrication processes in the future.

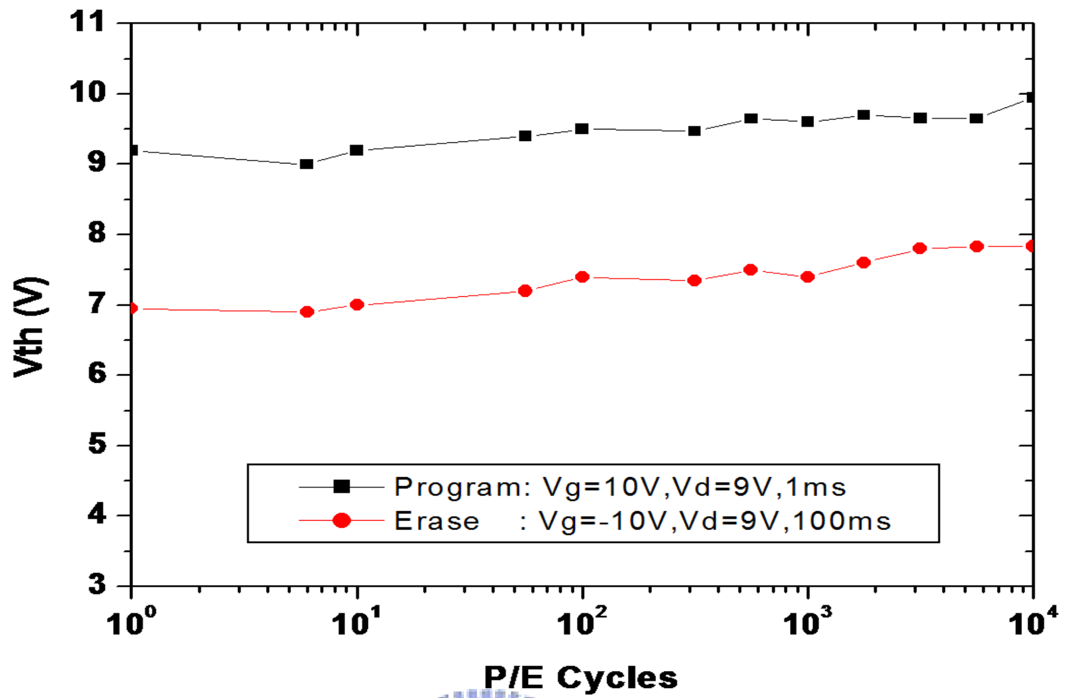

Fig. 2-20 The data endurance of (CoLi)Si_xO_y-M_xO_y NC devices

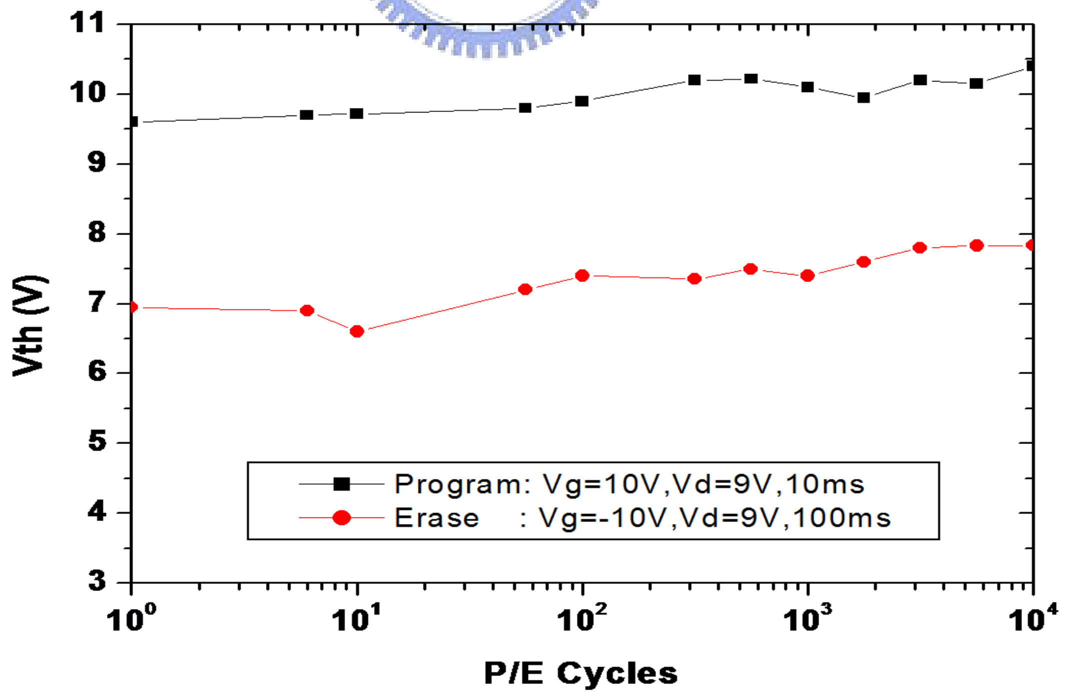

Fig. 2-21 The data endurance of (CoLi)Ge_xO_y-M_xO_y NC devices

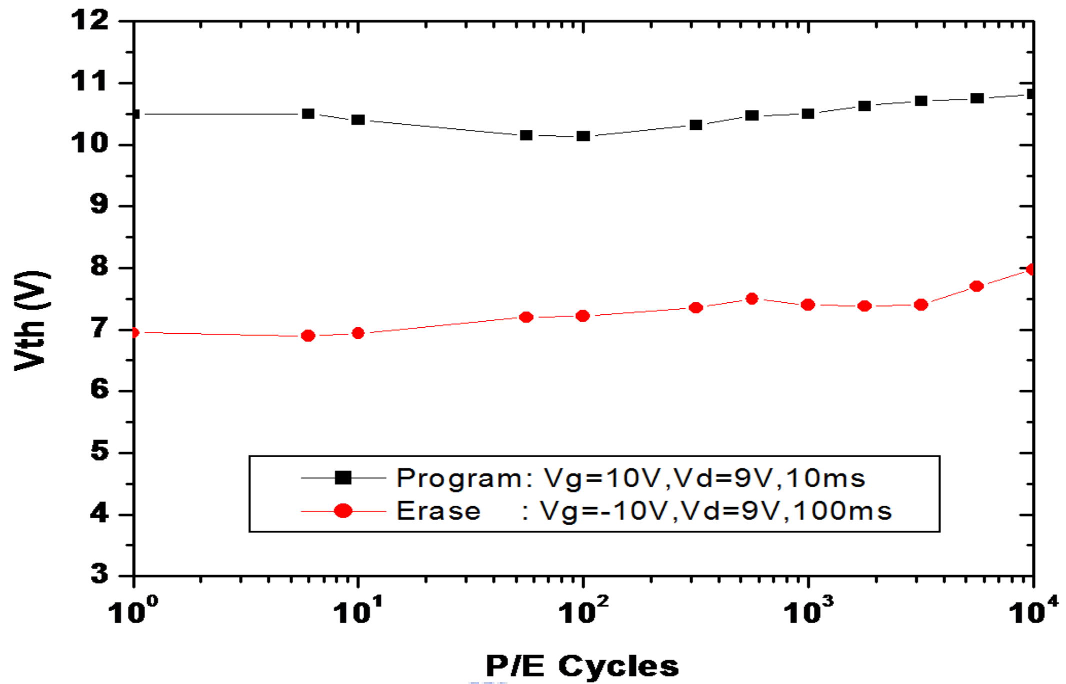

Fig. 2-22 The data endurance of (CoLiZr)Si_xO_y-M_xO_y NC devices

2-4.1.5 Gate/Drain Disturbance

Fig. 2-23 describes the schematic structure of G/D disturbance of Flash memory cells. The measurement of gate disturbance demonstrated in Fig. 2-24, Fig. 2-25, and Fig. 2-26 of the devices was two stress conditions: Vg = 8 V and Vg = 9 V with Vd = Vs (source voltage) = Vb (body voltage or substrate voltage) = 0 V. After 1000 sec. stress, the initial or fresh state △Vth increased to 0.03 V and 0.3 V with the Vg = 8 V and Vg = 9 V, respectively. These findings yielded that the supplied Vg would attract silicon substrate electrons tunneling through gate oxide to the M_xO_y trapping layer by FN tunneling mechanism and lead to the Vth increase.

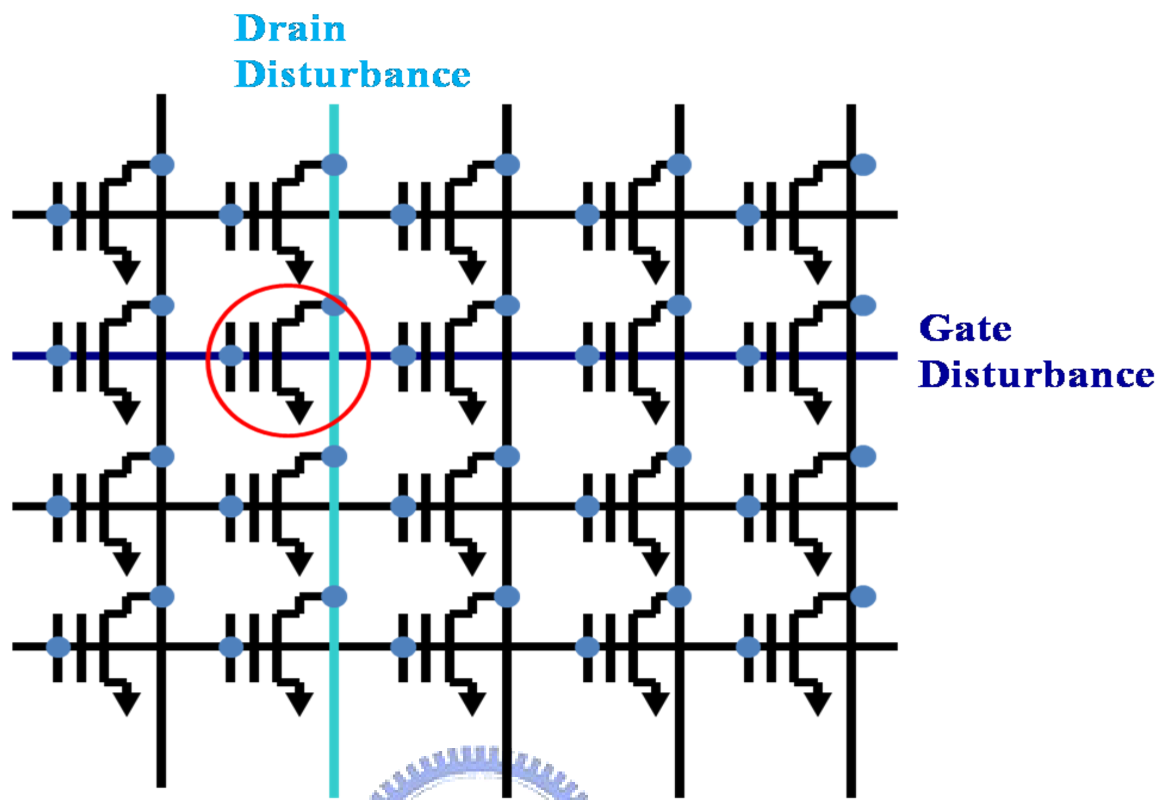

Fig. 2-23 The G/D Disturbance schematic structure of Flash memory cells

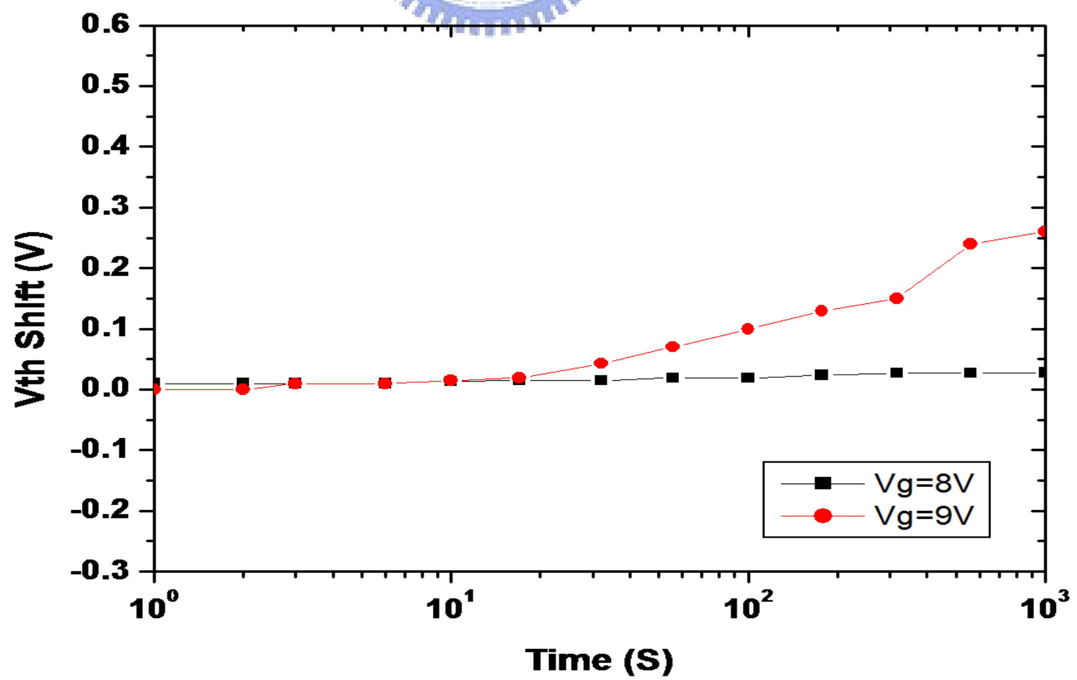

Fig. 2-24 The gate disturbance of (CoLi)Si_xO_y-M_xO_y NC devices

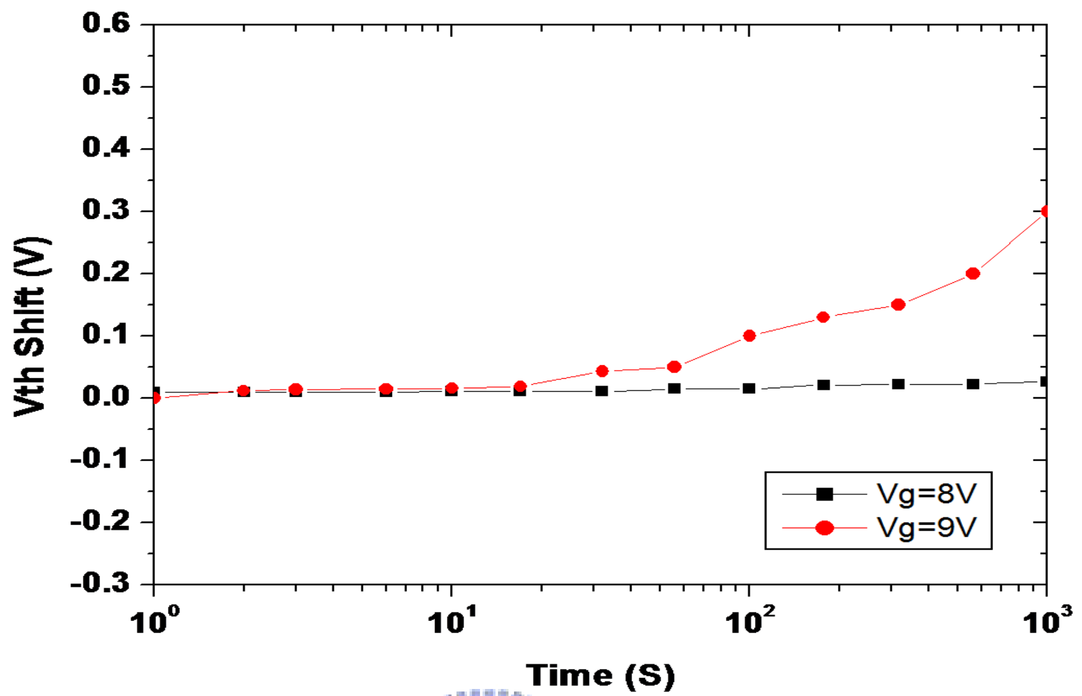

Fig. 2-25 The gate disturbance of (CoLi)Ge_xO_y-M_xO_y NC devices

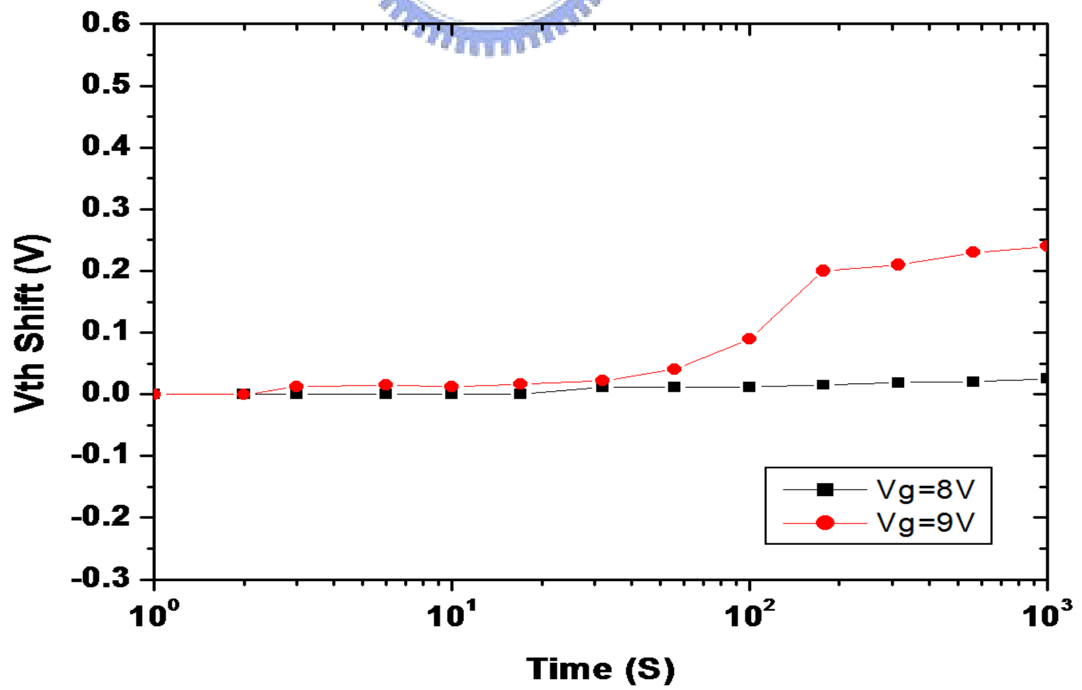

Fig. 2-26 The gate disturbance of (CoLiZr)Si_xO_y-M_xO_y NC devices

The measurement of drain disturbance was two stress conditions: Vd = 9 V and Vd = 10 V with Vg = Vs = Vb = 0 V to the devices as revealed in Fig. 2-27, Fig. 2-28, and Fig. 2-29 as well. From the three Figs., after 10^3 sec., each programmed state △ Vth had only a little charge loss of 0.05 V within reasonable range.

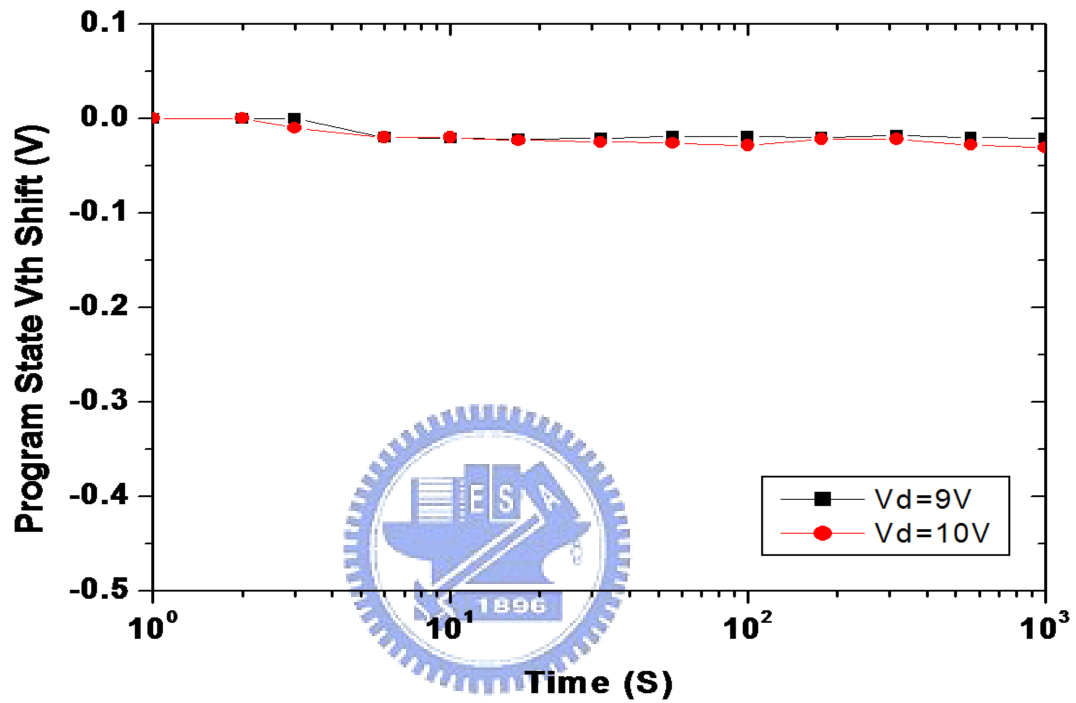

Fig. 2-27 The drain disturbance of $(CoLi)Si_xO_y$-M_xO_y NC devices

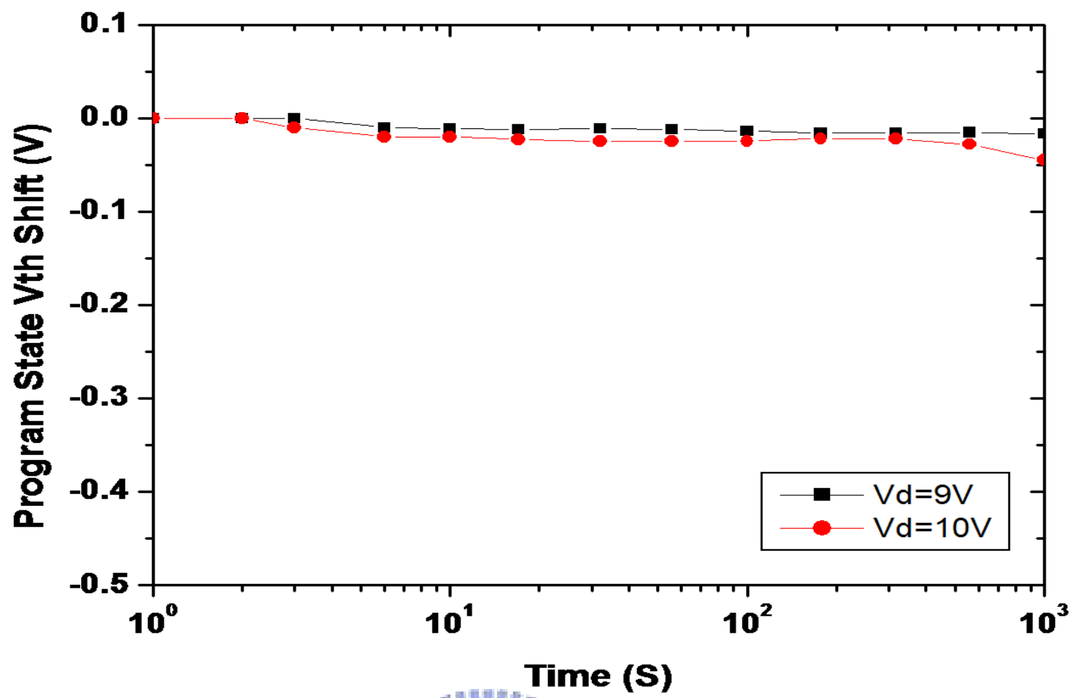

Fig. 2-28 The drain disturbance of (CoLi)Ge_xO_y-M_xO_y NC devices

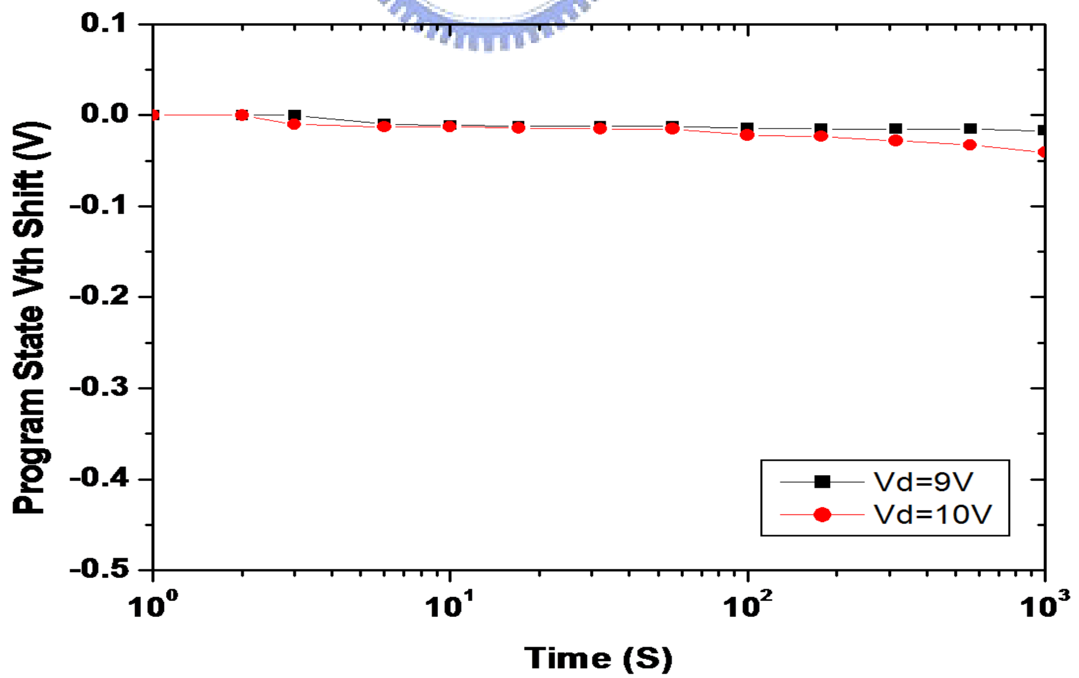

Fig. 2-29 The drain disturbance of (CoLiZr)Si_xO_y-M_xO_y NC devices

2-4.2 Physical Properties

The physical property research of various kinds of the M_xO_y thin film and binary or ternary NCs as the charge-trapping layer was carried out by the HRTEM instrument of the memory devices. From the following three HRTEM images as summarized in Fig. 2-30, Fig. 2-31, and Fig. 2-32, each trapping layer of the devices truly was shaped into nano-sized round balls or oval-shaped NCs or a composite thin film after the 1050° C 60 sec. ORTA step. The average nano-composite crystal size was around 5-10 nm. The crossed grids of lattice fringes could clearly be seen with crystallization into prominently nano-structured features typically [19]-[20].

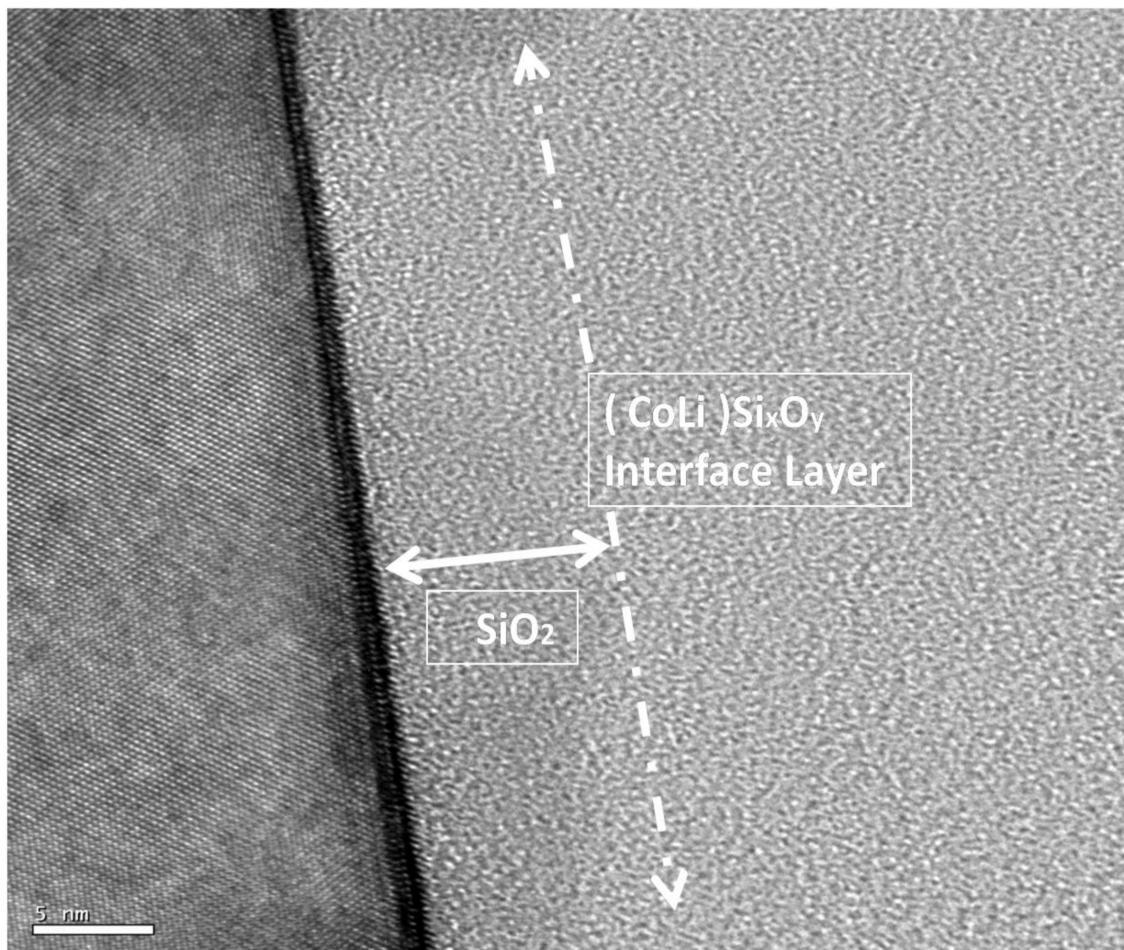

Fig. 2-30 The HRTEM image of the (CoLi)Si_xO_y-composite thin film on SiO_2 after the 1050° C 60 sec. ORTA step

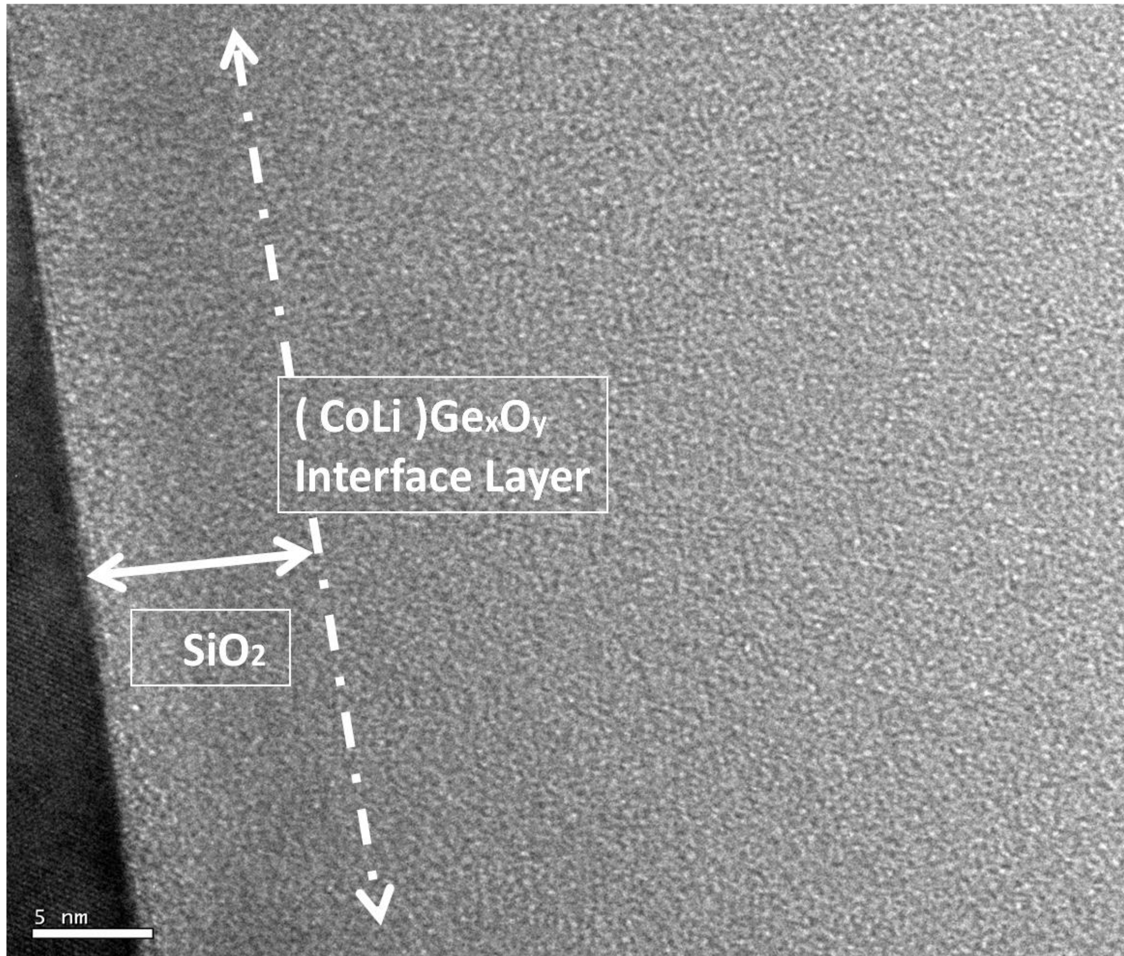

Fig. 2-31 The HRTEM image of the $(CoLi)Ge_xO_y$-composite thin film on SiO_2 after the 1050° C 60 sec. ORTA step

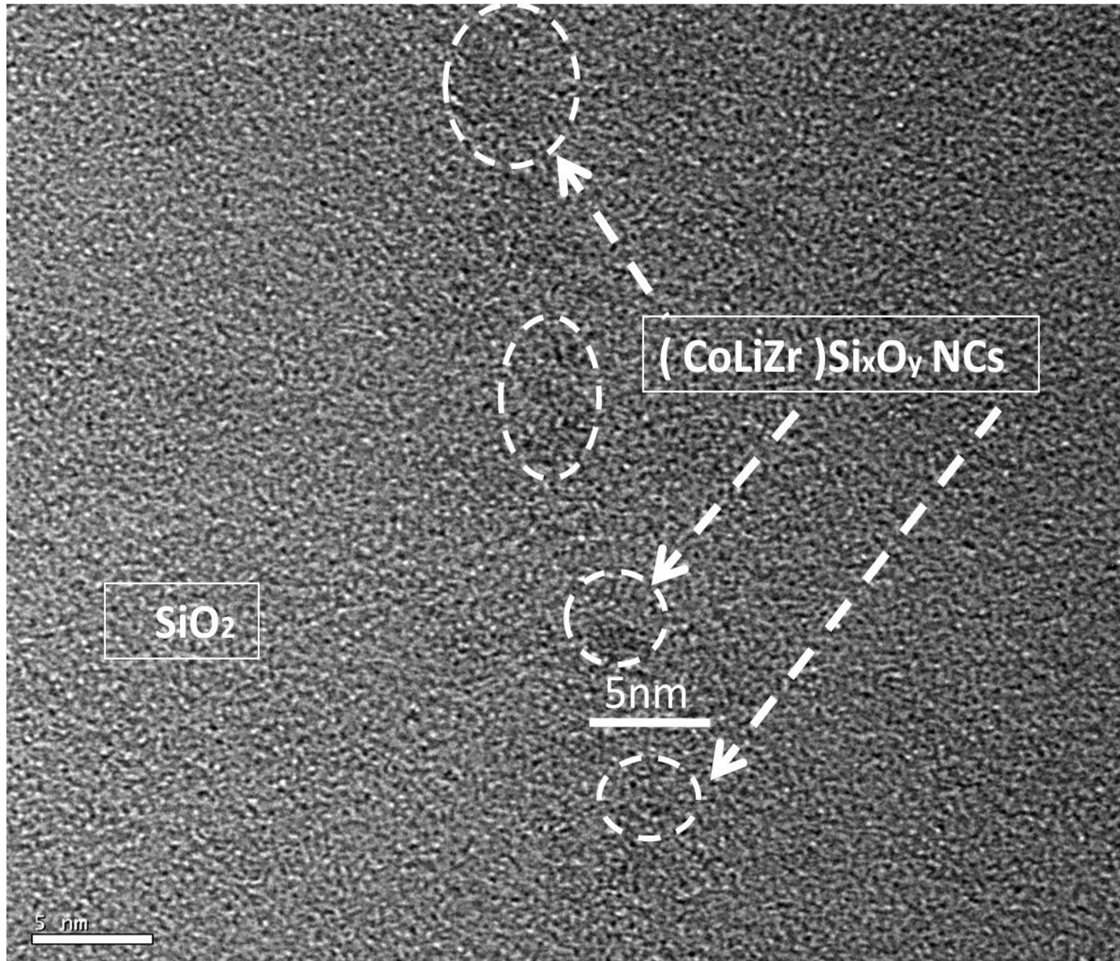

Fig. 2-32 The HRTEM image of $(CoLiZr)Si_xO_y$-composite NCs on SiO_2 after the 1050° C 60 sec. ORTA step

2-5 Summary

In this chapter, we presented the Sol-Gel technique to form the composite M_xO_y thin film and NCs for the trapping layer of NC Flash memory devices. The common programming and erasing methods are the CHEI and BTBHHI. We have displayed the electrical properties of devices such as Id-Vg transfer curves, charge retention time, endurance cycles, and G/D disturbance describing the better performance of a Sol-Gel derived M_xO_y charge-trapping layer.

As far as we are concerned, it has some good characteristics for relative 3-4 V

memory window. The longer retention time is due to binary or ternary M_xO_y NCs or the composite thin film in the charge-trapping layer, good endurance up to 10^4 P/E cycles with only a little memory window narrowing, and little G/D disturbance after 10^3 sec.

The HRTEM images also verify the formation of NCs or a composite M_xO_y thin film in the trapping layer. The easily proposed Sol-Gel spin coating method exhibits high potential to be incorporated into the future NC Flash memory fabrication.

Chapter 3

Electrical and Physical Properties of Metal Oxide Nanocrystal Flash Memory Devices by the Sol-Gel Spin Coating Method with C_2H_5OH Solvent

3-1 Introduction

The Si_3N_4 dielectric constant of SONOS memory is 7.5 eV and 2.05 eV BH versus silicon. Its electron trap level is about 0.8 eV below the nitride conduction band. The SONOS memory has better data retention time than FGNVM due to its spatially discrete trapping defects with the tunnel oxide thickness below 10 nm, but one issue is programming or erasing speed. The conduction band offset between Si_3N_4 and SiO_2 is 1.05 eV. Fig. 3-1 gives the energy-band diagram of ZrO_2 dielectric SONOS-type memory. With the reasons of small BH to silicon and large conduction band offset to SiO_2, high-k dielectrics and metal NCs like ZrO_2, Au, Co, Ge, and Ni elements are required to achieve high P/E speed, long retention/endurance time, and little disturbance properties for the Flash memory trapping layer [1].

The NC Flash memory can hold the trapped charges tightly to avoid the data loss and reduction of the charge retention storage. It also possesses many advantages in high speed work efficiency, low power consumption, and fast transistor on/off ratio contrary to the conventional SONOS memory [2]-[3].

In this chapter, we still utilized the simple Sol-Gel spin coating method for the NC Flash memory manufacturing with six metal chlorides as chemical reactions in C_2H_5OH solvent; the 1050° C 60 sec. ORTA step followed to deposit multiplexed

separation of NC mixtures as the memory device charge-trapping layer. We analyzed the physical and electrical properties of diversely distributed M_xO_y NCs for a lot of charge-trapping sites of the NC Flash memory devices in the HRTEM instrument, Id-Vg transfer curves, P/E speed, retention time, endurance cycles, and G/D disturbance as well [4]-[5].

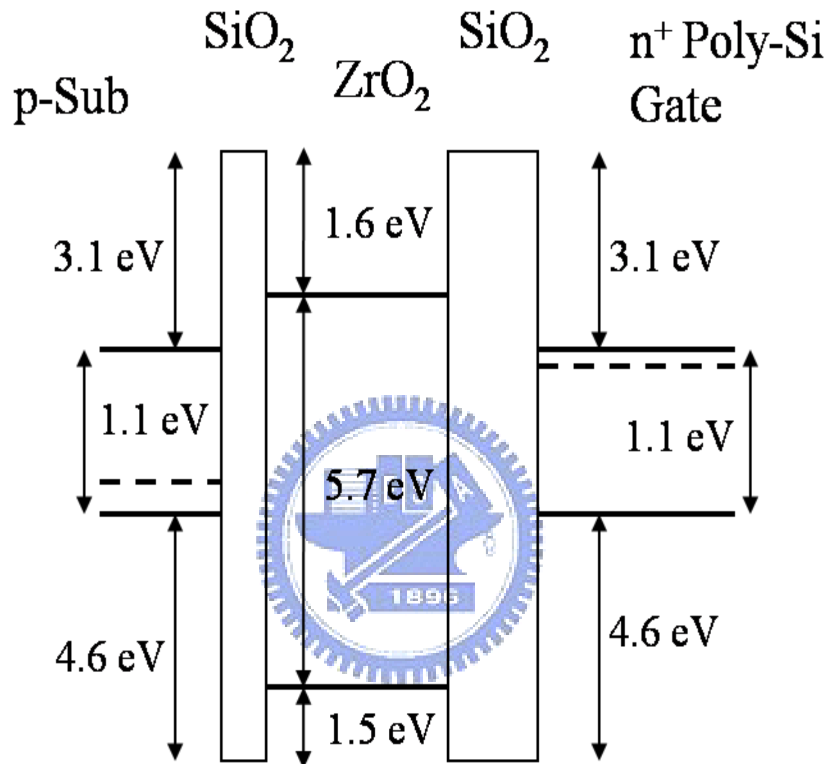

Fig. 3-1 The energy-band diagram of ZrO_2 dielectric SONOS-type memory

3-2 Experiments

First, ($CoCl_2 \cdot 6H_2O$), $GeCl_4$, ($HAuCl_4 \cdot 3H_2O$), ($NiCl_2 \cdot 6H_2O$), $SiCl_4$, and $ZrCl_4$ metal chlorides were used as chemical reaction precursors for the synthesis of M_xO_y NC materials. A mother Sol solution was obtained by mixing and dissolving metal chlorides into C_2H_5OH (Fluka, 99.5%) under the vigorous stirring condition for about 1 hour. Second, the Sol solution was prepared by entirely hydrolyzing metal chlorides

with the stoichiometric amount of water in C_2H_5OH to yield a 1:1000 molar ratio mixture of M_x : C_2H_5OH.

The Flash memory manufacturing processes were started with LOCOS isolation on p-type (100) 150-mm silicon substrate wafers. Next, a 10 nm tunnel oxide layer was thermally grown at 900° C by vertical furnace oxidation. The chemical solution of a 1:1000 molar ratio mixture of M_x : C_2H_5OH was coated on the tunnel oxide film by spin coater at 3000 rpm for 60 sec. at normal temperature (25° C).

The as-deposited thin film was followed by the 1050° C 60 sec. ORTA step in the oxygen environment to form nano-composite M_xO_y crystals for each device trapping layer. The 30-nm-thin block oxide layer was deposited by the HDPCVD SiO_2 in N_2 densification, and then with a 200-nm-thick poly-gate layer on the block oxide.

After the polysilicon-gate layer deposition, the step-by-step followed semiconductor processes were gate electrode patterning, S/D extension implanted by the dosage of 2E14 cm^{-2} As at 10 keV ion energy, oxide sidewall spacer formation, G/S/D implantation by the high dose of 5E15 cm^{-2} As at 20 keV ion energy, silicon substrate contact patterning and ion implantation with the high dosage of 5E15 cm^{-2} BF_2 at 40 keV ion energy, S/D dopant activation, passivation layer deposition by the HDPCVD SiO_2, contact hole openings, and metal pads; the rest of the standard MOS manufacturing steps were finished to fabricate all the NC Flash memory devices later.

The flow chart, semiconductor process flow, and cross section of the presented M_xO_y NC Flash memory devices are also described in Fig. 3-2, Fig. 3-3, and Fig 3-4, respectively.

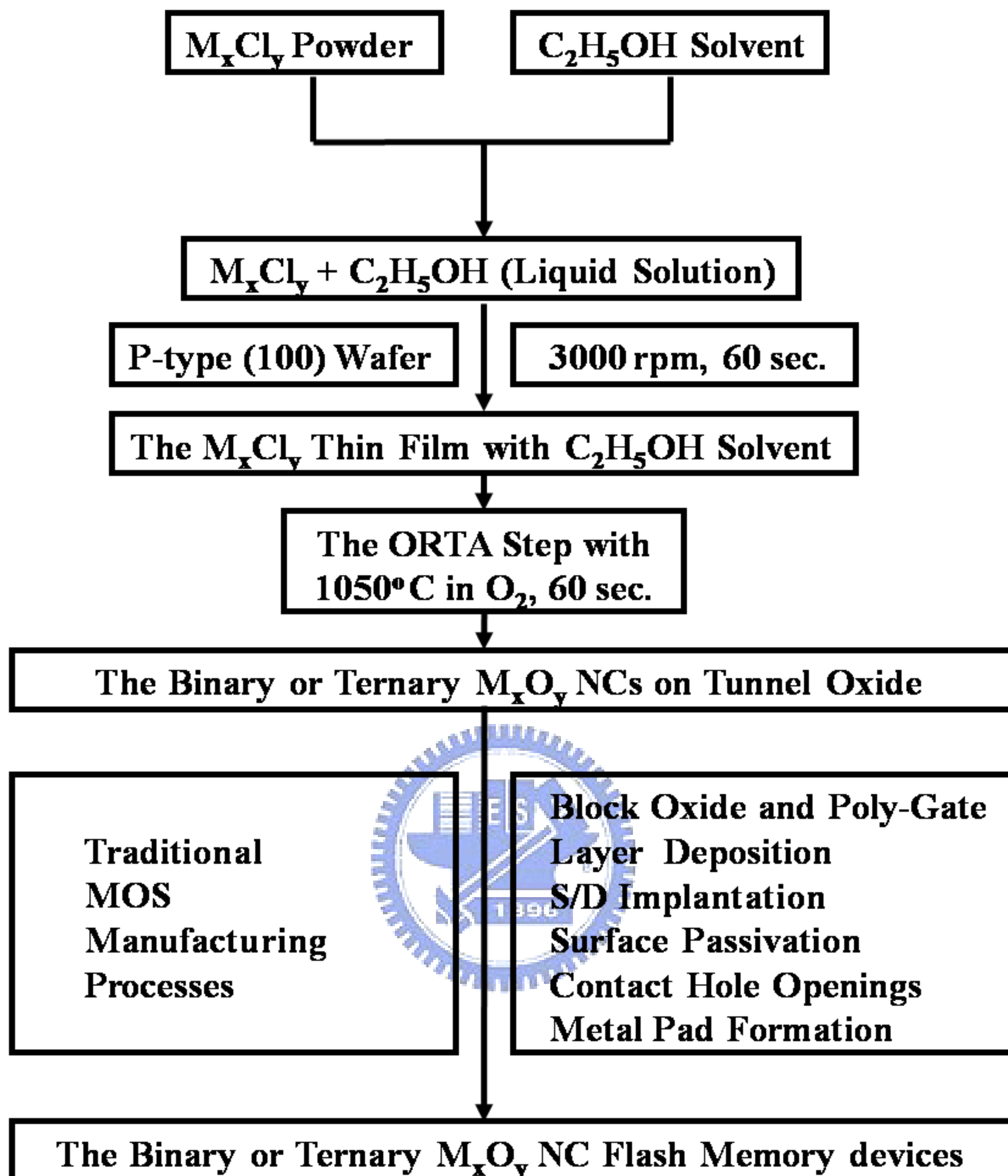

Fig. 3-2 The flow chart of C_2H_5OH Sol-Gel derived Flash memory devices

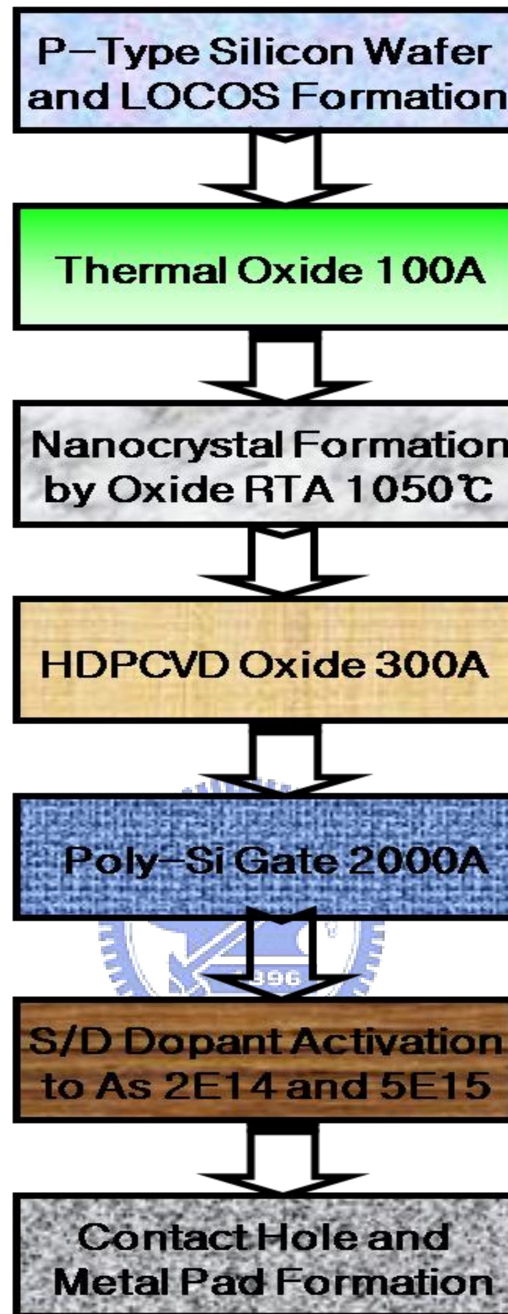

Fig. 3-3 The semiconductor process flow of C_2H_5OH Sol-Gel derived NC Flash memory cells

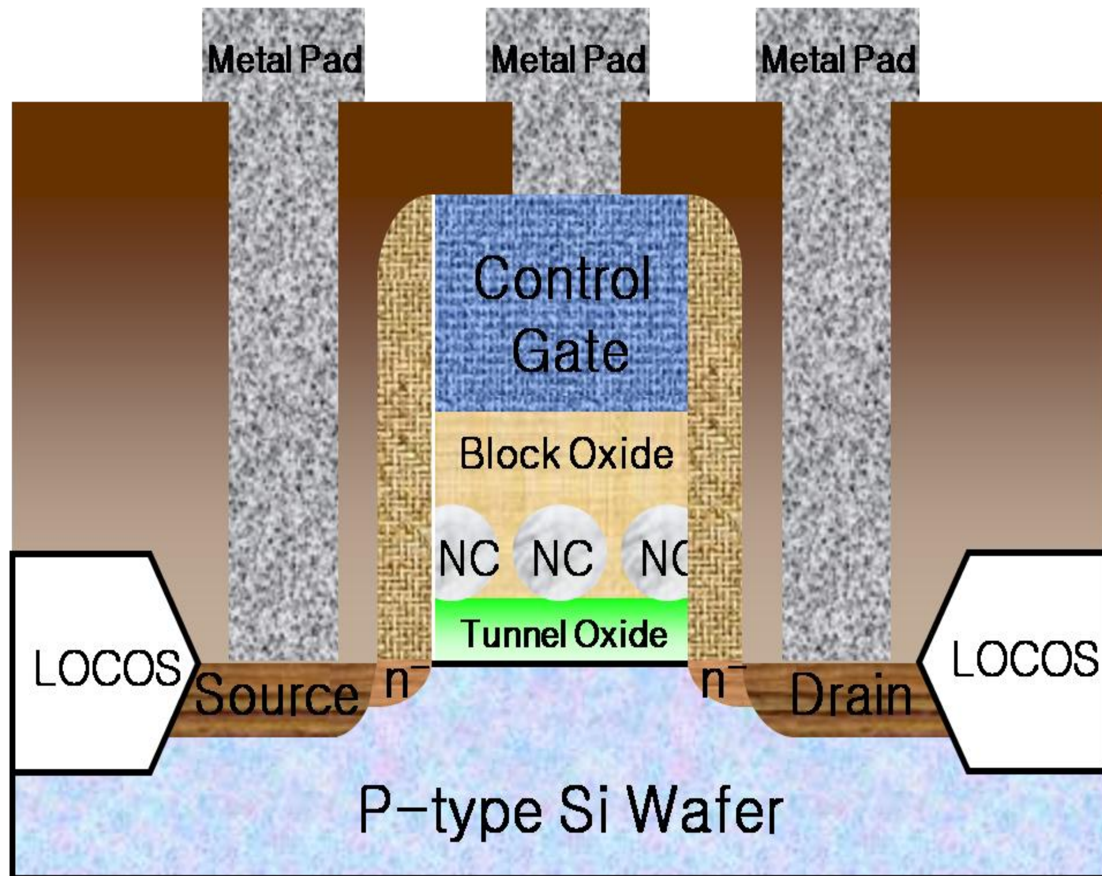

Fig. 3-4 The presented C_2H_5OH Sol-Gel derived NC Flash memory cross section

3-3 Results and Discussion

In this section, the electrical and physical properties of the C_2H_5OH Sol-Gel derived nano-composite NC Flash memory devices were discussed.

3-3.1 Electrical Properties

3-3.1.1 Id-Vg Transfer Curves

Fig 3-5, Fig. 3-6, and Fig. 3-7 depict the Id-Vg transfer curves of $AuGe_xO_y$, $(CoZr)Ge_xO_y$, and $(NiZr)Si_xGe_zO_y$ M_xO_y mixtures of the devices under programming and erasing operations. We used CHEI mechanism for programming and BBHHI

mechanism for erasing charges in these memory devices [5]-[7]. The programming conditions were as follows: Vg = 10 V and Vd = 9 V with 100 msec. stress. The erasing conditions were Vg = -6 V and Vd = 10 V with 10 msec. stress. The relatively large memory window of each device was around 3.2-4 V.

These results indicated a striking effect of polarization of Vg in our devices. Owing to the trapped electrons in the NC charge-trapping layer, the Vth or V_T shifted rightward. When the positive voltage Vg and Vd are applied, the channel electrons gain energy from +Vg and +Vd. Nevertheless, while the -Vg and +Vd voltage conditions are supplied, hot hole charges are generated from the p-type silicon substrate at the same time to balance the △Vth or △V_T for erasing. The hot holes can reach to the NC charge-trapping layer and result in the leftward △Vth or △V_T of following three Id-Vg transfer curves.

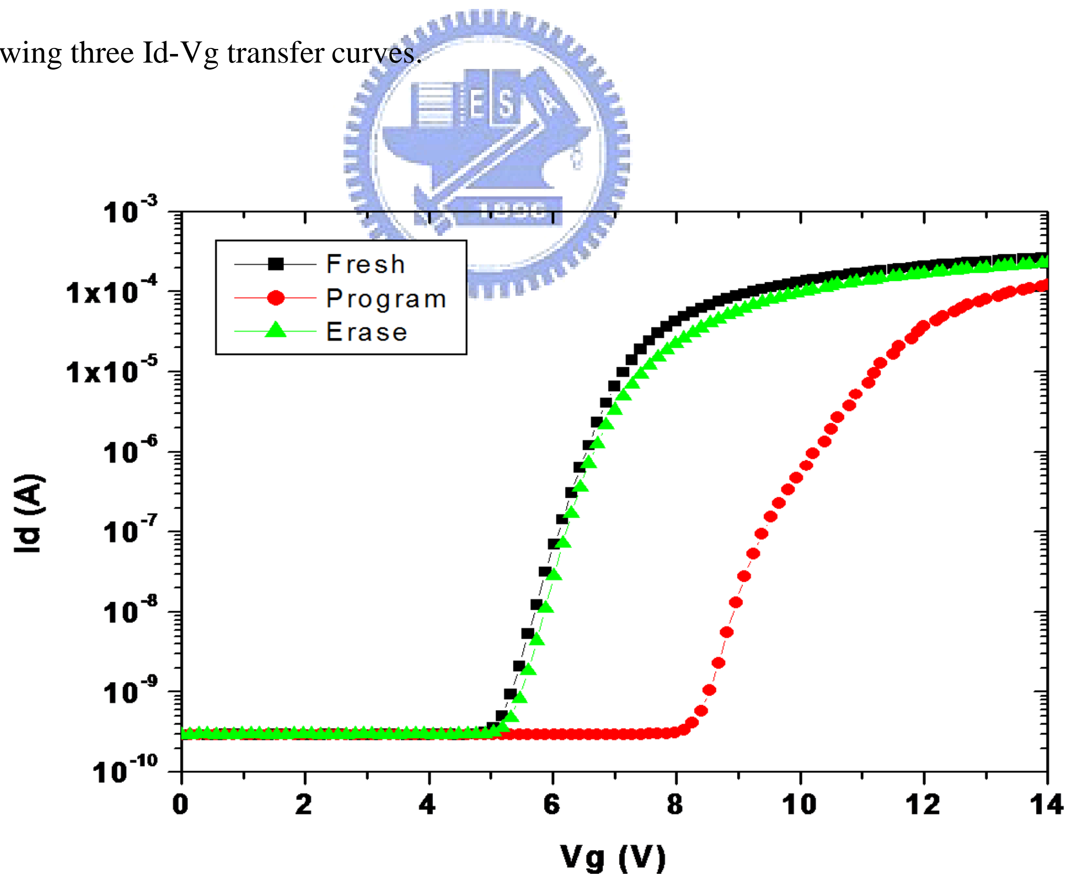

Fig. 3-5 The Id-Vg transfer curves of $AuGe_xO_y$-M_xO_y NC devices

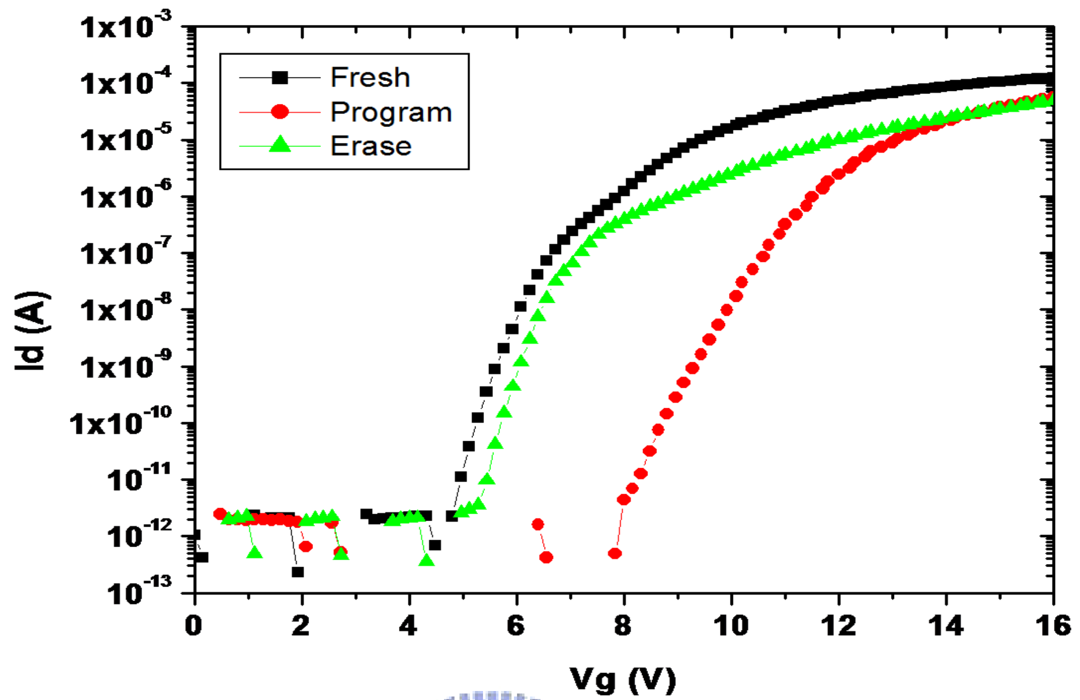

Fig. 3-6 The Id-Vg transfer curves of $(CoZr)Ge_xO_y\text{-}M_xO_y$ NC devices

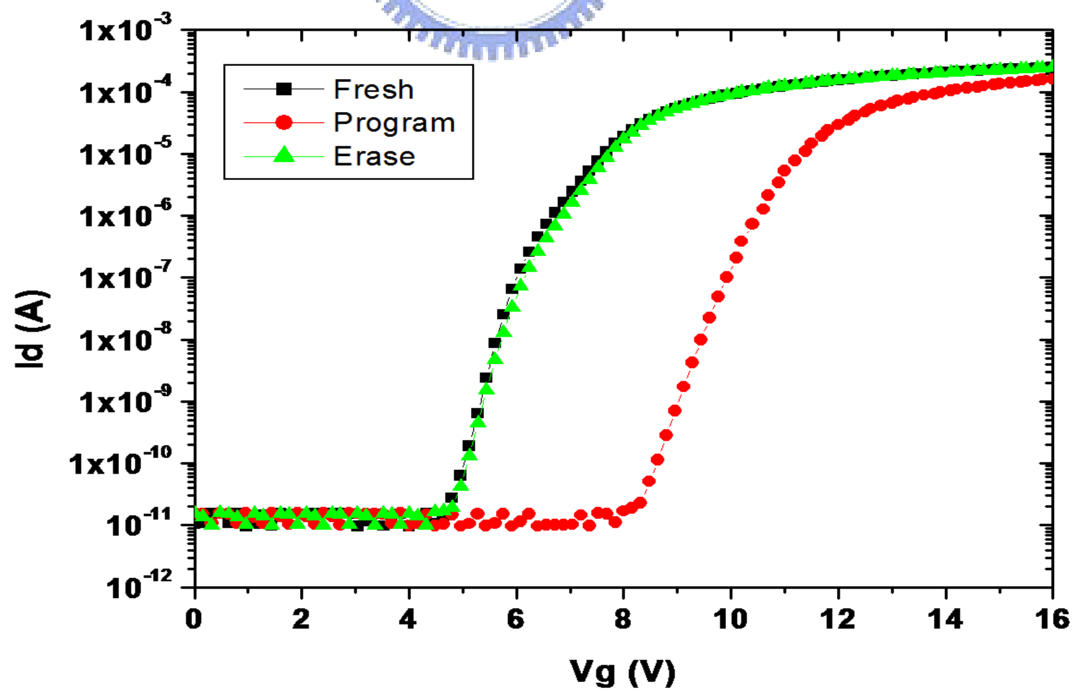

Fig. 3-7 The Id-Vg transfer curves of $(NiZr)Si_xGe_zO_y\text{-}M_xO_y$ NC devices

3-3.1.2 Programming/Erasing Speed

The three programming speed curves of the $AuGe_xO_y$, $(CoZr)Ge_xO_y$, and $(NiZr)Si_xGe_zO_y$ M_xO_y-composite NCs for each memory device trapping layer are revealed in Fig. 3-8, Fig. 3-9, and Fig. 3-10 under programming operations. They showed three different stress conditions: Vg = 8 V, 9 V, 10V and Vd = 9 V. While the Vg was increasing, the △Vth increases and the programming speed was faster as well.

Fig. 3-11, Fig. 3-12, and Fig. 3-13 give the three erasing speed curves of devices for differently erasing voltage conditions: Vg = -9 V, -10 V, and -6 V with Vd = 9 V and 10 V of the $AuGe_xO_y$, $(CoZr)Ge_xO_y$, and $(NiZr)Si_xGe_zO_y$ M_xO_y-NC mixtures, respectively.

We also could find the Vth shifting downward by the more negative gate voltage. The reason for relative variation in the △Vth is more channel electrons or substrate holes trapped in the charge-trapping layer as the increased or decreased gate voltage.

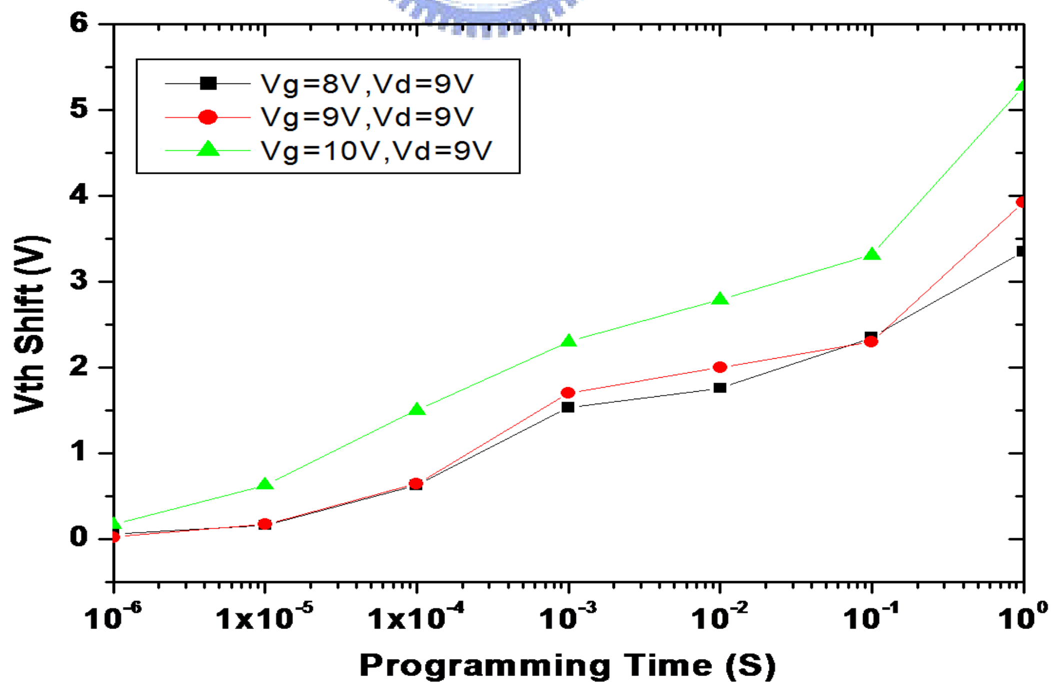

Fig. 3-8 The programming speed of $AuGe_xO_y$-M_xO_y NC devices

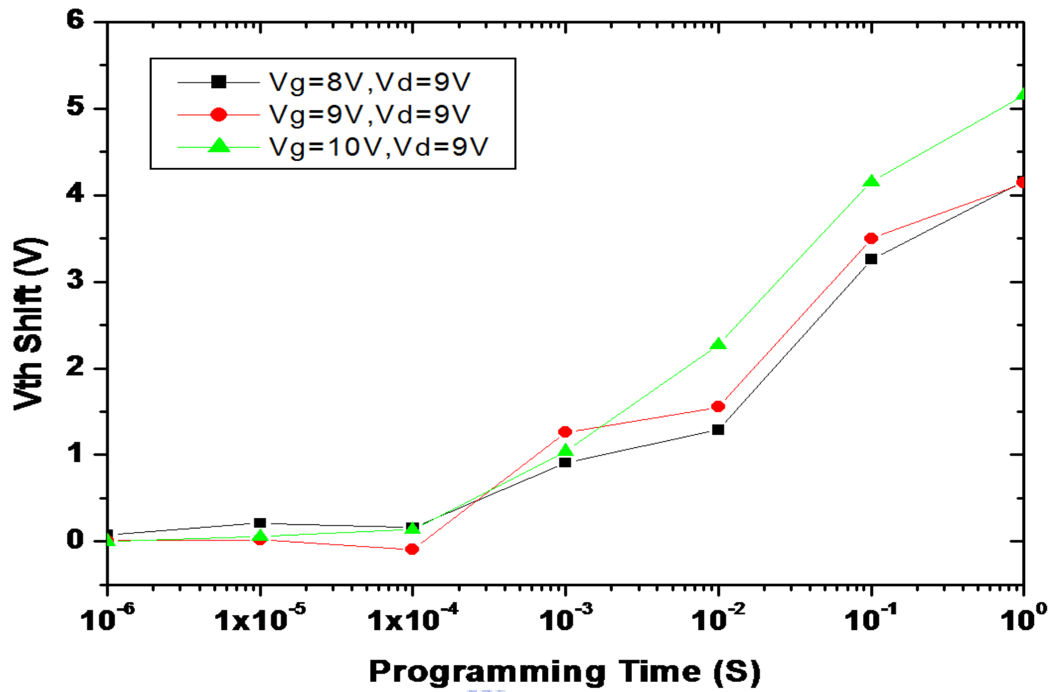

Fig. 3-9 The programming speed of $(CoZr)Ge_xO_y$-M_xO_y NC devices

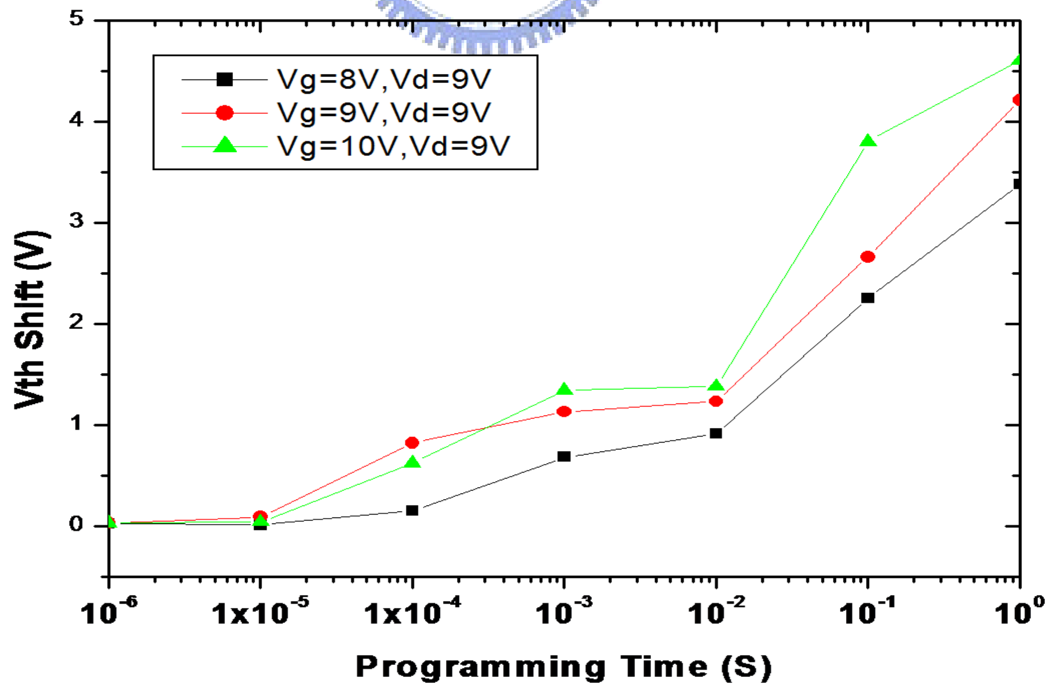

Fig. 3-10 The programming speed of $(NiZr)Si_xGe_zO_y$-M_xO_y NC devices

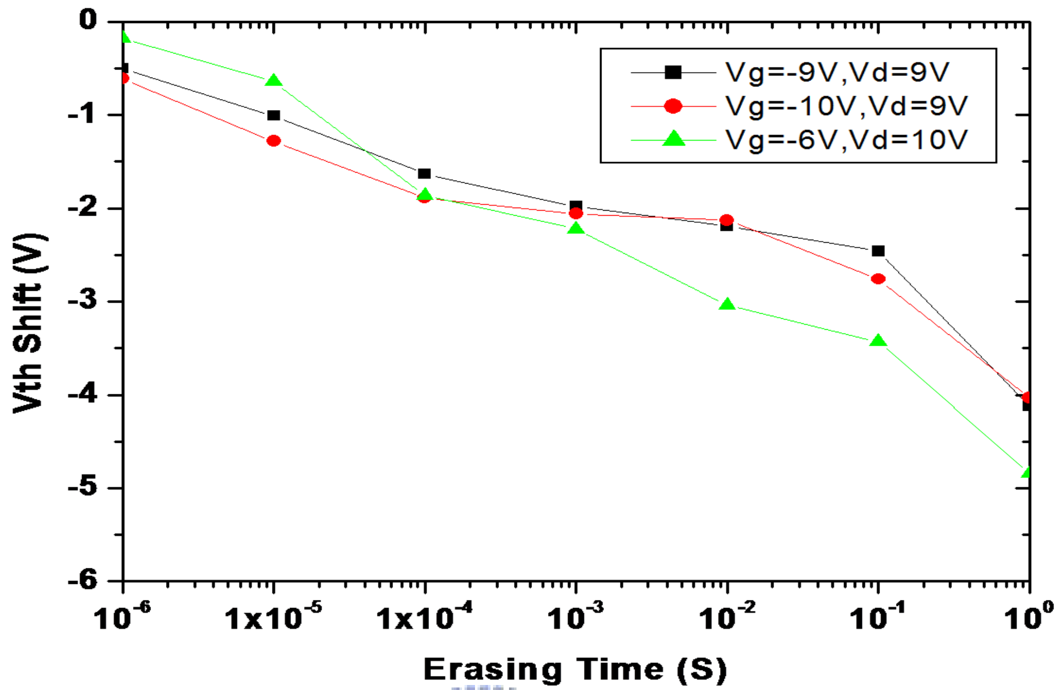

Fig. 3-11 The erasing speed of $AuGe_xO_y$-M_xO_y NC devices

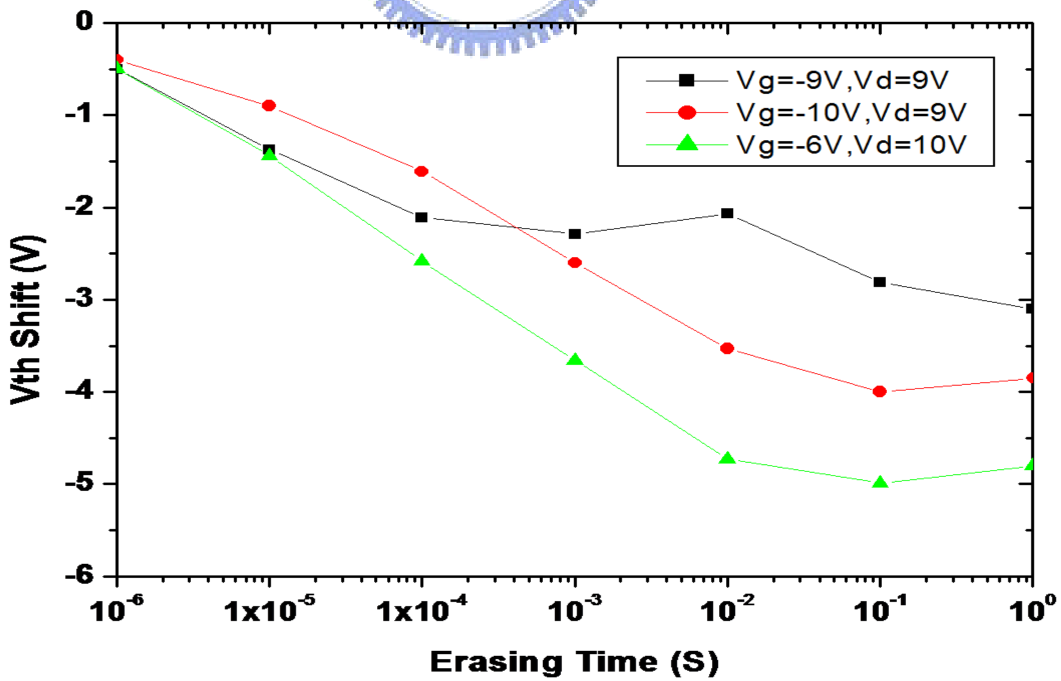

Fig. 3-12 The erasing speed of $(CoZr)Ge_xO_y$-M_xO_y NC devices

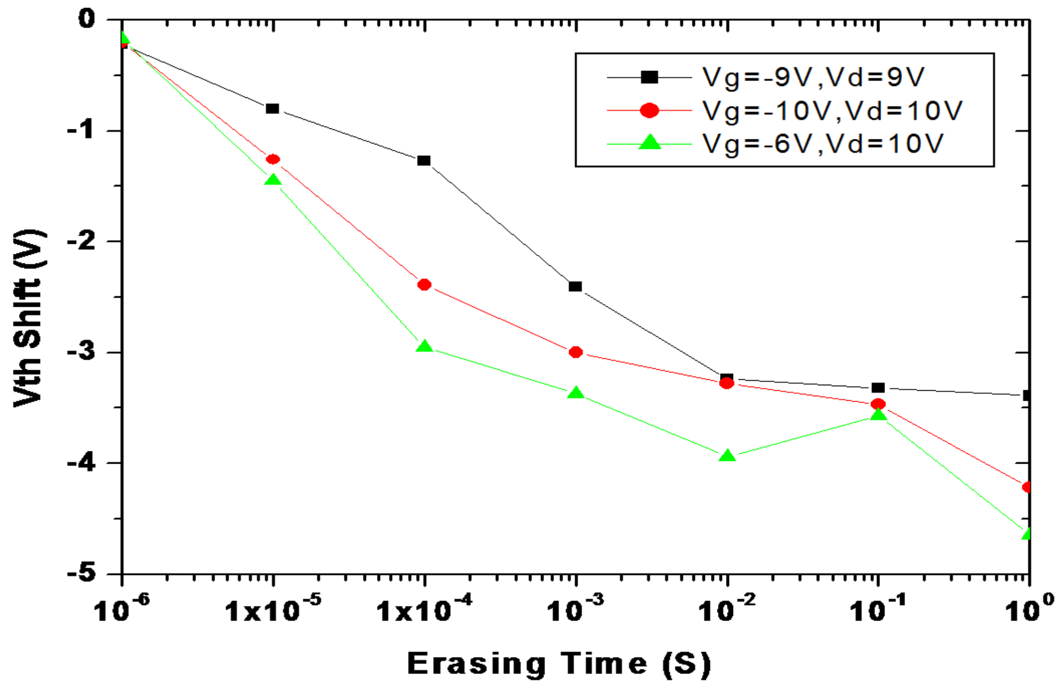

Fig. 3-13 The erasing speed of (NiZr)$Si_xGe_zO_y$-M_xO_y NC devices

3-3.1.3 Retention Time

The data retention time of memory devices was measured at 25° C and 85° C as illustrated in Fig. 3-14, Fig. 3-15, and Fig. 3-16. We found the small charge loss from 10^0 to 10^4 sec. in the devices. Each following curve displayed charge loss less than 5% at room temperature and below 11% at 85° C as measure time up to 10^4 sec.

We can infer the storage charges leak out from deep-level electron traps of the NC charge-trapping layer at 25° C and 85° C. The three Figs. have described only 5% charge loss at 25° C and about 10% at 85° C as measure time up to 10^4 sec. as well.

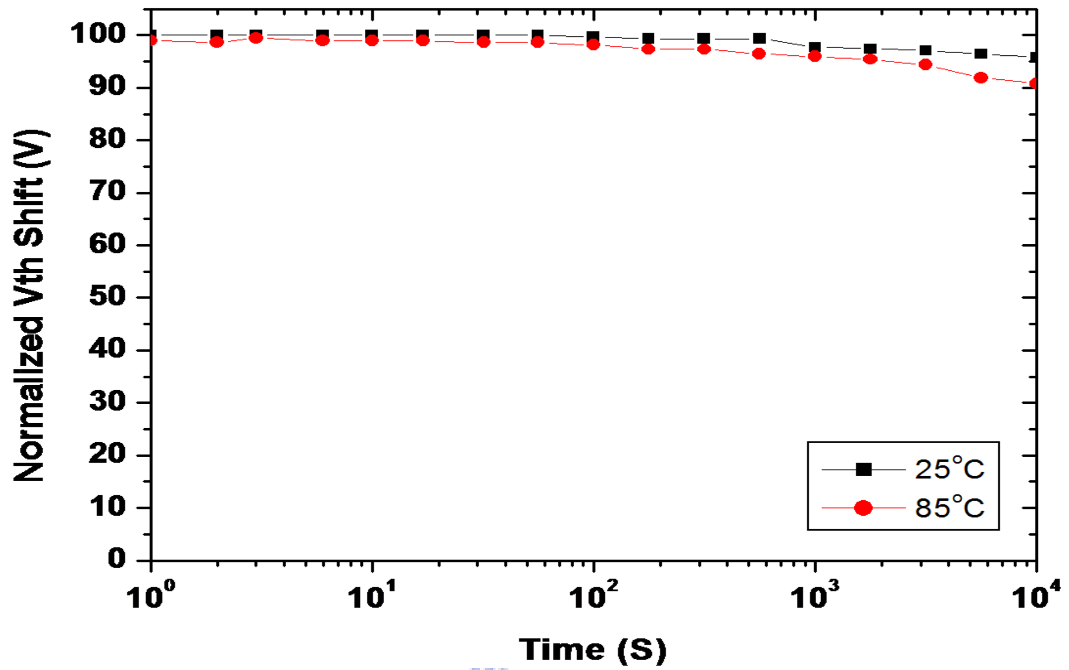

Fig. 3-14 The data retention time of $AuGe_xO_y$-M_xO_y NC devices

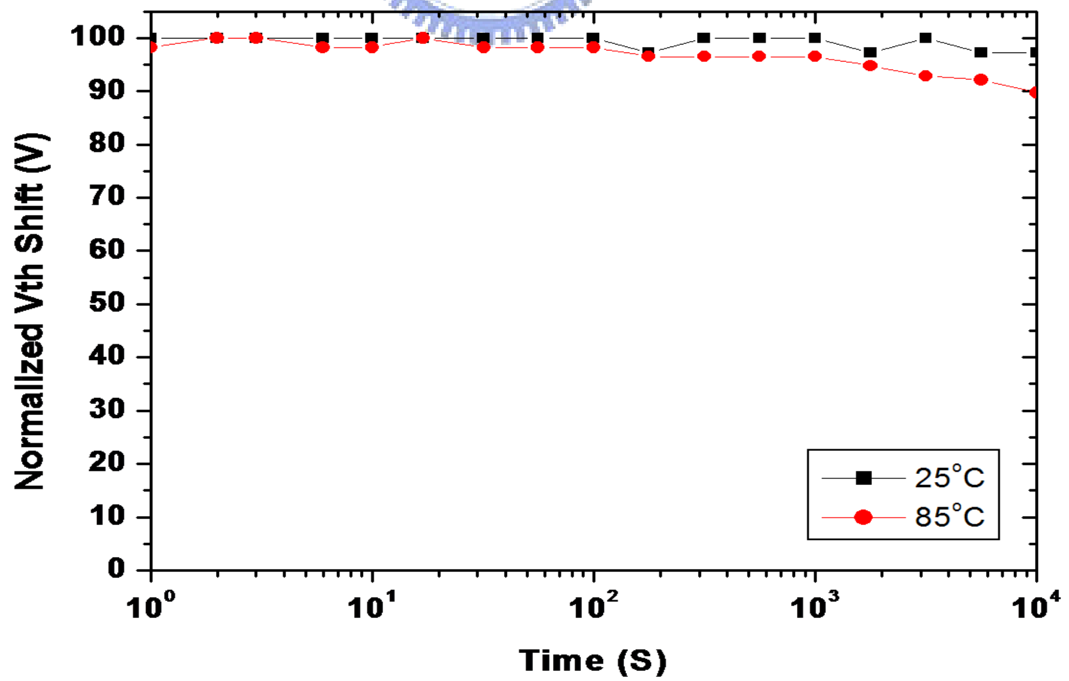

Fig. 3-15 The data retention time of $(CoZr)Ge_xO_y$-M_xO_y NC devices

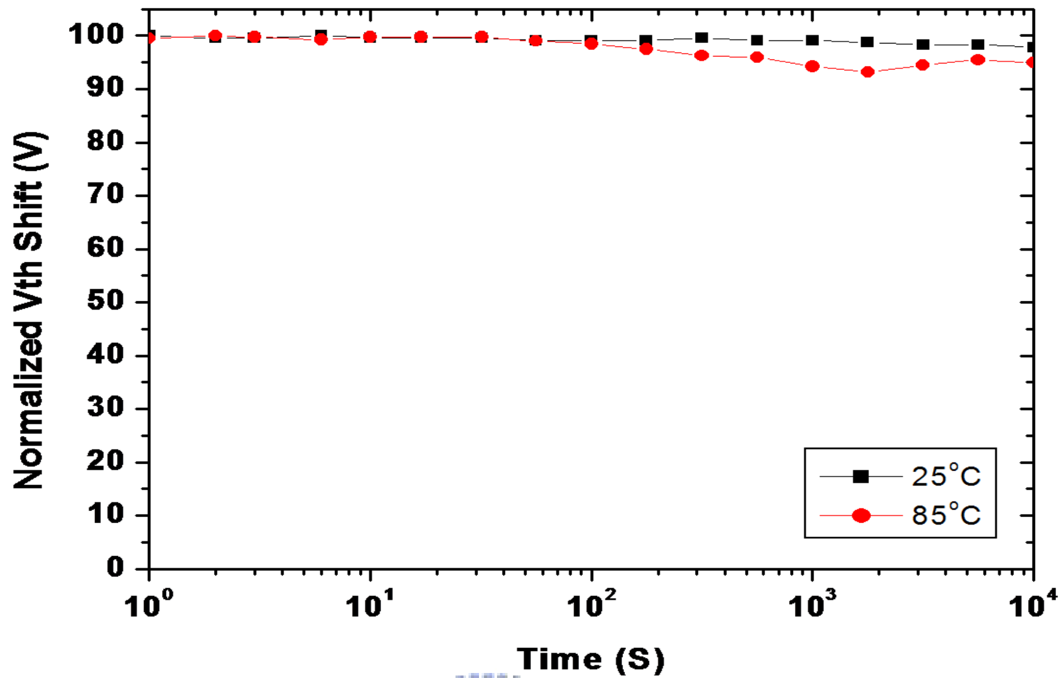

Fig. 3-16 The data retention time of $(NiZr)Si_xGe_zO_y$-M_xO_y NC devices

3-3.1.4 Endurance Cycles

Three endurance characteristics of the NC Flash memory devices are depicted in Fig. 3-17, Fig. 3-18, and Fig. 3-19. The measured voltage conditions were as follows: Vg = 10 V and Vd = 9 V with 10 msec. and 100 msec. for memory programming, Vg = -10 V and Vd = 9 V with 100 msec. for memory erasing.

A small increase of the erasing Vth is observed from the following Figs. due to hard erasure by deep-level trapped charges; in addition, only a little window narrowing effect may be observed.

After 10^4 cycles, the relative memory window was remained around 2.6-3 V. The findings suggested that more different M_xO_y-composite materials be used in order to form the novel NC Flash memory charge-trapping sites discretely in the future.

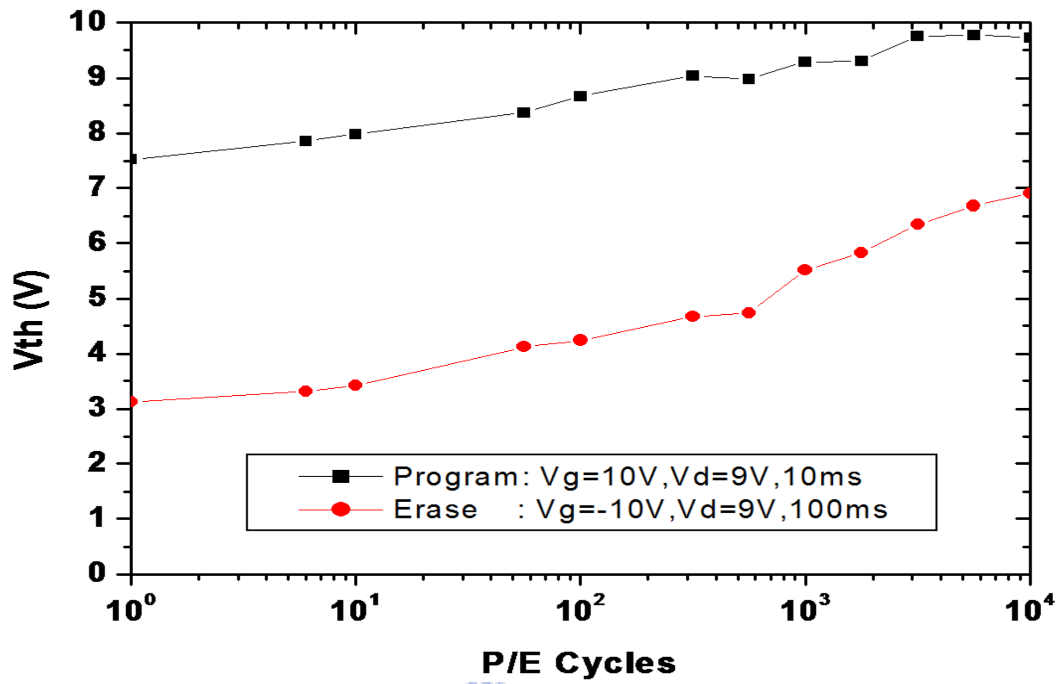

Fig. 3-17 The data endurance of $AuGe_xO_y$-M_xO_y NC devices

1896

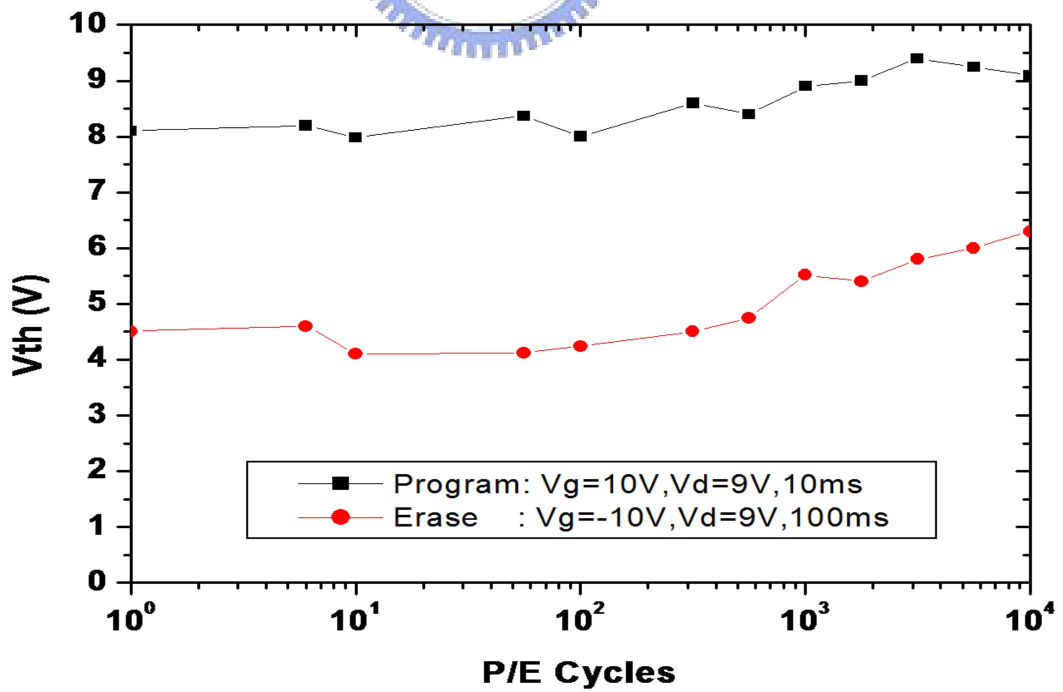

Fig. 3-18 The data endurance of $(CoZr)Ge_xO_y$-M_xO_y NC devices

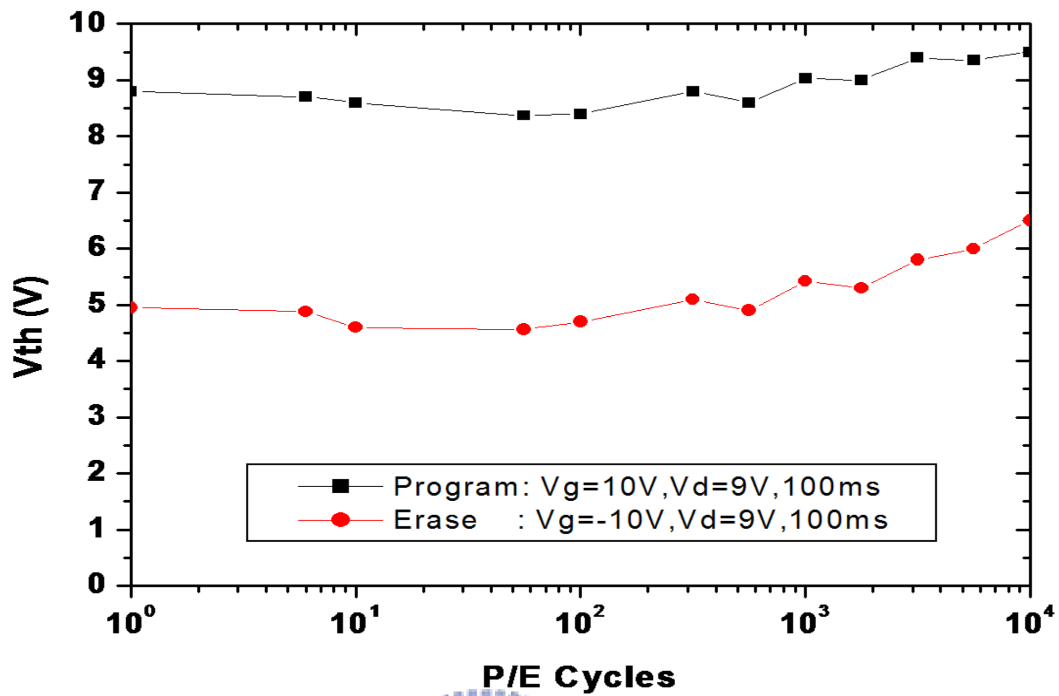

Fig. 3-19 The data endurance of (NiZr)$Si_xGe_zO_y$-M_xO_y NC devices

3-3.1.5 Gate/Drain Disturbance

Fig. 3-20, Fig. 3-21, and Fig. 3-22 show three gate disturbance Figs. of the devices. The measurement was two stress conditions: Vg = 8 V and Vg = 9 V with Vd = Vs = Vb = 0 V. The applied Vg would attract substrate electrons tunneling from gate oxide to the NC-trapping layer by FN mechanism and result in the splitting distribution of charges. After 10^3 sec. stress, the initial or fresh state △Vth increased to 0.05 V and 0.45 V with the Vg = 8 V and Vg =9 V, respectively.

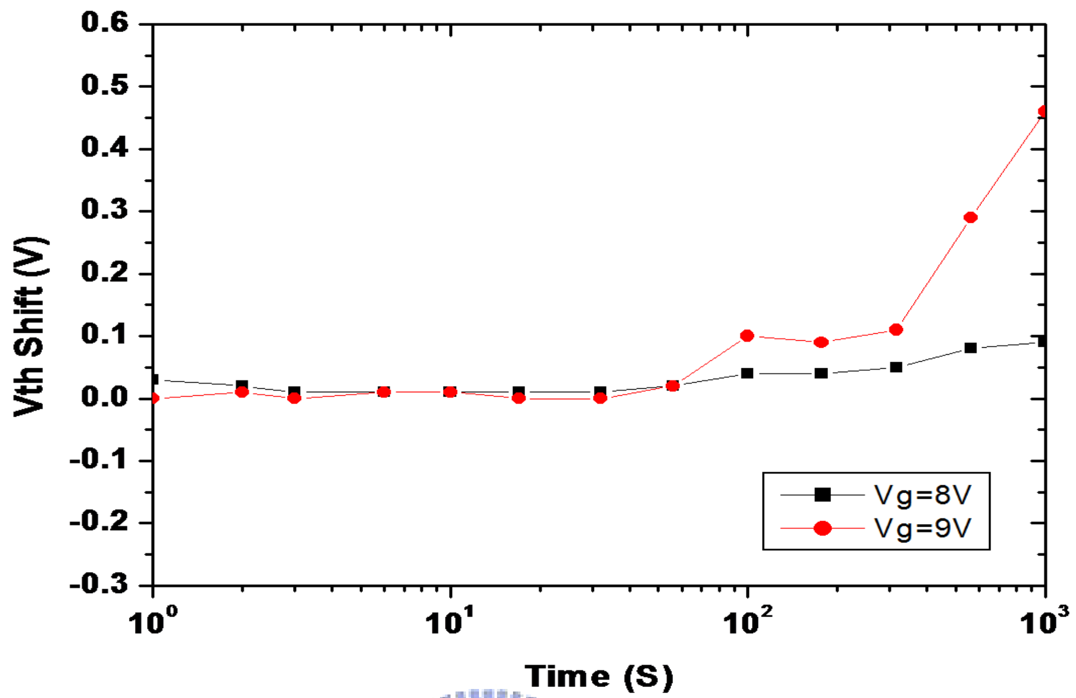

Fig. 3-20 The gate disturbance of $AuGe_xO_y$-M_xO_y NC devices

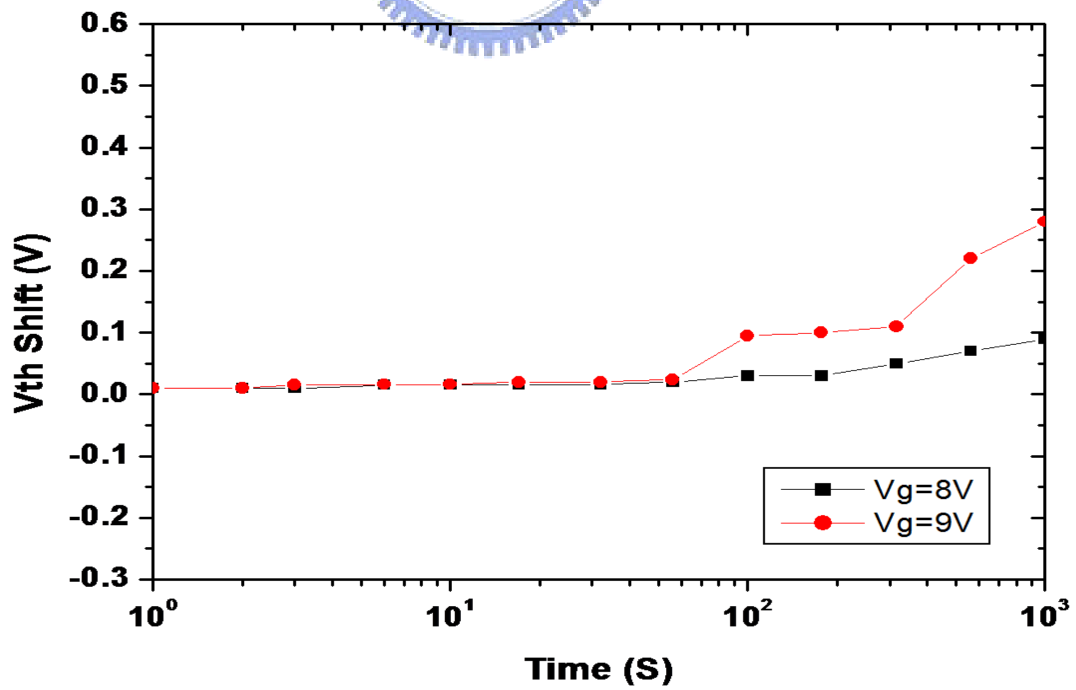

Fig. 3-21 The gate disturbance of $(CoZr)Ge_xO_y$-M_xO_y NC devices

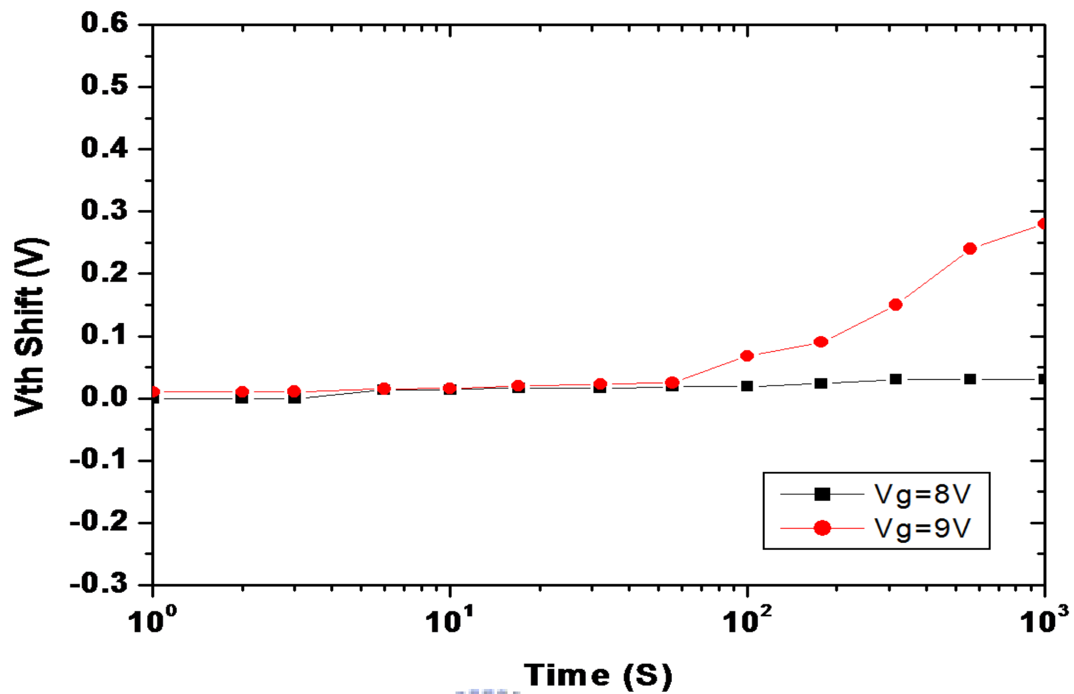

Fig. 3-22 The gate disturbance of (NiZr)$Si_xGe_zO_y$-M_xO_y NC devices

The measurement of each drain disturbance is yielded in Fig. 3-23, Fig. 3-24, and Fig. 3-25, respectively. Two stress conditions were as follows: Vd = 9 V and Vd = 10 V with Vg = Vs = Vb = 0 V to the devices. After 10^3 sec. stress for three Figs., each programmed state △Vth had only about 0.05 V charge loss as well.

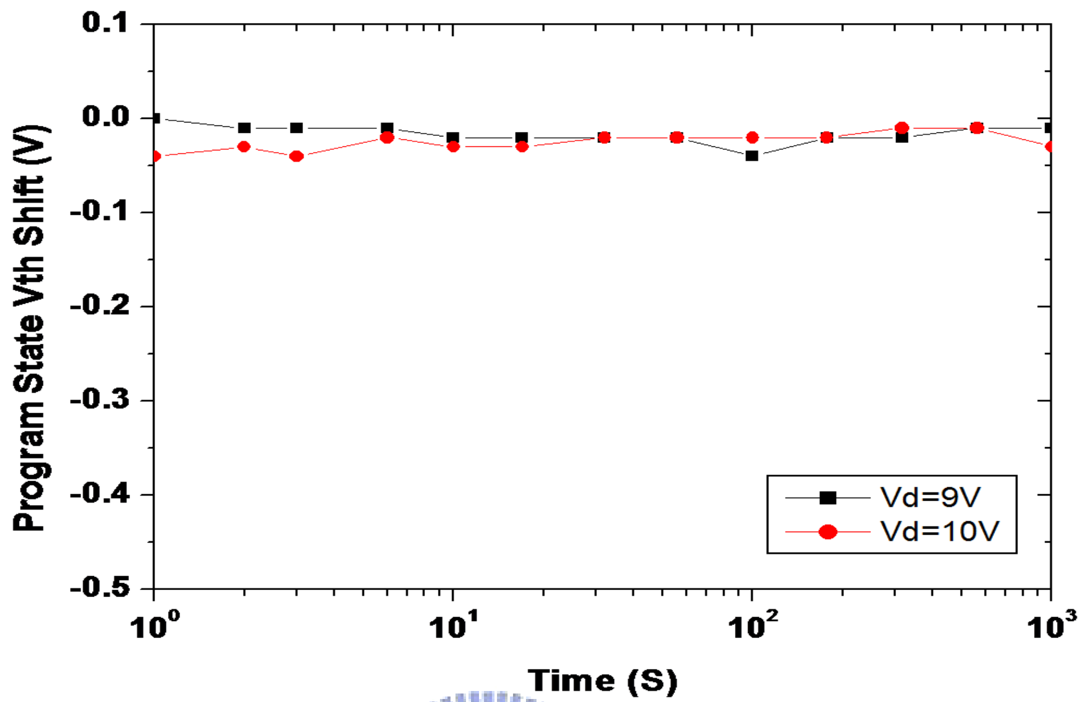

Fig. 3-23 The drain disturbance of $AuGe_xO_y$-M_xO_y NC devices

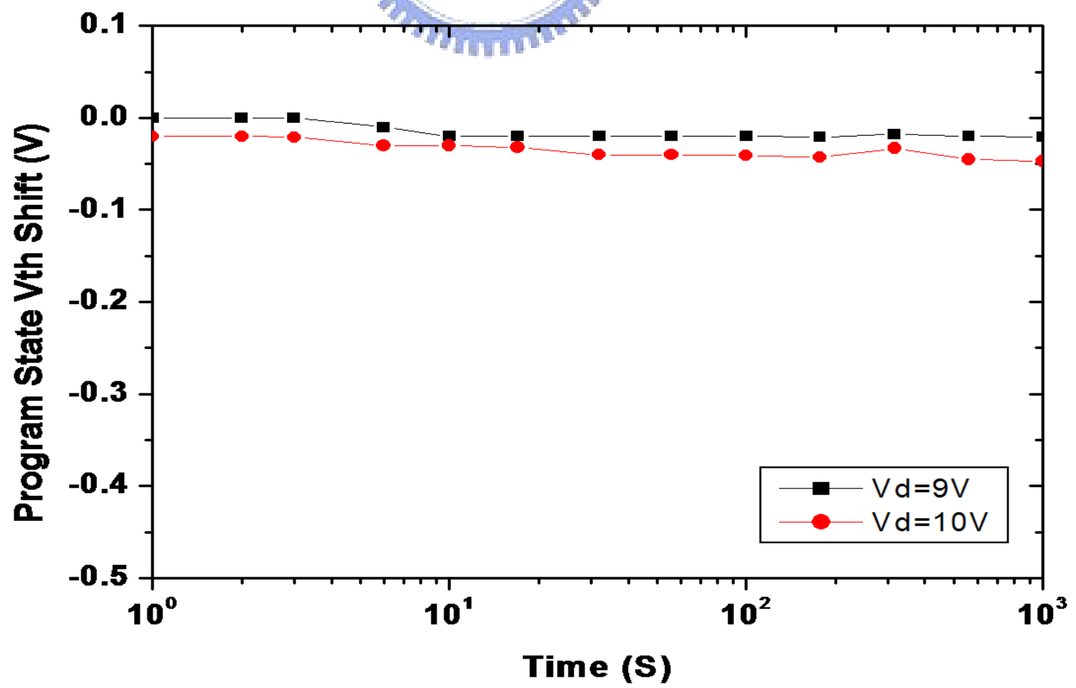

Fig. 3-24 The drain disturbance of $(CoZr)Ge_xO_y$-M_xO_y NC devices

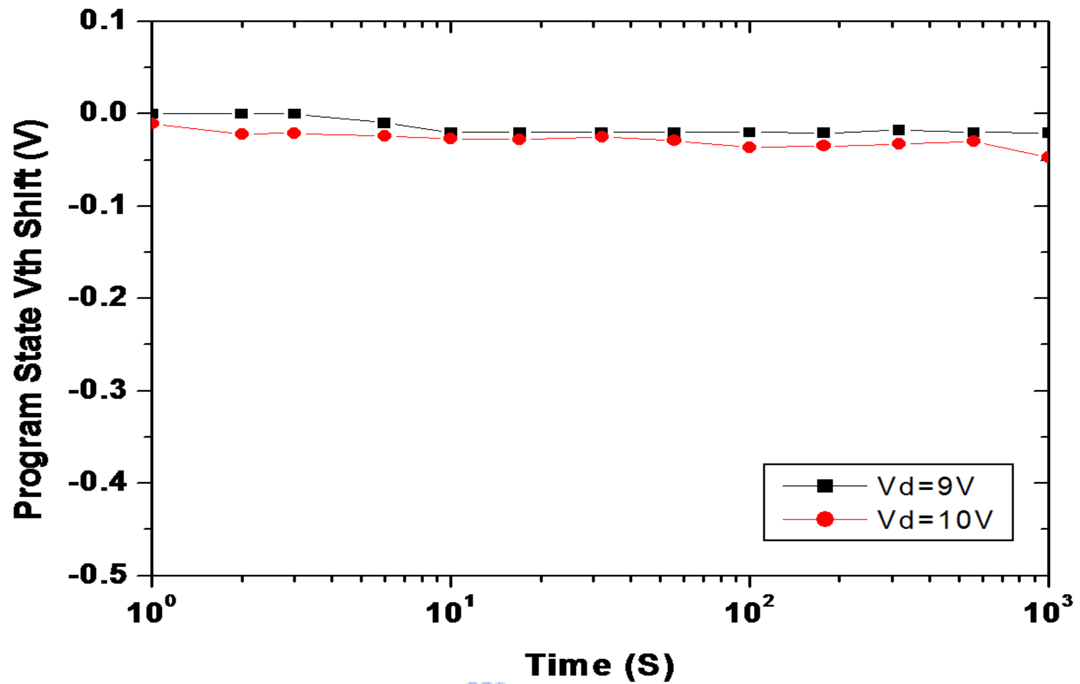

Fig. 3-25 The drain disturbance of (NiZr)$Si_xGe_zO_y$-M_xO_y NC devices

3-3.2 Physical Properties

For analyzing the chemical composites of the Sol-Gel thin-film trapping layer, various elements were detected by the HRTEM instrument of the devices. Fig. 2-26, Fig. 2-27, and Fig. 2-28 reveal three HRTEM images of M_xO_y NCs on SiO_2 after the 1050° C 60 sec. ORTA step. Each charge-trapping layer of the devices truly was shaped into nano-sized or oval-shaped crystals. The average NC size was around 5-10 nm. The visible lattice fringes could denote crystallization into well-ordered nano-structured features typically in each picture clearly [8]-[9].

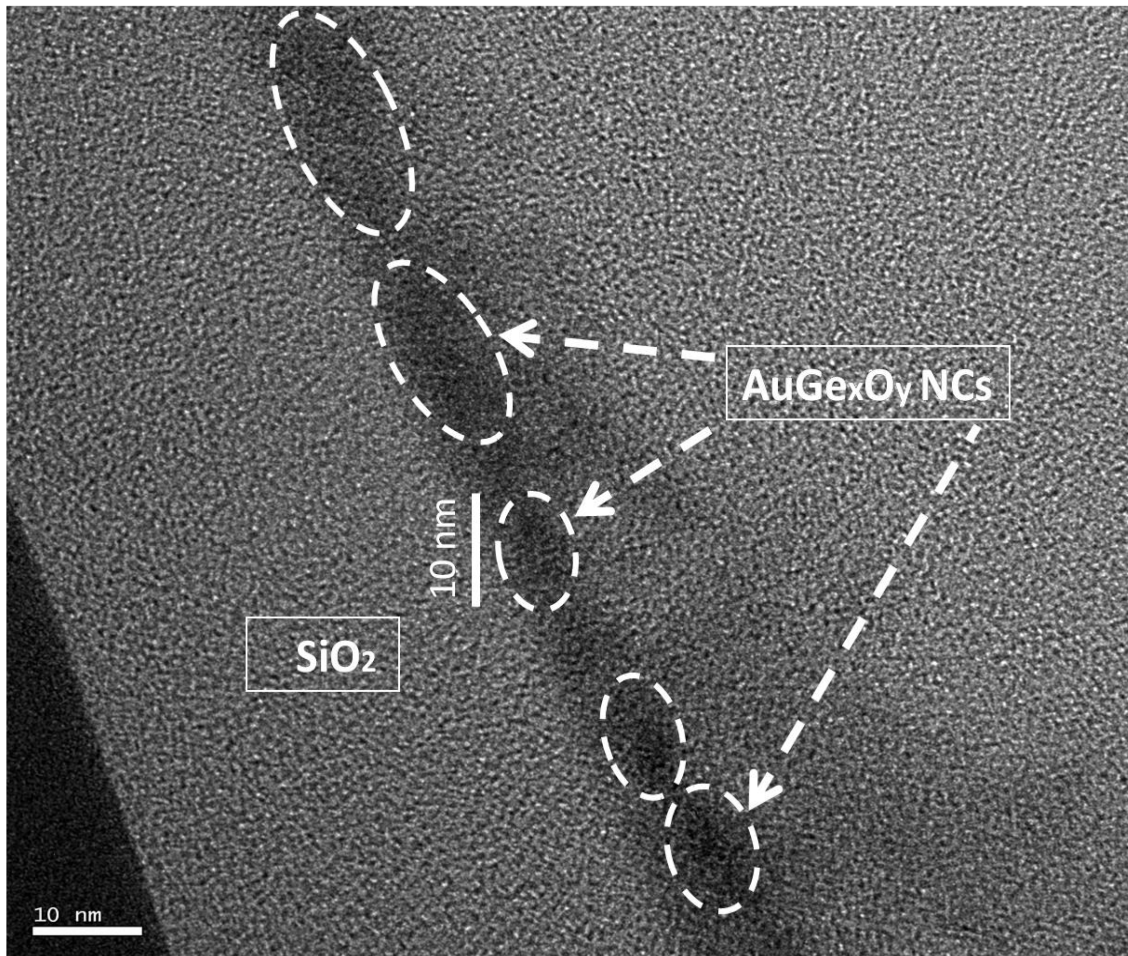

Fig. 3-26 The HRTEM image of $AuGe_xO_y$-composite NCs on SiO_2 after the 1050° C 60 sec. ORTA step

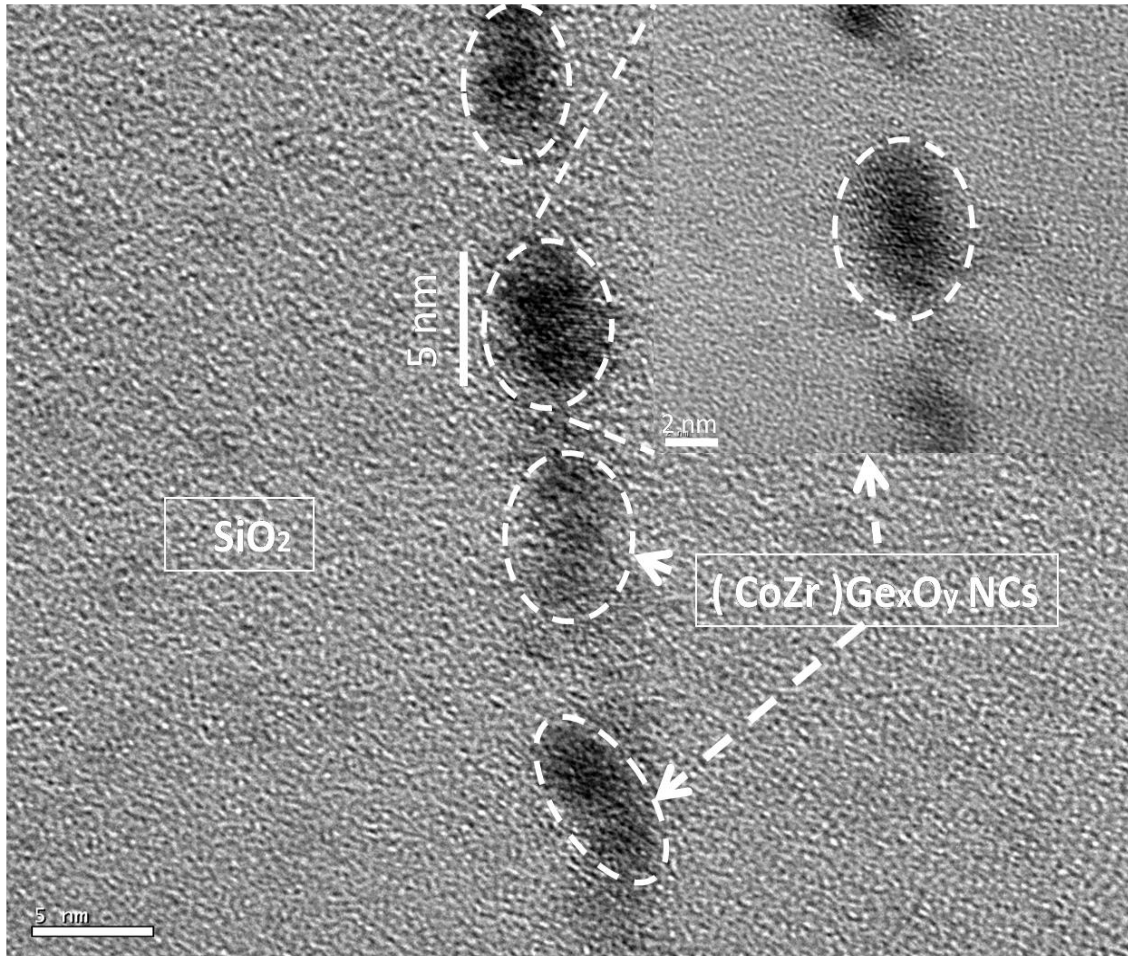

Fig. 3-27 The HRTEM image of $(CoZr)Ge_xO_y$-composite NCs on SiO_2 after the 1050° C 60 sec. ORTA step

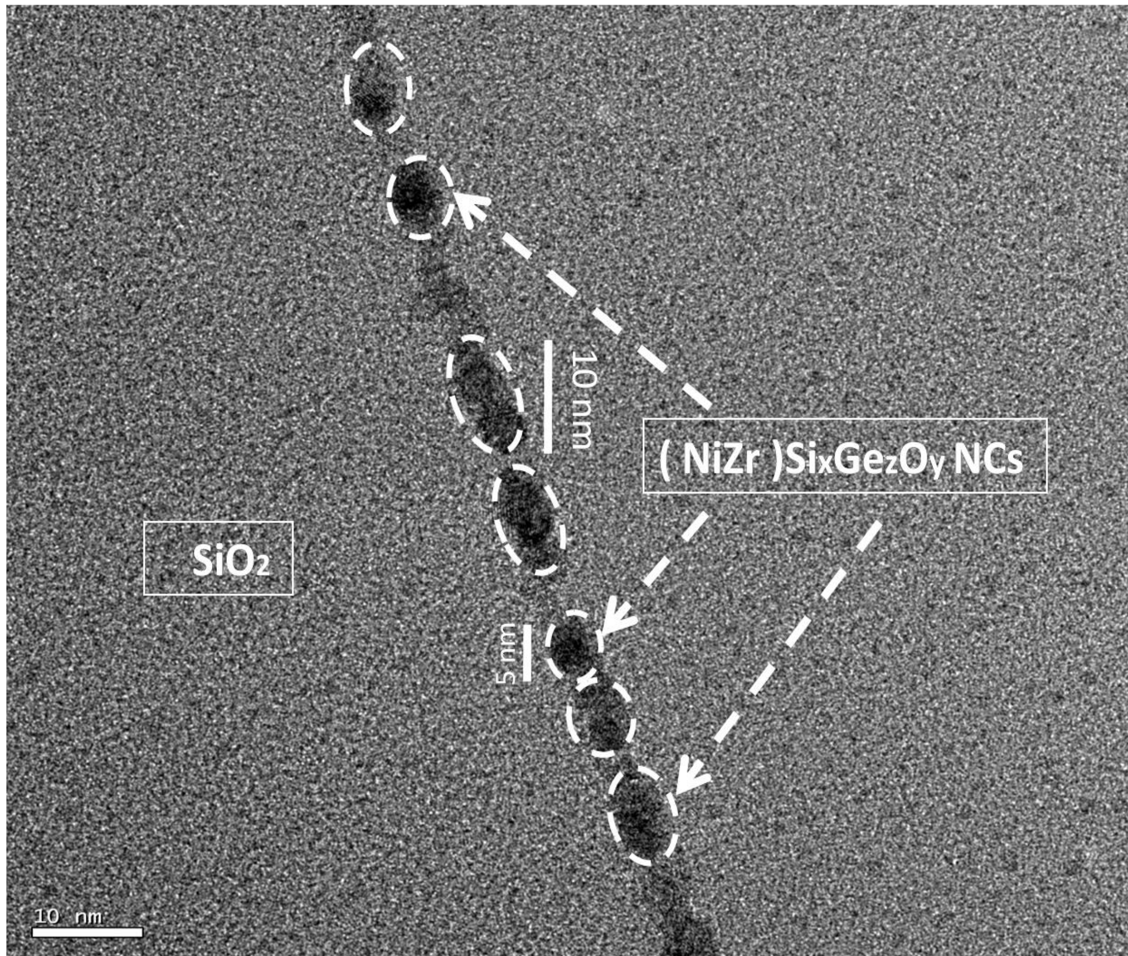

Fig. 3-28 The HRTEM image of $(NiZr)Si_xGe_zO_y$-composite NCs on SiO_2 after the 1050° C 60 sec. ORTA step

3-4 Summary

In this chapter, we proposed other M_xCl_y materials to form various binary or ternary NCs for the trapping layer of memory devices. The HRTEM images verify the formation of nano-composite crystals in the charge-trapping layer. We also have indicated the device electrical performance such as Id-Vg transfer curves, retention time, charge endurance, and G/D disturbance demonstrating the better characteristics in both relatively large 3.2-4 V memory window and little signal disturbance after 10^3 sec.

The longer charge retention is due to binary or ternary NCs in the charge-trapping layer, and good endurance is up to 10^4 cycles with only a little narrowing. The presented Sol-Gel technique is a very easy way to integrate the NC Flash memory fabrication into non-volatile semiconductor memory devices.

Chapter 4
Conclusions and Recommendations for Future Research

4-1 Conclusions

The overview of Flash memory was given with a brief background of NVM and the used terminology in the NVSM industry. This thesis of "The Study of Flash Memory Devices with Metal Oxide Nanocrystals in Sol-Gel Technique" was presented. The results of chapters 1-3 are summarized as follows. The benefits of Sol-Gel spin coating technique to deposit the M_xO_y thin film or NCs as the Flash memory charge-trapping layer are lower costs, more convenient tools, and easier processes to synthesize the combination of binary or ternary M_xO_y NCs in the normal pressure environment.

In the chapter 2, the NC Flash memory devices were fabricated. These experimental memory devices included the thin film of M_xO_y mixtures or NCs as the charge-trapping layer by the Sol-Gel spin coating procedure from IPA. The HRTEM pictures have listed the M_xO_y NCs on SiO_2 after the 1050° C 60 sec. ORTA step. The average size of binary or ternary NCs is about 5 nm. These memory devices have good electrical properties such as high P/E speed, small retention time loss of 5% charge loss as measure time up to 10^4 sec. at room temperature, and only a little window narrowing effect may be found as endurance up to 10^4 P/E cycles.

Next, in the chapter 3, we also fabricated Flash memory devices including the nano-composite M_xO_y crystals as the charge-trapping layer from C_2H_5OH with numerous metal chlorides as precursors. We have discussed the physical properties of

Sol-Gel derived NCs with the diameter of 5-10 nm after the 1050°C 60 sec. ORTA step. The memory electrical properties like Id-Vg transfer curves, P/E speed, retention time, endurance cycles and G/D signal disturbance are described in this chapter as well.

Finally, we have used the Sol-Gel spin coating method to fabricate various kinds of the M_xO_y thin film and binary or ternary NCs as the Flash memory charge-trapping layer for the devices and each of them has good characteristics. We have verified the good performance in terms of the larger △Vth or $\triangle V_T$ due to more trapping sites, longer retention time of only 5% charge loss up to 10^4 sec., better endurance of only a little window narrowing up to 10^4 P/E cycles, and less G/D disturbance for NCs surrounded by the increased tunnel oxide thickness. So the Sol-Gel technique is a simple method for the charge-trapping layer deposition of NC Flash memory devices. These results lead us to believe that the simple Sol-Gel technique will be linked to the novel NC Flash memory processes in the future.

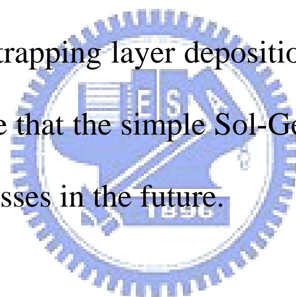

4-2 Recommendations for Future Research

There are two main themes suggested for future research. Thus we have the following topics for the devices. First, for physical analyses, the HRTEM measurement of nano-dot density may be done, and other metal chlorides to form nano-composite NCs with the formation mechanism can be studied. Then, for electrical analyses, the research of vertical migration, lateral migration, and the activation energy in chemical reactions may be undertaken in the future.

References

Chapter 1

[1] S. M. Sze and Kwok K. Ng, "Physics of Semiconductor Devices, 3rd Edition," John Wiley & Sons, 2007.

[2] S. Keeney, "A 130nm Generation High Density ETOX™ Flash Memory Technology," in *IEDM Tech. Dig.*, 2001, pp. 41-44.

[3] A. Thean and J. P. Leburton, "Flash Memory: towards single electronics," *IEEE Potentials*, pp. 35-41, 2002.

[4] R. Bez, E. Camerlenghi, A. Modelli, and A. Visconti, "Introduction to flash memory," in *Proc. of the IEEE*, 2003, pp. 489-502.

[5] P. Pavan, R. Bez, P. Olivo, and E. Zanoni, "Flash memory cells-an overview," in *Proc. of the IEEE*, 1997, pp. 1248-1271.

[6] B. D. Salvo, C. Gerardi, R. V. Schaijk, S. A. Lombardo, D. Corso, C. Plantamura, T. Serafino, G. Ammendola, M. V. Duuren, P. Goarin, W. Y. Mei, K. V. D. Jeugd, H. Baron, M. Gély, P. Mur, and S. Deleonibus, "Performance and reliability features of advanced nonvolatile memories based on discrete traps (silicon nanocrystals, SONOS)," *IEEE Trans. on Devices and Materials Reliability*, vol. 4, pp. 377-389, 2004.

[7] Y. N. Tan, W. K. Chim, B. J. Cho, and W. K. Choi, "Over-erase phenomenon in SONOS-type flash memory and its minimization using a hafnium oxide charge storage layer," *IEEE Trans. on Electron Devices*, vol. 51, pp. 1143-1147, 2004.

[8] "Test and Test equipment" in the *International Technology Roadmap for Semiconductors (ITRS)*, 2001, pp.27-28.

[9] Y. N. Tan, W. K. Chim, W. K. Choi, M. S. Joo, T. H. Ng, and B. J. Cho, "High-k HfAlO charge trapping layer in SONOS-type nonvolatile memory device for high speed operation," in *IEDM Tech. Dig.*, 2004, pp.889-892.

[10] W. J. Zhu, T. P. Ma, T. Tamagawa, J. Kim, and Y. Di, "Current Transport in Metal/Hafnium Oxide/Silicon Structure," *IEEE Electron Device Letters*, vol. 23, no. 2, pp. 97-99, 2002.

[11] G. D. Wilk, R. M. Wallace, and J. M. Anthony, "High-k gate dielectrics: Curent status and materials properties considerations," *Journal of Applied Physics*, vol. 89, pp. 5243-5275, 2001.

[12] T. Yamaguchi, H. Satake, and N. Fukushima, "Band diagram and carrier conduction mechanisms in ZrO/sub 2/MIS structures," *IEEE Trans. on Electron Devices*, vol. 51, pp. 774-779, 2004.

[13] W. Zhu, T. P. Ma, T. Tamagawa, Y. Di, J. Kim, R. Carruthers, M. Gibson, and T. Furukawa, "HfO_2 and HfAlO for CMOS: thermal stability and current transport," *IEDM*, vol. 463, pp. 20.1.1-20.1.4, 2001.

[14] S. Jeon, J. H. Han, J. Lee, C. J. Choi, S. Choi, H. Hwang, and C. Kim, "High work function metal gate and high-k dielectrics for charge trap flash memory device applications," in *Proc. of ESSDERC Symp.*, 2005.

[15] S. Jeon, J. H. Han, J. Lee, S. Choi, H. Hwang, and C. Kim, "Impact of Metal Work Function on Memory Properties of Charge-Trap Flash Memory Devices Using Fowler–Nordheim P/E Mode," *IEEE Trans. on Electron Devices*, vol. 27, 2006.

[16] J. J. Lee and D. L. Kwong, "Metal Nanocrystal Memory with High-k Tunneling Barrier for Improved Data Retention," *IEEE Trans. on Electron Devices*, vol. 52, 2005.

[17] K. J. Hubbard, et al., "Thermodynamic stability of binary oxides," *J. Mater. Res.*, vol.11, no. 11, 1996.

[18] S. Haukka, E. L. Lakomaa, and T. Suntola, in *Adsorption and Its Applications in Industry and Environmental Protection: Stud. Surf. Sci. Catal.*, ed. A. Dabrowski, vol. 120, 1998, pp. 715-750.

[19] S. Ek, Helsinki University of *Technology Inorganic Chemistry Publication Series*, no. 4, Espoo, 2004.

[20] S. K. Gandhi, "The Theory and Practice of Microelectronics," John Wiley & Sons, 1984.

Chapter 2

[1] H. Aozasa, I. Fujiwara, A. Nakamura, and Y. Komatsu, "Analysis of Carrier Traps in Si_3N_4 in Oxide/Nitride/Oxide for Metal/ Oxide/Nitride/Oxide Silicon Non-volatile Memory," *Japanese Journal of Applied Physics*, vol.38, part 1, no. 3, pp.1441-1447, 1999.

[2] Y. Yang and M. H. White, "Charge retention of scaled SONOS non-volatile memory devices at elevated temperatures," *Solid State Electronics*, vol. 44, pp. 949-958, 2000.

[3]G. D. Wilk, R. M. Wallace, and J. M. Anthony, "High-k gate dielectrics: Current status and materials properties considerations," *Journal of Applied Physics*, vol. 89, pp. 5243-5275, 2001.

[4] M. Takata, S. Kondoh, T. Sakaguchi, H. Choi, J. C. Shim, H. Kurino, and M. Koyanagi, "New nonvolatile memory with extremely high density metal nano-dots," in *IEDM Tech. Dig.*, 2003, pp. 553-557.

[5] M. She and T. J. King, "Impact of crystal size and tunnel dielectric on semi-conductor nanocrystal memory performance," *IEEE Trans. on Electron Devices*, vol. 50, pp. 1934-1940, 2003.

[6] T. F. Lei, et al., "High Performance Multi-bit Nonvolatile HfO_2 Nanocrystal Memory Using Spinodal Phase Seperation of Hafnium Silicate," *Intl. Elec. Dev. Meeting*, pp. 1080-1081, 2004.

[7] H. C. You, F. H. Ko, and T. F. Lei, "Physical characterization and electrical properties of sol-gel-derived zirconia films," *Journal of The Electrochemical Society*, vol. 153, no. 6, pp. F94-F99, 2006.

[8] C. W. Turner, Sol-Gel Process-Principles and Applications, *Ceramic Bulletin*, vol. 70, pp. 1487-1490, 1991.

[9] C. J. Brinker, A. J. Hurd, P. R. Schunk, C. S. Ashley, R. A. Cairncross, J. Samuel, K. S. Chen, C. Scott, and R. A. Schwartz , *Metallurgical and Ceramic Protective Coatings*, Chapman & Hall, London, pp. 112-151, 1996.

[10] T. Troczynski and Q. Yang, US patent, May, 2001.

[11] T. Olding, M. Sayer, and D. Barrow, "Ceramic sol-gel composite coatings for electrical insulation," *Thin Solid Films*, vol. 398-399, pp. 581-586, 2001.

[12] T. Kololuoma, S. M. Nissila, and J. T. Rantala, "Sol-Gel Optics V. Society of Photo-Optical Instrumentation 54 Engineers," in *Proc. of SPIE*, 2000, pp. 218.

[13] C. J. Brinker and G. W. Scherer, *Sol-Gel Science: The Physics and Chemistry of Sol-Gel Processing*, Academic Press, Inc. New York, 1990.

[14] A. Eisenberg and M. King, *Ion-Containing Polymers: Physical Properties and Structure,* Academic Press, New York, vol. 2, pp. 163-169, 1977.

[15] G. Trimmel, C. Lembacher, G. Kickelbick, and U. Schubert, *New Journal of Chemistry*, 2002.

[16] M. Marvola, J. Kiesvaara, K. Järvinen, M. Lindén, and A. Urtti, *Sol-Gel Derived Silica Gel Monoliths And Microparticles As Delivery in Tissue Admonistration,* Division of Biopharmaceutics and Pharmacokinetics Department of Pharmacy University of Helsinki, 2001.

[17] F. M. Yang, T. C. Chang, P. T. Liu, P. H. Yeh, Y. C. Yu, J. Y. Lin, S. M. Sze, and J. C. Lou, "Memory characteristics of Co nanocrystal memory device with HfO_2 as blocking oxide," *Appl. Phys. Lett.*, vol. 90, pp. 132102, 2007.

[18] T. Baron, B. Pellissier, L. Perniola, F. Mazen, J. M. Hartmann, and G. Polland, "Chemical vapor deposition of Ge nanocrystals on SiO_2," *Appl. Phys. Lett.*, vol. 83, pp. 1444-1446, 2003.

[19] G. D. Wilk and D. A. Muller, "Correlation of annealing effects on local electronic structure and macroscopic electrical properties for HfO_2 deposited by atomic layer deposition," *Appl. Phys. Lett.*, vol. 83, pp. 3984-3986, 2003.

[20] F. H. Ko, H. C. You, C. M. Chang, W. L. Yang, and T. F. Lei, "Fabrication of SONOS-Type Flash Memory with the Binary High-*k* Dielectrics by the Sol-Gel Spin Coating Method," *Journal of The Electrochemical Society*, vol. 154, no. 4, pp. H268-H270, 2007.

[21] C. J. Brinker, D. M. Smith, R. Deshpande, P. M. Davis, S. Hietala, G. C. Frye, C. S. Ashley, and R. A. Assink, *Catal. Today* 1992.

[22] C. J. Brinker, A. J. Hurd, P. R. Schunk, G. C. Frye, and C. S. Ashley, *J. Non-Cryst. Solids*, 1992.

[23] Hong Xiao, "Introduction to Semiconductor Manufacturing Technology," Prentice Hall, 2001.

Chapter 3

[1] T. H. Hsu, H. C. You, F. H. Ko, and T. F. Lei, "PolySi-SiO_2-ZrO_2-SiO_2-Si Flash Memory Incorporating a Sol-Gel-Derived ZrO_2 Charge Trapping Layer," *Journal of The Electrochemical Society*, vol. 153, no. 11, pp. G934-G937, 2006.

[2] Z. Liu, C. Lee, V. Narayanan, G. Pei, and E. C. Kan, "Metal Nanocrystal

Memories-Part I: Device Design and Fabrication," *IEEE Trans. on Electron Devices*, vol. 49, pp. 1606-1613, 2002.

[3] Z. Liu, C. Lee, V. Narayanan, G. Pei, and E. C. Kan, "Metal Nanocrystal Memories-Part II: Electrical Characteristics," *IEEE Trans. on Electron Devices*, vol. 49, pp. 1614-1622, 2002.

[4] J. H. Chen, Y. Q. Wang, W. J. Yoo, Y. C. Yeo, G. Samudra, D. SH Chan, A. Y. Du, and D. L. Kwong, "Nonvolatile Flash Memory Device Using Ge Nanocrystals Embedded in HfAlO High-k Tunneling and Control Oxides: Device Fabrication and Electrical Performance," *IEEE Trans. on Electron Devices*, vol. 51, pp. 1840-1848, 2004.

[5] Y. Liu, S. Tang, D. Yu, G. Hwang, and S. Banerjee, "Tunnel oxide thickness dependence of activation energy for retention time in SiGe quantum dot flash memory," *Appl. Phys. Lett.*, vol. 88, pp. 213504, 2006.

[6] F. M. Yang, T. C. Chang, P. T. Liu, P. -. Yeh, Y. C. Yu, J. Y. Lin, S. M. Sze, and J. C. Lou, "Memory characteristics of Co nanocrystal memory device with HfO_2 as blocking oxide," *Appl. Phys. Lett.*, vol. 90, pp. 132102, 2007.

[7] D. U. Lee, M. S. Lee, J. H. Kim, E. K. Kim, H. M. Koo, W. J. Cho, and W. M. Kim, "Floating gated silicon-on-insulator nonvolatile memory devices with Au nanoparticles embedded in $SiO_{1.3}N$ insulators by digital sputtering method," *Appl. Phys. Lett.*, vol. 90, pp. 093514, 2007.

[8] H. C. You, T. H. Hsu, F. H. Ko, J. W. Huang, and T. F. Lei, "Hafnium Silicate Nanocrystal Memory Using Sol–Gel-Spin-Coating Method," *IEEE Electron Device Letters*, vol. 27, no.8, pp. 644-646, 2006.

[9] F. H. Ko, H. C. You, and T. F. Lei, "Sol-gel-derived double-layered nanocrystal memory," *Appl. Phys. Lett.*, vol. 89, pp. 252111, 2006.

[10] U. Schubert, “Chemical Modification of Titanium Alkoxides for Sol-Gel Processing,” *J. Mater. Chem.*, vol. 15, pp. 3701-3715, 2005.

[11] S. M. Sze and C.Y. Chang, “ULSI Technology,” McGraw-Hill, 1996.